# Wear Mechanisms in Cutting Tools for Machining Applications

## Interfacial Phenomena, Characterization, and Relation to Performance

Lindvall, Rebecka

2024

*Document Version:*
Publisher's PDF, also known as Version of record

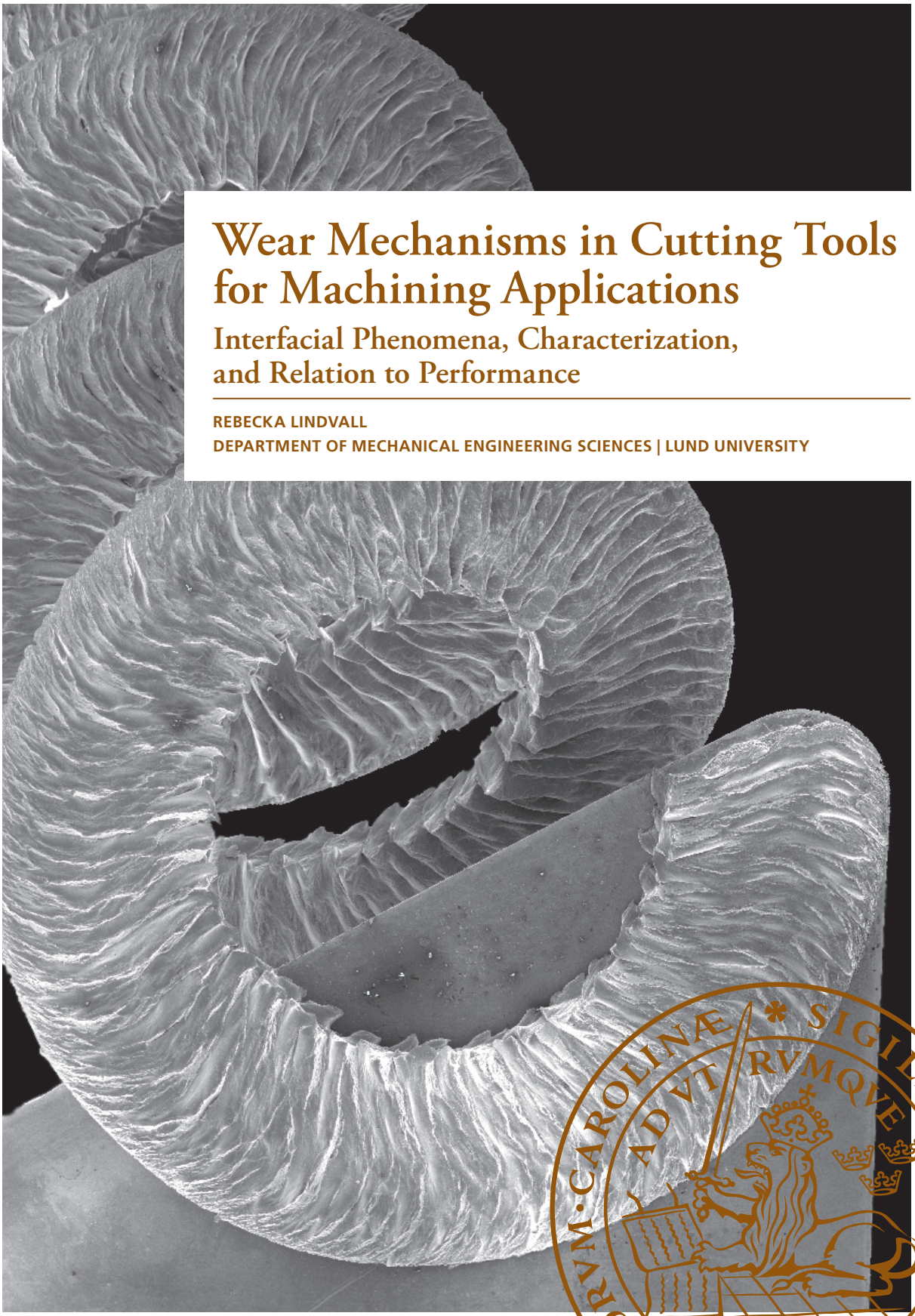

# Wear Mechanisms in Cutting Tools for Machining Applications

## Interfacial Phenomena, Characterization, and Relation to Performance

REBECKA LINDVALL
DEPARTMENT OF MECHANICAL ENGINEERING SCIENCES | LUND UNIVERSITY

# Wear Mechanisms in Cutting Tools for Machining Applications

## Interfacial Phenomena, Characterization, and Relation to Performance

Rebecka Lindvall


LUND
UNIVERSITY

DOCTORAL DISSERTATION

Doctoral dissertation for the degree of Doctor of Philosophy (PhD) at the Faculty of Engineering, Lund University, to be publicly defended on the 24th of May at 10.00 in lecture hall M:D, Department of Mechanical Engineering Sciences, Ole Römers väg 1, Lund.

*Faculty opponent*
Associate professor Giuliano Bissacco

Technical University of Denmark (DTU), Department of Civil and Mechanical Engineering, Lyngby, Denmark

**Organization** Division of Production and Materials Engineering, Faculty of Engineering, LUND UNIVERSITY

**Document name** DOCTORAL DISSERTATION **Date of issue** 2024-05-24

**Author** Rebecka Lindvall **Sponsoring organization**

**Title and subtitle** Wear Mechanisms in Cutting Tools for Machining Applications – Interfacial Phenomena, Characterization, and Relation to Performance

**Abstract**

Metal cutting technology plays an important role in the automotive and aeronautic sectors, both of which are important for the Swedish economy. Both make use of traditional grey cast iron and difficult-to-machine materials like titanium alloys and compacted graphite iron. The tools used to machine these materials wear at varying rates depending on factors such as contact temperature, pressure, and the relative motion of the workpiece material and the tool surface. Given that the machining process and the production of tool and workpiece materials are energy intensive and generate waste, it is important to improve the process sustainability. This can be achieved by improving machining conditions and tooling solutions, and by developing more wear-resistant tooling. Doing so requires knowledge of the wear mechanisms that contribute to tool degradation.

The aim of this work is to expand knowledge of wear mechanisms in commercial tooling during machining, to explore the phenomena occurring at the tool-chip/workpiece interface, and to explore the driving forces that govern their intensity and relation to performance. Tools worn in turning and milling applications and the related interfacial phenomena were explored after controlled variations in the cutting environment. The methods used included freezing the cutting action, imitational experiments, and to a lesser extent simulations or models of the wear processes. Samples generated by these experimental methods were studied using scanning electron microscopy, X-ray energy-dispersive spectroscopy, electron backscatter diffraction, ion channeling contrast, transmission electron microscopy, and X-ray diffraction.

The major tool wear mechanisms include diffusional dissolution and formation of reaction products that are either easily removed with the chip flow or that work as diffusion barriers. Additional chemical wear through oxidation may occur in milling operations. Tool coatings are subject to mechanical wear and also to some degree to diffusional dissolution. The combination of several titanium alloys including commercially pure titanium, near-α Ti-6Al-2Sn-4Zr-2Mo, α+β Ti-6Al-4V, α+β Ti-6Al-2Sn-4Zr-6Mo, and near-β Ti-5Al-5V-5Mo-3Cr, compacted graphite iron, and grey cast iron with tooling including polycrystalline diamond, polycrystalline cubic boron nitride, uncoated cemented carbide grades and coated versions including physical vapor deposition applied $Ti_{0.45}Al_{0.55}N$ with or without NbN overlayer and chemical vapor deposition applied Ti(C,N)-$Al_2O_3$ makes for many variants of reaction products, intensity of wear mechanisms, performance, and ways to decrease the wear rate.

**Keywords** Machining, Tool wear, Wear mechanisms, Diffusion, Chemical wear

Classification system and/or index terms (if any) Supplementary bibliographical information

**ISBN** 978-91-8039-962-3 (print) **ISSN and key title**:

**ISBN** 978-91-8039-963-0 (electronic) **Language** English

Recipient's notes **Number of pages**: 270

Price Security classification



Signature Date 2024-04-10

# Wear Mechanisms in Cutting Tools for Machining Applications

## Interfacial Phenomena, Characterization, and Relation to Performance

Rebecka Lindvall


LUND
UNIVERSITY

Coverphotos by Rebecka Lindvall
Copyright Rebecka Lindvall




Faculty of Engineering
Department of Mechanical Engineering Sciences
Division of Production and Materials Engineering



ISBN 978-91-8039-962-3 (print)
ISBN 978-91-8039-963-0 (electronic)

Printed in Sweden by Media-Tryck, Lund University
Lund 2024


# Acknowledgments

The first time I saw the M-house was in August 2013, a week before I started the mechanical engineering program. I thought, yes, this is where I will spend a lot of time the coming five years. It turned out to be a bit more than double, but I have no regrets. The wear of cutting tools fascinated me early in my master's studies, and I am thankful to have had the opportunity to dig deeper into the subject in the doctoral program. During these years of exploring tool wear mechanisms, I have come to realize how much there is to investigate and learn. This thesis represents a fraction of the knowledge pool.

My supervision team consisted of Volodymyr Bushlya, Jan-Eric Ståhl, Filip Lenrick, and Rachid M'Saoubi. I am thankful that each of you has generously shared inspiration, support, and challenges during these years. I would also like to thank my colleagues at the division of Production and Materials Engineering for support, discussions, and feedback on my research and working life in general. I would also like to thank the co-authors of my papers, the people with whom I collaborated on research projects, and the industries I have had the pleasure of visiting. I would also like to thank the editors and reviewers, who are rarely acknowledged but who have given constructive feedback on research papers and who have encouraged and often believed in the content.

I thank Bengt-Göran Rosén for conducting the midway review of my doctoral studies. I am also thankful for the travel scholarship I was awarded by the Engineering Club of Skåne (Skånska Ingenjörsklubben). My doctoral studies were made possible by the financial support and collaboration of Seco Tools AB, the European Union's Horizon 2020 Research and Innovation Program under the *Flintstone2020* project (Grant Agreement Number 689279), the Sustainable Production Initiative, which is a cooperative venture between Lund University and Chalmers University of Technology, the Element Six Group, the Swedish Governmental Agency for Innovation Systems (VINNOVA) project *Competitive gray cast iron for sustainable development* (Grant Agreement Number 2017-03213), and the FFI Strategic Vehicle Research and Innovation project *Sustainable product realization of cast iron components in an extended value chain* (Grant Agreement Number 2019-03118).

# Table of Contents

# Abstract

Metal cutting technology plays an important role in the automotive and aeronautic sectors, both of which are important for the Swedish economy. Both make use of traditional grey cast iron and difficult-to-machine materials like titanium alloys and compacted graphite iron. The tools used to machine these materials wear at varying rates depending on factors such as contact temperature, pressure, and the relative motion of the workpiece material and the tool surface. Given that the machining process and the production of tool and workpiece materials are energy intensive and generate waste, it is important to improve the process sustainability. This can be achieved by improving machining conditions and tooling solutions, and by developing more wear-resistant tooling. Doing so requires knowledge of the wear mechanisms that contribute to tool degradation.

The aim of this work is to expand knowledge of wear mechanisms in commercial tooling during machining, to explore the phenomena occurring at the tool-chip/workpiece interface, and to explore the driving forces that govern their intensity and relation to performance. Tools worn in turning and milling applications and the related interfacial phenomena were explored after controlled variations in the cutting environment. The methods used included freezing the cutting action, imitational experiments, and to a lesser extent simulations or models of the wear processes. Samples generated by these experimental methods were studied using scanning electron microscopy, X-ray energy-dispersive spectroscopy, electron backscatter diffraction, ion channeling contrast, transmission electron microscopy, and X-ray diffraction.

The major tool wear mechanisms include diffusional dissolution and formation of reaction products that are either easily removed with the chip flow or that work as diffusion barriers. Additional chemical wear through oxidation may occur in milling operations. Tool coatings are subject to mechanical wear and also to some degree to diffusional dissolution. The combination of several titanium alloys including commercially pure titanium, near-α Ti-6Al-2Sn-4Zr-2Mo, α+β Ti-6Al-4V, α+β Ti-6Al-2Sn-4Zr-6Mo, and near-β Ti-5Al-5V-5Mo-3Cr, compacted graphite iron, and grey cast iron with tooling including polycrystalline diamond, polycrystalline cubic boron nitride, uncoated cemented carbide grades and coated versions including physical vapor deposition applied $Ti_{0.45}Al_{0.55}N$ with or without NbN overlayer and chemical vapor deposition applied Ti(C,N)-$Al_2O_3$ makes for many variants of reaction products, intensity of wear mechanisms, performance, and ways to decrease the wear rate.

**Keywords**: Machining, Tool wear, Wear mechanisms, Diffusion, Chemical wear.

# Populärvetenskaplig sammanfattning

Skärande bearbetning är en viktig men kostsam tillverkningsmetod. En kostnadsdrivare är användningen av skärverktyg som slits ned eller går sönder och behöver bytas. Grundläggande arbetsmaterial i de ekonomiskt viktiga bil- och flygindustrin inkluderar bland annat svårbearbetade titanlegeringar och kompaktgrafitjärn men även traditionellt gråjärn. Bearbetningen, avfallet som genereras samt produktionen av verktygs- och arbetsmaterial är energikrävande och deras hållbara utveckling behöver förbättras. Det kan uppnås genom förbättringar i maskinförhållanden och i verktygslösningar, men också genom utveckling av mer hållfasta och slittåliga verktyg. Då behövs kunskap om underliggande utslitningsmekanismer som bidrar till verktygsslitaget.

Målet med avhandlingen är att öka kunskapen om utslitningsmekanismer i vanliga skärverktyg vid bearbetning av dessa arbetsmaterial. Det görs genom att använda lämpliga experimentella metoder och karaktäriseringstekniker. Verktygsslitage skapas genom bearbetning av arbetsmaterialen i svarv- och fräsmaskiner. Fenomen vid gränsytan utforskas efter kontrollerade processvariationer, efter skapande av en stillbild av skärprocessen genom quick-stop-försök, efter imitationsexperiment och till en mindre del genom simuleringar och modeller av utslitningsprocesserna. Prover genererade genom dessa experiment studeras via djupgående mikroskopitekniker för att kunna identifiera utslitningsmekanismerna.

Höga processhastigheter som behövs i industriella verksamheter skapar höga processtemperaturer och relativ rörelse mellan spåna och verktyg. Då skapas förhållanden där huvudsakliga utslitningsmekanismer inkluderar diffusionsupplösning och skapande av reaktionsprodukter som antingen lätt avlägsnas med spånflödet eller som skyddar verktyget från slitage genom minskad diffusionshastighet. Vid fräsning tillkommer kemisk förslitning i form av oxidering som orsakar sprickbildning. Verktygsbeläggningar som applicerats för att öka verktygslivslängden slits mestadels mekaniskt genom sprickbildning men också till viss del genom diffusionsupplösning. Kunskapen om utslitningsmekanismerna gör att riktade insatser kan göras vid val av processparametrar eller vid val av verktygsmaterial som båda kan minska utslitningshastigheten. Kunskapen kan också användas vid utvecklingen av nya, mer slitstarka verktygsmaterial som bidrar till mer hållbara tillverkningsförhållanden.

**Nyckelord**: Skärande bearbetning, Verktygsförslitning, Utslitningsmekanismer, Diffusion, Kemisk förslitning.

# Appended publications

The thesis is based on the following publications which in the text are referred to with by their respective Roman numerals.

**I** **Performance and Wear Mechanisms of PCD and pcBN Cutting Tools during Machining Titanium Alloy Ti6Al4V**
R. Lindvall, F. Lenrick, H. Persson, R. M'Saoubi, J-E. Ståhl, and V. Bushlya
*Wear* **454–455** (2020) 203329
https://doi.org/10.1016/j.wear.2020.203329

**II** **Performance and Wear Mechanisms of Uncoated Cemented Carbide Cutting Tools in Ti6Al4V Machining**
R. Lindvall, F. Lenrick, R. M'Saoubi, J-E. Ståhl, and V. Bushlya
*Wear* **477** (2021) 203824
https://doi.org/10.1016/j.wear.2021.203824

**III** **On the Wear Mechanisms of Uncoated and Coated Carbide Tools in Milling Titanium Alloys**
R. Lindvall, J. M. Bello Bermejo, A. Bjerke, J. M. Andersson, E. Vikenadler, F. Lenrick, R. M'Saoubi, and V. Bushlya
*International Journal of Refractory Metals and Hard Materials* (2024) Submitted.

**IV** **Degradation of Multi-Layer CVD-Coated Cemented Carbide in Finish Milling Compacted Graphite Iron**
R. Lindvall, J. M. Bello Bermejo, B. Cámara Herrero, S. Sirén, L. Magnusson Åberg, S. Norgren, R. M'Saoubi, V. Bushlya, and J-E. Ståhl
*Wear* **522** (2023) 204724
https://doi.org/10.1016/j.wear.2023.204724

**V** **Wear Mechanisms in Ti(C,N)-$Al_2O_3$ Coated Carbide during Sustainable Machining CGI**
R. Lindvall, K. Monroe Diaz, R. Lin Peng, O. Gutnichenko, S. Sirén, L. Magnusson Åberg, S. Norgren, R. M'Saoubi, V. Bushlya, and
J-E. Ståhl
*International Journal of Refractory Metals and Hard Materials* **119** (2024) 106550
https://doi.org/10.1016/j.ijrmhm.2023.106550

**VI** **Effect of Ageing on Machining Performance of Grey Cast Iron and Its Compensation by Cutting Speed Management**

V. Bushlya, R. Lindvall, F. Lenrick, L. Magnusson Åberg, R. M'Saoubi, and J-E. Ståhl

*CIRP Annals Manufacturing Technology* (2024) Accepted.

**VII** **A Combined Experimental and Modelling Approach to Understand Chemical Wear in Titanium Turning**

A. Graves, R. Lindvall, A. Salmasi, W. Wan, C. Xiao, H. Larsson, V. Bushlya, M. Jackson, and S. Norgren

*The 15th World Conference on Titanium proceedings* (2024) In press.

**VIII** **Predicting Wear Mechanisms of Ultra-Hard Tooling in Machining Ti6Al4V by Diffusion Couples and Simulation**

R. Lindvall, A. Bjerke, A. Salmasi, F. Lenrick, R. M'Saoubi, J-E. Ståhl, and V. Bushlya

*Journal of the European Ceramic Society* **43**(2) (2023) 291–303 https://doi.org/10.1016/j.jeurceramsoc.2022.10.005

**IX** **On Wear of TiAlN Coated Tools with and Without NbN Overlayer in Machining Titanium Alloys**

R. Lindvall, F. Lenrick, J. M. Andersson, R. M'Saoubi, and V. Bushlya

*International Journal of Machine Tools and Manufacture* (2024) 104148 https://doi.org/10.1016/j.ijmachtools.2024.104148

**X** **Characterisation of Worn WC Tool using STEM-EDS Aided by Principal Component Analysis**

I. Lazar, R. Lindvall, F. Lenrick, V. Bushlya, and M. Ek

*Journal of Microscopy* **283**(1) (2021) 64–73 https://doi.org/10.1111/jmi.13009

**XI** **Assessment of Metal Cutting Tools using Cost Performance Ratio and Tool Life Analyses**

D. Johansson, R. Lindvall, C. Windmark, R. M'Saoubi, A. Can, V. Bushlya, and J-E. Ståhl

*Procedia Manufacturing* **38** (2019) 816–823 https://doi.org/10.1016/j.promfg.2020.01.114

# Author's contribution

**I** Lindvall was the main author and performed the majority of the experimental work and data analysis.

**II** Lindvall was the main author, performed the majority of the experimental work and data analysis, and presented the paper at the 23rd International Conference on Wear of Materials in April 2021.

**III** Lindvall was the main author, performed the majority of the experimental work in collaboration with Bello Bermejo, analyzed the results, and presented the paper at the 12th International Conference on the Science of Hard Materials in March 2024.

**IV** Lindvall was the main author, performed the majority of the experimental work in collaboration with Bello Bermejo and Cámara Herrero, analyzed the results, and presented the paper at the 24th International Conference on Wear of Materials in April 2023.

**V** Lindvall was the main author, performed the majority of the experimental work in collaboration with Diaz, and analyzed the results.

**VI** Lindvall performed parts of the experimental work, data analysis, and paper writing.

**VII** Lindvall performed parts of the experimental work, data analysis, and paper writing. Graves was the main author and presented the paper at the 15th World Conference on Titanium in June 2023.

**VIII** Lindvall was the main author and performed the majority of the experimental work. Bjerke and Salmasi performed the modeling and simulations and wrote parts of the paper.

**IX** Lindvall was the main author, performed the majority of the experimental work in collaboration with Bushlya, and analyzed the results.

**X** Lindvall performed the experimental work and Lazar analyzed the data and wrote the majority of the paper in collaboration with Ek.

**XI** Lindvall performed the experimental work and presented the paper at the 29th International Conference on Flexible Automation and Intelligent Manufacturing in June 2019. Johansson performed cost modeling and wrote major parts of the paper in collaboration with Windmark and Lindvall.

# Publications not appended to the thesis

The author contributed to the following papers, but they are beyond the scope of the thesis.

**xii** **Equivalent Chip Thickness and Its Influence on Tool Life**
D. Johansson, R. Lindvall, M. Fröström, V. Bushlya, and J-E. Ståhl
*Procedia Manufacturing* **25** (2018) 344–350
https://doi.org/10.1016/j.promfg.2018.06.102

**xiii** **A Machine Learning Based Approach for Determining the Stress-Strain Relation of Grey Cast Iron from Nanoindentation**
J. Weng, R. Lindvall, K. Zhuang, J-E. Ståhl, H. Ding, and J. Zhou
*Mechanics of Materials* **148** (2020) 103522
https://doi.org/10.1016/j.mechmat.2020.103522

**xiv** **Improvement of Tool Utilization when Hard Turning with cBN Tools at Varying Process Parameters**
O. Gutnichenko, M. Nilsson, R. Lindvall, V. Bushlya, and M. Andersson
*Wear* **477** (2021) 203900
https://doi.org/10.1016/j.wear.2021.203900

# Selected abbreviations and symbols

| | | |
|---|---|---|
| bcc | Body Centered Cubic | |
| CP | Commercially Pure | |
| CVD | Chemical Vapor Deposition | |
| EBSD | Electron Backscatter Diffraction | |
| fcc | Face Centered Cubic | |
| FIB | Focused Ion Beam | |
| HAADF | High Angle Annular Dark Field | |
| hcp | Hexagonal Close Packed | |
| HPDC | High Pressure Directed Coolant | |
| ICCI | Ion Channeling Contrast Imaging | |
| LAADF | Low Angle Annular Dark Field | |
| MQL | Minimum Quantity Lubrication | |
| PcBN | Polycrystalline Cubic Boron Nitride | |
| PCD | Polycrystalline Diamond | |
| PVD | Physical Vapor Deposition | |
| SAED | Selected Area Electron Diffraction | |
| SEM | Scanning Electron Microscopy | |
| STEM | Scanning Transmission Electron Microscopy | |
| TEM | Transmission Electron Microscopy | |
| VB | Flank wear | |
| XEDS | X-ray Energy-Dispersive Spectroscopy | |
| XRD | X-ray Diffraction | |
| $a_e$ | Width of cut | mm |
| $a_p$ | Depth of cut | mm |
| $f$ | Feed | mm/rev |
| $f_z$ | Feed per tooth | mm/tooth |
| $h_1$ | Equivalent chip thickness | mm |
| $v_c$ | Cutting speed | m/min |
| $v_{ch}$ | Chip speed | m/min |
| $r$ | Nose radius | mm |
| $r_\varepsilon$ | Edge radius | µm |
| $z$ | No inserts | - |
| α | Clearance angle | degree |
| γ | Rake angle | degree |
| vol.% | Volume percent | % |
| wt.% | Weight percent | % |

# 1 Introduction

In 2022, the total value of Swedish exports was 3,140 billion SEK, representing slightly more than half of the GNP [1]. Seventy percent of these exports were goods, many of them produced by the automotive and aeronautic industries, machine and workshop industry, and mining industries [2, 3]. All these industries use various methods to shape metallic components [4]. Shaping without losing volume can be done using deformation methods, and metals can be merged by melting processes such as welding or additive manufacturing. However, a key value-adding production process is machining, which is a subtractive process in which parts of the material are removed by the shearing action of a cutting tool. Machining can provide high-dimensional tolerance, surface finishes, and complex shapes that cannot be achieved using other methods [5, 6]. It has been estimated that some 80% of all manufactured parts require some machining [5].

In an attempt to reduce their footprint as the second largest source of $CO_2$ emissions globally, the automotive and aeronautical transport industries are working on sustainability by reducing their emissions and increasing their energy efficiency [7, 8]. Weight reductions can contribute significantly to lowering emissions, but reducing weight requires smarter design or replacement of currently used materials with materials that are as strong or stronger but with lighter weight [2]. In the automotive industry, compacted graphite iron (CGI) or austempered ductile iron (ADI) are advanced high–strength cast materials that are replacing conventional grey cast iron in many products, including the engine blocks and cylinder heads for diesel engines [9, 10]. This change will have a significant effect as ninety-seven percent of the Swedish truck fleet are registered as diesel powered, and this fleet will be slower to move away from fossil fuels than personal cars and buses [11]. Electrification and hybrid solutions are rapidly emerging technologies, and CGI is also a suitable material for the smaller engines in hybrids [12]. In the aerospace industry, aluminum and titanium alloys are established materials due to their lightness and strength, and composite materials are the latest addition [13]. Both CGI and Ti alloys are considered difficult-to-machine materials, and sustainable machining with efficient tooling solutions is needed.

The removal of metal by machining is done through the shearing action by a cutting tool. The process is energy intensive and creates high temperatures in the cutting tool and in the material being cut. The contact regions where the tool and the material meet is the focus of this thesis. It is here that high contact pressures, high

temperatures, and the relative motion of the workpiece material and the tool surface cause degradation of the cutting tool. The intensity of these factors affects how long a tool will last before it degrades to the point where it can no longer function efficiently to produce the surfaces or dimensions required, or where it poses a risk of damaging the part or the equipment.

In 2013, the market share for cutting tool materials was as follows: cemented carbide (53%), high-speed steel (20%), ceramics (8%), cermets (6%), polycrystalline diamond (PCD) (7%), and cubic boron nitride (cBN) (6%) [14]. More than half of the products using cemented carbide were related to metal cutting [15]. The global production of cemented carbide has grown steadily [15] since it was first patented in 1923 [16, 17]. The Swedish company Sandvik AB added cemented carbide products to their range of cutting tools in 1942, a move that has contributed to their status as a world market leader in metal cutting products and solutions today [18].

Cemented carbide consists of WC grains in a Co matrix, with WC providing wear resistance and Co providing impact resistance [15]. However, both W and Co are critical raw materials (CRMs), meaning that they are economically important and that there are risks associated with the raw material supply for the European Union [19]. Accordingly, such materials should be used efficiently in the many cutting tool materials or their coatings that contain CRMs [19, 20]. Attention should also be paid to the increasing supply risks posed by the emergence of electric vehicles with batteries containing CRMs, their health risks, and the ethical issues associated with their handling and mining [21–23].

## 1.1 Objective and hypotheses

Advanced materials with higher strength and lighter weight can contribute to reduced emissions and increased energy efficiency in the auto and aero industries. However, these materials are difficult to machine, adding to the already high energy consumption during machining as well as to tool wear rates and so tool material consumption. Moreover, the production of advanced materials and cutting tool materials is energy intensive, and the machining process generates waste in the form of chips and products that do not meet quality requirements. It is thus important to improve the sustainability of the machining process. Much work has already been done to improve machining conditions and tooling solutions. The work includes matters like the development of lubrication and cooling technologies, tooling geometries, tool materials and their grades, coating technology, and optimization of tool paths and cutting data. All of this work can be done without in-depth knowledge of the underlying causes of tool material failure.

The next step in improving machining sustainability and tooling efficiency involves more in-depth exploration of active tool wear mechanisms in order to select suitable

tool (and coating) materials for machining applications and to develop new, more wear-resistant tool materials. The objective of this thesis is to expand knowledge of active wear mechanisms in cutting tools, of how these are manifested as phenomena observable at the interface between tool and workpiece material, and of the driving forces that govern their intensity. This will contribute to more precise control of the wear processes and to tool material development.

The hypothesis for this work is that reducing the wear and degradation of cutting tools used in machining can be successfully achieved based on knowledge of wear mechanisms and related phenomena. At the same time, experimental and characterization techniques can be identified and selected such that wear phenomena across the tool-chip/workpiece interfaces are captured adequately. This information can serve as a prerequisite for an increased understanding and knowledge on active tool wear mechanisms and their combination across multiple length scales.

## 1.2 Research questions

Three research questions were formulated:

1. Which experimental and characterization techniques can be used to adequately capture wear mechanisms and related phenomena across tool-chip/workpiece interfaces?
2. How can knowledge about individual wear mechanisms and their combination across multiple length scales be brought together to describe tool wear?
3. How do the identified wear mechanisms and reaction products contribute to the wear rate and tooling performance and what can be done to reduce the wear rate?

## 1.3 Methodology

In the machining of a workpiece material where the metal or alloy is sheared off and removed by a cutting tool, the active processes of degradation of the tool material occur in the tool-chip/workpiece contact region. In turning and milling processes, this contact region is shielded by the chip on the tool rake face and by the workpiece material on the flank side. As the cutting proceeds, the tool morphology and microgeometry gradually change due to tool wear. However, it is not yet possible to follow these changes *in-operando* along with the cutting action. An ideal experimental situation would involve simultaneous studies of atomic movements,

the formation and development of reaction products and diffusion paths at the nano or atomic scale at the interface, and the evolution of morphology and mechanically induced cracks or other damage at a micrometer scale. This is not yet possible, and the actual wear mechanisms that occur during machining can be represented by a black box (Fig. 1).

Currently, researchers have to combine different experimental methods that each in their own way resemble the active wear mechanisms in machining. By combining them it is possible to draw conclusions about the probability of observed wear phenomena actually occurring in machining. The limitations, differences, and formation of artifacts in the methods need to be understood to be able to make realistic correlations with the actual wear mechanisms in machining. A proper combination of experiments can become a powerful way to understand the active processes in tool wear, and Fig. 1 shows some identified methods.

A common approach is to study as-worn tools with varying levels of wear. Parameters like cutting data, tool and holder geometries, environments, and tool and workpiece materials can be varied, which then alters temperature, pressure, and sliding conditions. In this study, this type of experiment is called a controlled variability experiment. A negative aspect of studying as-worn tools is that the cutting depth or contact width is gradually reduced as the tool disengages, which slightly alters the conditions that previously operated on the cutting tool. As the tool cools after disengagement, some phases may change and may thus not resemble those present during machining. Another less common option is process freezing experiments that provide a way to examine the tool-chip/workpiece wear interface. Such experiments can be done using the quick stop method, which gives a freeze-frame of the cutting process [24–26].

Imitational experiments are another method of studying wear mechanisms. The diffusion couple method is gradually increasing in popularity and may become the new standard for examining diffusional and chemical wear mechanisms [27–34]. There are also other types of imitational experiments including tribo-tests such as pin-on-disk tests [35–38], sliding or adhesion tests [39–43], and oxidation tests [44–46]. These are easily quantifiable, reproducible, and can be done in a safe environment. However, the extent to which they represent the actual wear processes and mechanisms needs to be analyzed. Wear mechanisms can also be studied using modeling and simulations of the wear processes at the interface [47–50].

However, even this broad scope of tests and analysis does not reveal all wear phenomena and their progress, and there is scope for more approaches to studying wear mechanisms (Fig. 1). In this work, a combination of methods is used to study wear mechanisms. These include studies of as-worn tools and their cross-sections in controlled variability experiments, process freezing experiments using the quick stop method, imitational experiments using diffusion couples, and thermodynamic modeling and diffusion simulations. Samples are studied using a range of

microscopy techniques that capture wear phenomena in different ways and at different scales. These approaches complement each other, resulting in a wider understanding of the wear mechanisms present.

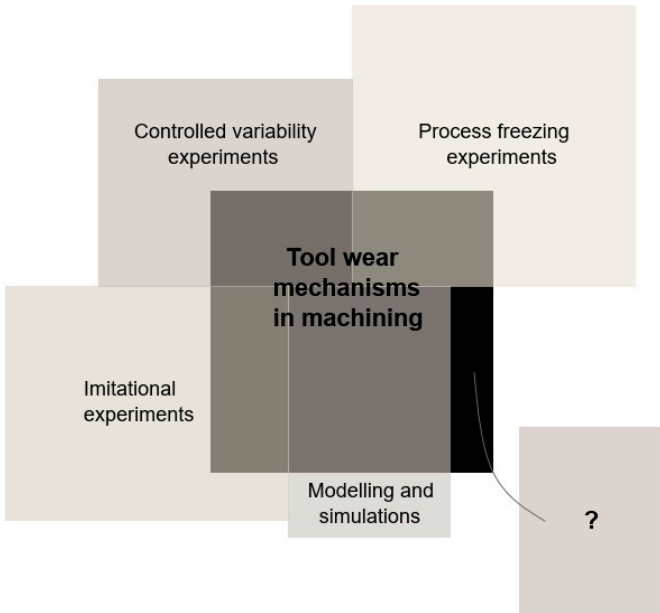


**Fig. 1** Venn diagram of methods that contribute to the understanding of active wear mechanisms in machining [**IX**].

The work is primarily deductive with initial literature studies that provided information on the current state of tooling performance and its evolution and identified, or suggested, wear mechanisms. However, the research reported in this thesis did not set out to replicate previous studies to check their validity. Instead, performance tests were done with industrially relevant environmental and cutting data, bearing in mind the importance of industrial usability. The evaluation of performance and the exploration of the mechanisms that are the underlying cause of the observed tool wear morphology and tool performance involve deductive reasoning. The approach of successively narrowing the scale in the samples prepared and the microscopy investigations allows exploration and tracing of wear mechanisms.

The exploration of wear mechanisms also falls within a qualitative framework. It is challenging to quantify how much each identified wear mechanism contributes to the overall wear of the tool, and this work does not intend to do so. The qualitative way of identifying wear mechanisms is based on the overall information gathered with the different methods in Fig. 1 together with the range of microscopy

techniques that combine to give a picture of the wear mechanisms present. However, when evaluating the performance of tools in machining, quantitative measures were used to find the tool life at a predefined wear criterion using the respective ISO standards for tool wear monitoring.

## 1.4 Scope and limitations

The scope of this work includes the exploration of active wear mechanisms in commercial cutting tools (uncoated and coated cemented carbide, PCD, and pcBN) used in industrially relevant machining operations (turning and milling) of difficult-to-cut and economically important materials (Ti alloys, CGI, and GCI). The range of microscopy techniques used to characterize the wear mechanisms includes light optical microscopy, scanning electron microscopy, X-ray energy-dispersive spectroscopy, electron backscatter diffraction, ion channeling contrast imaging, transmission electron microscopy, and X-ray diffraction.

Tooling performance was evaluated using ISO standards for tool life testing, and the wear mechanisms were linked to the wear rate. This work is limited to wear mechanisms observable using the above microscopy techniques and by the available methods for observing the tool-chip/workpiece interface, including as-worn tools and tools attached to the workpiece after quick stop tests, their cross-sections, and diffusion couples. Other complementary methods like electron energy loss spectroscopy (EELS), atom probe tomography (APT), and neutron or synchrotron sources could also be used to characterize tool wear mechanisms, but these fall outside the scope of this work.

Tool wear during machining is here limited to a laboratory environment. The cutting operations are limited to continuous turning and down face and external circular milling, mostly at finishing conditions in order to be economic in workpiece material consumption. Cutting data and cooling conditions are limited to recommendations by tool manufacturers. Variations in workpiece and tooling material quality were not the primary focus of the work, although these can play a role in the wear rate due to varying microstructural and material properties.

The study is limited to commercial tool and coating grades and geometries. Tool life testing was limited to a maximum of two repeats due to the long test times and the need to be economical in material use. Different cutting data parameters were used when evaluating cost performance. For in-depth transmission electron microscopy based investigations, a maximum of four lamellae a few μm in size and <200 nm thickness were studied per investigated tool and workpiece material system. Such small samples may not represent the full wear region and may not capture all wear phenomena, but they still offer in-depth insight that yield valuable information on some of the active wear mechanisms.

# 2 Machining

Machining is a value-adding material shaping process that is economically important in industrialized countries [6]. It is a subtractive process that includes turning, milling, drilling and other cutting operations [51]. In this research, I have focused on longitudinal turning, down face milling, and external circular milling. Metal cutting allows for great variability, as almost all metals or alloys can be machined. Complicated shapes are achievable, and sizes can range from watch parts to aircraft wing spars. High precision is possible. As cutting speeds can vary from more than 1000 m/min to less than 0.01 m/min, the cutting time can range from several hours to a fraction of a second [6, 51]. Metal cutting is directly or indirectly related to other manufacturing processes such as the making of dies for sheet metal forming [6, 51]. Annual investment in metal machining has been approximately three times the investment in metal forming, despite improvements in replacement materials and near-net shape processes [51]. International competition creates a need for higher productivity, which requires advances in tooling for high speed machining [6].

## 2.1 Longitudinal continuous turning

The longitudinal turning process is displayed in Fig. 2. The workpiece is clamped on one side with a chuck that provides the rotational speed and torque to the workpiece, while the other end can be supported by a tailstock (Fig. 2a). The diameter of the workpiece and the rotational speed give the cutting speed $v_c$, expressed in m/min, at which the material approaches the cutting tool surface, while the evacuated chip has another, lower, speed, $v_{ch}$ (Fig. 2b). The cutting tool mounted in the tool holder moves radially towards the workpiece material to a specified diameter. This radial ingress is the cutting depth $a_p$, expressed in mm (Fig. 2c). The tool holder moves along the axis of the workpiece at a feed rate $f$ in mm/rev and removes material in the form of chips (Fig. 2c). The cutting depth and the feed in combination with the major cutting edge angle $\kappa$ give the contact area of the cutting tool, which is marked in blue in Fig. 2c. The major cutting edge angle together with the feed rate gives the theoretical chip thickness $h_1$, expressed in mm (Fig. 2c). The nose radius $r$ in mm and the feed rate generate the theoretical surface roughness in µm (Fig. 2c). The material removal rate is used to assess efficiency. It is calculated

by multiplying the depth of cut, feed, and cutting speed [6]. Chip removal induces a force acting on the tool that can be divided into three orthogonal cutting force components. These are in the cutting speed direction, the feed direction, and the cutting depth direction. The forces are called the main cutting force $F_c$, the feed force $F_f$, and the passive force $F_p$ respectively (Fig. 2c).

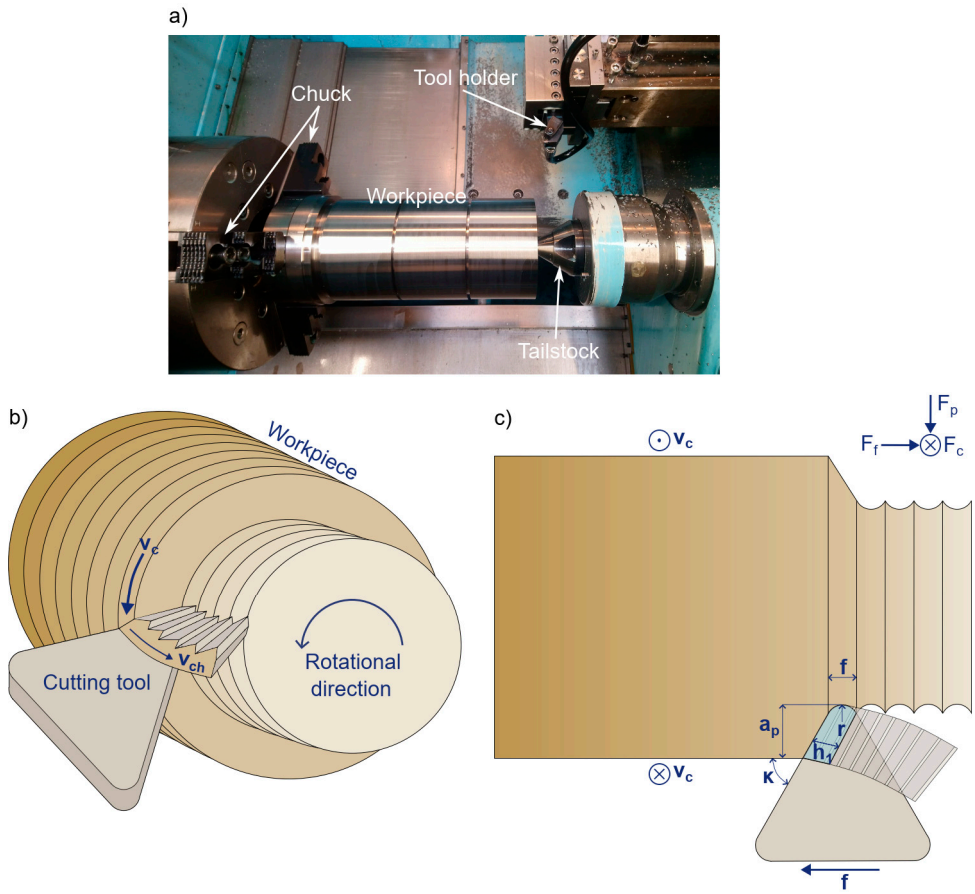


**Fig. 2** (a) Machine setup for longitudinal turning in an SMT 500 Swedturn lathe. (b) Illustration of the turning process in 2.5D and in (c) 2D showing the cutting parameters.

Fig. 3 shows the cross-sectioned turning process and a magnified view of the cutting zone. The cross-sectioned cutting zone shows the cutting speed and chip speed, the feed direction, and the theoretical chip thickness, as well as the edge radius $r_\beta$ of the cutting tool, the clearance angle α, and the rake angle γ. The clearance angle prevents the flank side of the tool from rubbing against the freshly cut surface. The rake angle is adjusted for optimal cutting performance and chip evacuation. Tools with a highly positive rake angle in combination with a small edge radius and nose radius are mechanically weaker.

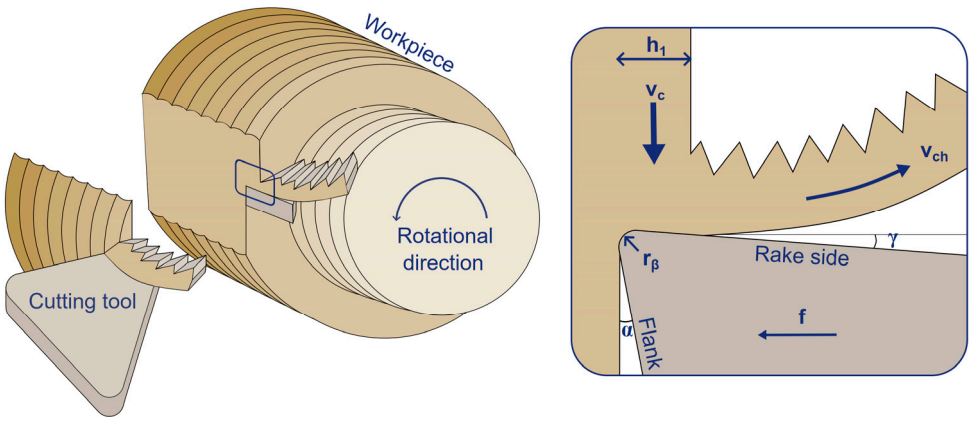


**Fig. 3** Illustrations of the cross-sectioned turning process and the cutting parameters [**IX**].

## 2.2 Down face milling

A milling process is generally more complex than a turning process as it is intermittent due to the cyclic engagement and exit of the tool. The work reported in this thesis employed down face milling, as shown in Fig. 4. Such operations are common when machining items like cylinder blocks [6]. One or more cutting tools are mounted in a milling cutter that rotates around its own axis, and so the material is removed in an arc shape as the cutter moves along the clamped workpiece material at a given feed rate $f$ in mm/min. This feed rate is divided by the number of cutting tools mounted $z$ (each cutting edge is called a tooth) and thus each milling cutter has its own feed per tooth $f_z$ expressed in mm/tooth. The cutting width is given by $a_e$ in mm, and its maximum is given by the diameter of the cutter. The cutting depth is given by $a_p$ in mm. Together with the feed per tooth $f_z$ the cutting width and depth give the volume removed per revolution of the tool edge. The rotational speed and diameter of the milling cutter give the cutting speed $v_c$ in m/min, and the evacuated chip has a chip speed $v_{ch}$. The periodic engagement of the teeth in the workpiece material give rise to thermal and mechanical cycling stresses [6].

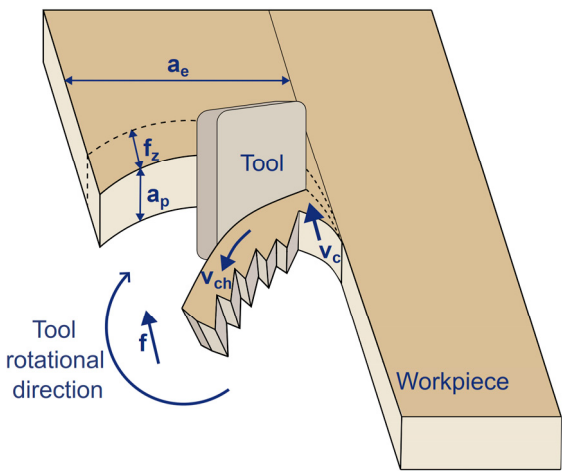


**Fig. 4** Illustration of the down face milling process and the cutting parameters.

## 2.3 External circular milling

Another milling method employed in this research is external circular milling. Fig. 5 shows a cylindrical workpiece clamped on the table of the machining center. The mill head rotates around its own axis and simultaneously moves around the workpiece diameter. This method was employed to make efficient use of the workpiece material supplied as cylindrical bars. Fig. 5 also illustrates the cutting parameters of feed per tooth $f_z$, cutting width $a_e$, cutting depth $a_p$, and how the diameter is reduced per workpiece revolution. In this test, the milling cutter was moved down along the workpiece axis to maintain the correct cutting depth in the next pass. The diameter of the workpiece, the diameter of the milling cutter, the selected cutting width $a_e$, and the feed per tooth $f_z$ determine the engagement angle Θ. However, the efficient contact width on the rake face $h_{1max}$ of the tool will be smaller than $f_z$ in the case applicable to this work, shown in Fig. 5.

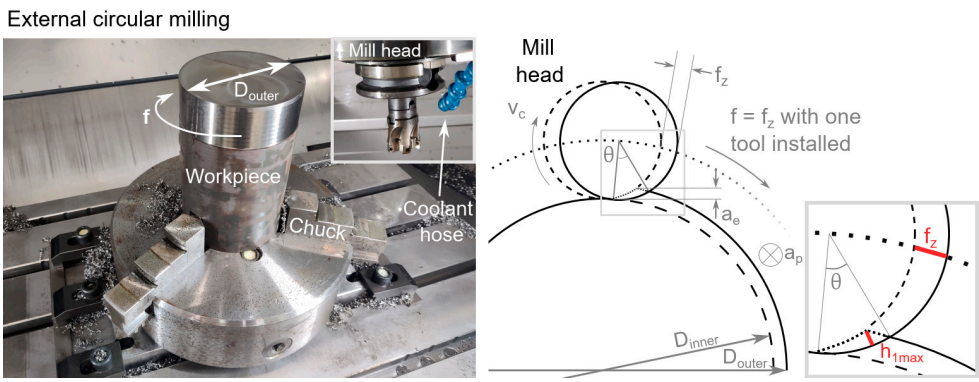


**Fig. 5** The external circular milling setup in a Mori Seiki SV 500 CNC mill and an illustration of the process with cutting data [**III**].

## 2.4 Quick stop in turning

The quick stop method can be employed to study material deformation in the cutting zone and the contact between cutting tool, chip, and workpiece material during a machining operation. The basic procedure of the quick stop method for a turning operation is presented in Fig. 6. The tool is engaged in the workpiece during turning until an impact rapidly disengages the tool holder. The supporting shear pin that the tool holder is resting on breaks and the tool holder is rotated around its pivot point. The impact must generate a movement of the tool holder to a speed greater than the cutting speed [51]. This is done by accelerating an impactor by a gunpowder charge in a gun. As a result, a frozen cutting process is obtained in the form of a, so called,

chip root, preserving the mechanics of chip formation. Sometimes, it is just as important to preserve the tool-chip/workpiece interface as well. This can be done by artificially introducing a weakness in the cutting tool by cutting a slot with a diamond disc in the rake of the tool outside the contact area so that the tool edge can break during cutting. Due to adhesive forces on the tool, the broken off tool edge can stick to the cutting zone in the workpiece material after impact. The contact regions between cutting tool, chip, and workpiece material can then be studied in a view like the right hand illustration in Fig. 3. While dynamic information is lost by freezing the action, microscopic detail is gained [6, 51].

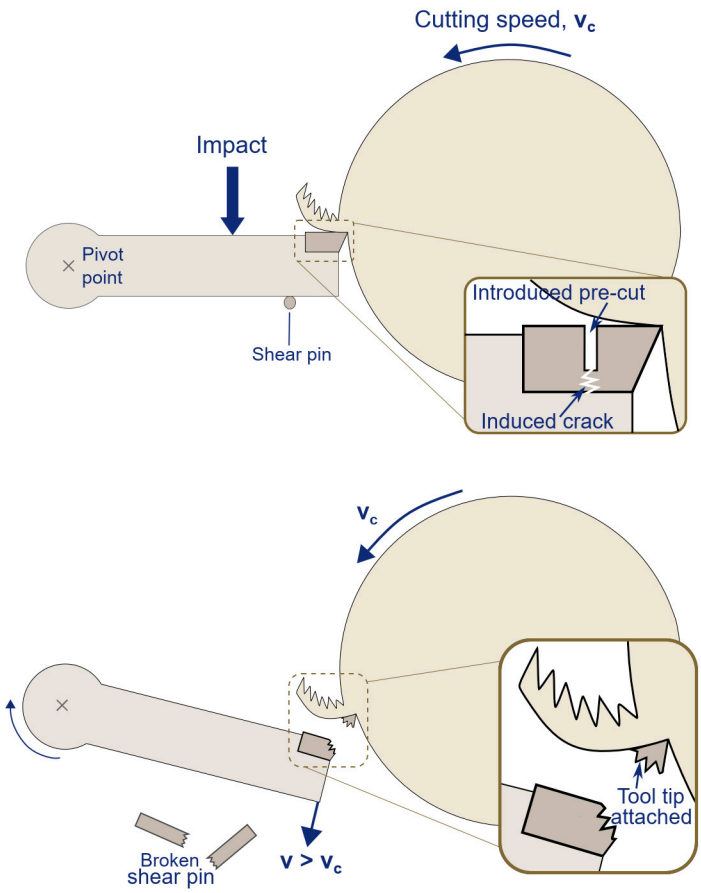


**Fig. 6** Illustration of the quick stop process in turning [**IX**].

## 2.5 Deformation and temperature

During a metal cutting operation, the material is either plastically deformed and sheared off or removed through brittle fracture. Plastic shearing is common in the machining of Ti alloys, while brittle fracture is more common in machining cast irons. Either deformation process requires large amounts of energy [6], while the rest of the mechanical work is related to the friction between the tool rake and chip [52]. Three deformation zones are present: the primary ($\varepsilon_I$), secondary ($\varepsilon_{II}$), and tertiary deformation zones ($\varepsilon_{III}$) as illustrated in Fig. 7a–b. The primary shear zone requires the majority of the work and the temperature becomes locally higher there [52]. Additional plastic work is done in the secondary and tertiary deformation zones [52]. The chip starts to form on the rake side of the stagnation zone (Fig. 7b) which is where the workpiece material flow approaches zero velocity. Chip segments like the ones shown in Fig. 7a cause an uneven loading cycle on the cutting tool [6] and are common when machining Ti alloys.

The plastic deformation of workpiece material causes high cutting temperatures. Some 70–85% of the work can dissipate as heat [52]. Increasing the cutting speed increases the cutting temperature as more energy is consumed in shearing off chips per unit of time [52]. The heat conducted into the tool depends on the thermal conductivity of both the tool and the workpiece material [52]. Knowledge about tool edge temperatures is valuable for predicting the formation of reaction products or phase transformations when studying tool wear mechanisms. However, measurement of tool edge temperatures can be challenging [53]. Common methods include measurement of the temperature on the side of a tool with infrared thermography or with thermocouples embedded within the tool body, as well as using models and simulations [54, 55]. The first two methods can only measure the temperature some distance from the cutting zone, and extrapolation is needed to determine the actual tool edge temperature [56]. Titanium alloys have a low thermal conductivity that combined with a short contact width, results in high tool edge temperatures of up to 900–1100 °C [57–60] like those shown in Fig. 7c.

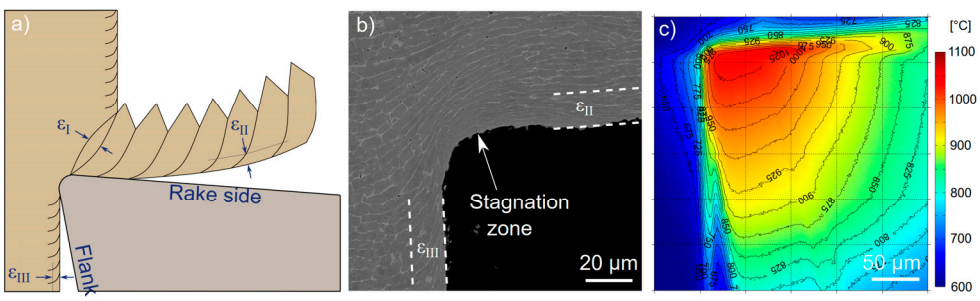


**Fig. 7** (a) Illustration and (b) example of deformation zones. (c) Tool temperature distribution [**I**].

## 2.6 Conclusions

This section has introduced subtractive metal cutting processes and the cutting parameters employed in this work. The methods include longitudinal turning, down face milling, and external circular milling. This work thus includes both continuous and intermittent cutting processes. A freeze-frame of the cutting process in turning can be achieved by using the quick stop method, which requires altering the tool if the tool-chip/workpiece contact is to be maintained. The processes of deformation and chip formation were introduced, as well as the temperature generated in the cutting tool and its effect on tool wear. Knowledge on the cutting process and environment that the cutting tool has been subjected to is important when analyzing the active tool wear mechanisms and relation to the tool cutting performance.

# 3 Materials

During the last century, higher machining rates and productivity were enabled by the introduction of high-speed steel and cemented carbide cutting tool materials that replaced the previously standard technology of carbon steel. The subsequent introduction of ceramics and ultra-hard tool materials (PCD and pcBN) has further contributed to increased productivity. At the same time, a vast number of new workpiece materials have been developed to meet the higher demands of stress, temperature, and corrosion resistance that are now required in industry. The improved material properties have made some of these alloys more difficult to machine than their traditional counterparts, and so increased the need for improved tool wear resistance [6, 61].

## 3.1 Tool materials

Cutting tools are used over a wide range of cutting conditions and it can be difficult to find cutting tool material specifications that suit the whole range. Some cutting tool materials may perform well in some conditions but worse in others, which is one reason for developing different grades and varieties of tool materials. The physical and metallurgical requirements of a cutting tool material include a high yield strength at elevated temperatures, hardness, fracture toughness, wear and fatigue resistance, thermal conductivity, thermal shock resistance, and low reactivity with the workpiece material and atmosphere [61].

### 3.1.1 Cemented carbide

Cemented carbide is produced through powder metallurgy by sintering hard and wear-resistant WC grains of micrometer size (0.2–10 μm) with a softer and ductile Co binder matrix (commonly 4–15 wt.% for metal cutting), which results in a unique combination of hardness and toughness [6, 15]. Other hard phases such as TiC, TaC, and NbC can be introduced to further strengthen the material; these grades are suited for machining steel [6, 15, 51]. Because WC has a hexagonal crystal structure that does not undergo structural transformations up to its melting point, which is 2750 °C [6, 62], heat treatment of WC does not alter its properties. While the hardness decreases with increased temperatures, it still exceeds that of steel [6, 62]. Small

fractions of Cr added to the Co binder inhibits grain growth during sintering [51, 62]. At temperatures below 417 °C, Co has a hexagonal crystal structure and the face centered cubic structure above, and a face centered cubic above. The fcc crystal structure is retained after sintering [15, 62].

A wide variety of microstructures and mechanical properties can be achieved by adjusting the composition and grain size of the hard phase(s), the binder material and its volume, and the production process parameters [15, 62]. Increased Co content reduces the hardness and compressive strength but increases the ability to resist fracture, while a finer WC grain size increases the hardness of the cemented carbide [6, 15, 51]. A grade with 6 wt.% Co and 2 µm WC suits the majority of applications [6, 62]. This study includes the cemented carbide microstructures displayed in Fig. 8 with WC-Co grades with fine grain size and 6 wt.% Co (Fig. 8a) or 12 wt.% Co (Fig. 8b), a coarse grain size with 15 wt.% Co (Fig. 8c), and a mixed substrate grade with fine grain size and 85.3 vol.% WC, 2.0 vol.% (Ta,Nb,W)C, and 12.7 vol.% (7.8 wt.%) Co binder (Fig. 8d).

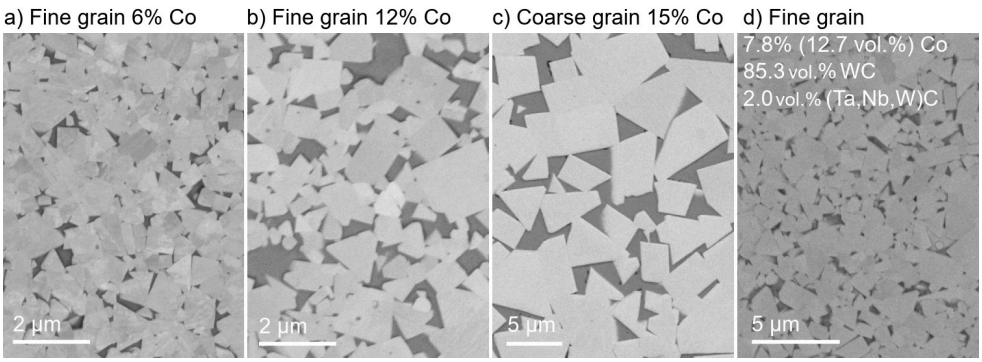


**Fig. 8** SEM-BSE microstructure images of cemented carbide grades. (a) Fine grain size and 6 wt.% Co binder [**II**, **VII**, **X**, **XI**]. (b) Fine grain size and 12 wt.% Co binder [**III**]. (c) Coarse grain size and 15 wt.% Co binder [**VIII**]. (d) Mixed substrate grade with fine grain size and 85.3 vol.% WC, 2.0 vol.% (Ta,Nb,W)C, and 12.7 vol.% (7.8 wt.%) Co binder [**IV**, **V**].

#### *3.1.1.1 Coatings*

Cemented carbide tools can be coated with a hard and wear-resistant coating to extend the tool life [51]. In this way, the bulk cemented carbide is optimized to resist failure and the surface is optimized to resist wear [51]. The coating should ideally also reduce friction and not only supply improved wear resistance but also resistance to oxidation. It should have thermal shock resistance, and the integrity of the coating needs to be stable during the cutting operation [63]. About 80% of cemented carbides for machining are coated [14, 51]. It is common to apply one or more layers of coating, combining different coating materials with specific characteristics [6, 63]. Coatings for cutting tools are commonly applied by chemical vapor deposition (CVD) or physical vapor deposition (PVD) techniques [6].

The CVD technique applies coatings of about 4–12 µm thickness [6, 51, 52]. Common materials are TiN, Ti(C,N), and $Al_2O_3$ [6, 14]. $Al_2O_3$ is usually applied on Ti(C,N) base layers. α-$Al_2O_3$ in the 001 orientation or texturing has shown superior cutting performance and wear resistance compared to other orientations [14, 64]. The CVD process involves heating the tools to about 800–1050 °C in a sealed chamber with a flow of hydrogen gas [6, 51, 52]. Gases that contain the coating elements are circulated in the chamber to form the ceramic coating with a fine grain size and equiaxed grains [6, 51, 52]. The thermal expansion coefficient is generally greater for the coated material than for the substrate, which introduces cracks and tensile stresses in the coating upon cooling [6, 51].

In the PVD process, ionized metal atoms are attracted to the tool by high voltage on the tool surface in the presence of low pressure gas containing nitrogen, carbon, or oxygen [6, 51, 63]. This process can be done at 500 °C or lower [6, 51] which results in lower residual stresses in the tool coating and less or no cracking compared to CVD-applied coatings [6]. PVD-applied coatings are normally thinner than CVD-applied coatings [65]. $Ti_{1-x}Al_xN$ (x = 0.4–0.7) is a common coating material for cutting tools and has an fcc crystal structure. However, it can undergo spinodal decomposition above 800 °C into fcc TiN and fcc AlN [51, 64]. Fig. 9 shows the microstructure of the coatings utilized in this work including PVD-applied $Ti_{0.45}Al_{0.55}N$ (Fig. 9a) and $Ti_{0.45}Al_{0.55}N$-NbN (Fig. 9b), and CVD-applied Ti(C,N)-$Al_2O_3$ (Fig. 9c).

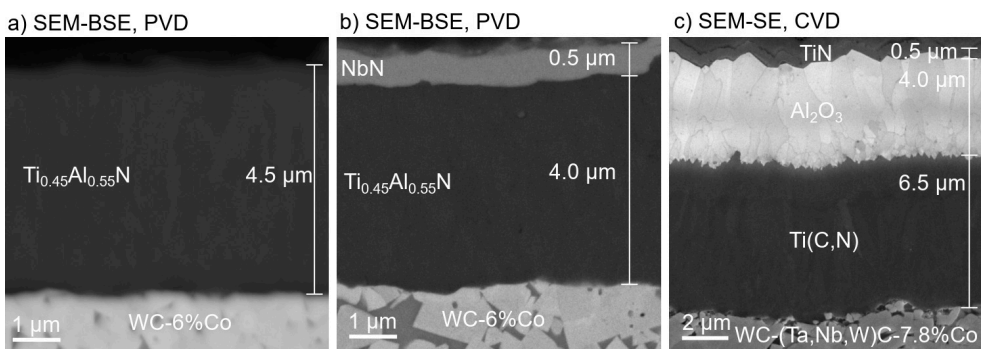


**Fig. 9** SEM microstructure images of coatings. (a) PVD-applied $Ti_{0.45}Al_{0.55}N$ on WC-6%Co using the BSE-detector [**IX**]. (b) PVD-applied $Ti_{0.45}Al_{0.55}N$-NbN on WC-6%Co or WC-12%Co using the BSE-detector [**III**, **IX**]. (c) CVD-applied Ti(C,N)-$Al_2O_3$-TiN on WC-(Ta,Nb,W)C-7.8%Co using the SE-detector [**IV**, **V**].

### 3.1.2 Polycrystalline diamond (PCD)

Polycrystalline diamond (PCD) tools consist of synthetic 2–25 µm-sized diamond grains that are surrounded by a metallic binder, commonly Co [6, 20, 51, 66]. Synthetic diamond consolidation is done at high pressure and temperature (HP-HT) [6, 20]. During densification, the Co melts and surrounds the diamond grains, stimulating the formation of diamond-diamond bonds [20]. Due to the high cost of PCD, cutting tools are rarely made of solid PCD. Instead an effective tip of PCD is bonded to a cemented carbide substrate [6, 20, 67]. The price of PCD tools is about ten to twenty times that of cemented carbide, which restricts its use to operations where other tool materials are not as efficient [6, 20]. PCD tools generally have a lower wear rate in abrasive environments due to their high hardness. This abrasion resistance increases with diamond grain size. A smaller grain size improves the edge quality and thus positively affects the surface roughness of the machined part [6, 20, 67]. Diamond is metastable and converts to graphite at approximately 600 °C in air [66].

PCD tools are commonly used in machining aluminum and aluminum-silicon casting alloys, copper and its alloys, cemented carbide in pre- and post-sintered state, as well as abrasive non-metallic materials like carbon fiber reinforced plastics [6, 67, 68]. PCD is not suited to machining iron-based materials as diamond is dissolved by iron at high temperatures [6, 51, 68]. The thermal conductivity of PCD is about five times higher than that of WC and cBN, which leads to lower heat accumulation at the tool-chip/workpiece interface during machining [20]. Commercial PCD with the microstructure presented in Fig. 10a displays a multimodal grain size distribution with 12 wt.% Co binder. Fig. 10b shows another type of fine grained PCD with 17 wt.% Co binder.

### 3.1.3 Polycrystalline cubic boron nitride (pcBN)

Cubic boron nitride (cBN) is the second hardest material after diamond [6]. It has a face-centered cubic crystal structure with boron and nitrogen each filling one face-centered set [6]. cBN is not found in nature and is synthesized and consolidated at HP-HT conditions. Densification is done with a metallic or ceramic binder to form polycrystalline cBN (pcBN) [6, 51]. Like PCD, pcBN is expensive, and thus only an effective tool tip is bonded to a cemented carbide substrate. However, solid pcBN inserts are also available [6, 68]. The cost of pcBN tools is about five to ten times that of cemented carbide [6]. Compared to diamond-based tools, cBN shows improved stability at high temperatures such as 1000 °C in air or in contact with iron and other metals. It reacts slowly with steel at such high temperatures [6]. PcBN tools are therefore used in machining hardened steel, superalloys, and hard cast irons at high speeds that make their use economic despite their high cost [6, 67, 68]. Fig. 10c shows a commercial pcBN tool material with fine grain size and 15 wt.%

metallic binder consisting of several phases mainly containing Al, Ti, Cr, Ni, Mo, Co, and W that was used in this work. Another pcBN coarse-grain grade with 10 wt.% binder of AlN and $AlB_2$ shown in Fig. 10d was also employed.

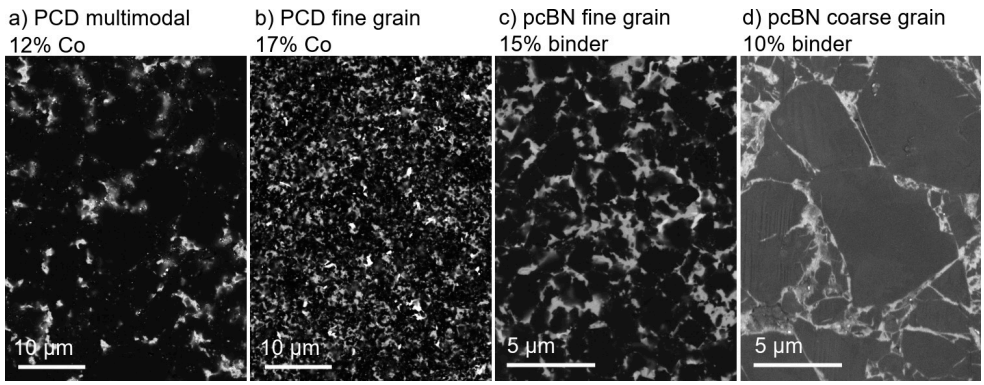


**Fig. 10** SEM-BSE microstructure images of PCD and pcBN grades. (a) PCD with multimodal grain size distribution and 12 wt.% Co binder [**I**, **VIII**, **XI**]. (b) PCD with fine grain size and 17 wt.% Co binder [**I**]. (c) pcBN with fine grain size and 15 wt.% metallic binder [**I**, **VIII**]. (d) pcBN with coarse grain size and 10 wt.% AlN and $AlB_2$ binder [**VI**].

## 3.2 Workpiece materials and their machinability

The two groups of workpiece materials studied are titanium alloys and cast irons, including compacted graphite iron and grey cast iron. Titanium alloys and compacted graphite iron can be considered difficult to machine. Machinability can be defined as *"the property of a material which governs the ease or difficulty with which a material can be machined using a cutting tool"* [61]. This definition is very broad, and can carry different meanings in different specialist contexts. There is no one generally accepted parameter to measure machinability, and attempts to define it focus on parameters like tool life, wear rate, energy consumption, or surface finish [61].

### 3.2.1 Titanium alloys

Titanium alloys were introduced in the 1950s and are thus relatively new engineering materials [9, 69, 70]. They have gained popularity due to their high strength-to-weight ratio, high corrosion resistance in air, marine, and many industrial environments, low thermal conductivity, and low thermal expansion [9, 69, 70]. These properties make Ti alloys suitable for use in the aerospace, automotive, chemical, and medical industries [9, 70, 71]. A negative aspect of

titanium is its high chemical affinity to other materials at elevated temperatures. This results in high tool wear rates when machining titanium. It also means that titanium alloys require nonconventional refining, melting, and casting techniques, which contribute to their high cost [9, 70, 72].

Titanium has a high melting point (1668 °C) and exists in the hcp α-phase up to 882 °C, above which it attains the bcc β-phase [6, 69]. The β-transus temperature can be adjusted by adding alloying elements that stabilize either phase. Al is an important α-stabilizer and solid-solution strengthener that also reduces the density of the alloy [69, 70]. β-stabilizers include β-isomorphous Mo, V, and Nb that have complete solubility in the β-phase and limited solubility in α [69, 70]. There are also β-eutectoid stabilizers like Cr and Fe [69, 70]. Titanium accepts interstitial solutes like the α-stabilizers C, N, and O, and β-stabilizer H [69]. The hcp α-phase has eight slip planes while the bcc β-phase has twelve [70], which improves forgeability and increases adhesiveness in β-alloys.

The wide range of Ti alloys are classified according to the phases in the microstructure and include commercially pure (CP) α-alloys, near-α alloys, α+β alloys, near-β alloys, and β-alloys [69, 70]. Oxygen is the main alloying element in CP-Ti in which the only phase present is α, while near-α alloys have a small fraction of β-phase [70]. CP-Ti has lower strength than other Ti alloys but is preferred for its corrosion resistance and creep resistance at elevated temperatures [70]. The α+β alloys are probably the most widely used as they exhibit good formability but lower creep resistance and weldability than the α-alloys. Among these, Ti6Al4V (Ti-64) is the most versatile [69–71]. The β-alloys have high strength due to fine α-phased precipitates in the β-structure and offer a unique combination of fracture toughness, high strength, deep hardenability, and simpler processing [69–71]. However, the same properties give β-alloys a reduced machinability, and the large amounts of β-stabilizers makes them heavier than the α+β alloys. They are also prone to embrittlement [70–72]. Near-β alloys like Ti-5Al-5V-5Mo-3Cr (Ti-5553) are replacing conventional α+β alloy Ti-64 in some critical aeronautic applications [71].

The material properties that make titanium alloys popular in combination with the high chemical affinity of Ti, make them difficult to machine. The high tool temperature generated during machining due to the low thermal conductivity of Ti alloys drives tool wear. About 80% of the generated heat is conducted to the tool when machining Ti-64. Tool temperatures as high as 730–1100 °C have been reported at cutting speeds ranging up to 200 m/min. Machining titanium alloys is also associated with a smaller contact width on the rake face compared to cutting Fe or Ni based alloys, which results in higher compressive stresses on the tool. The low elastic modulus causes workpiece deflection, vibration, and chatter. The chips are commonly segmented with shear localization in a narrow band, which results in variations in chip thickness on the active rake contact area and a cyclic load distribution. [6, 72]

The traditional approach to coping with the poor machinability of titanium alloys has been to use low cutting speeds and cutting fluids to reduce the cutting edge temperature, and a high feed rate and depth of cut to increase the naturally narrow contact zone. Cutting fluids, preferably involving water-soluble oil, rather than oil, applied at high pressure, have been shown to increase tool life when machining Ti alloys as they effectively penetrate the tool-chip interface and thus decrease the cutting temperature [72]. A further option is to use a tool material that has high thermal conductivity and so can dissipate much of the generated heat. Cemented carbide grades containing TiC wear more rapidly than straight grades of WC-Co because the Ti in mixed-crystal carbides diffuses faster into titanium alloy chips than WC does. The recommended cutting tool materials for machining Ti alloys include uncoated or coated cemented carbide, pcBN, and PCD [51]. [6, 72]

This work includes five Ti alloys ranging from α to near-β. Their microstructures are shown in Fig. 11. The Ti alloys are the α-phase CP-Ti (Fig. 11a), near-α Ti-6Al-2Sn-4Zr-2Mo (Ti-6242) (Fig. 11b), α+β Ti-6Al-4V (Ti-64) (Fig. 11c), α+β Ti-6Al-2Sn-4Zr-6Mo (Ti-6246) (Fig. 11d), and near-β alloy Ti-5Al-5V-5Mo-3Cr (Ti-5553) (Fig. 11e). Their respective compositions are shown in Table 1 and their heat treatment and mechanical properties are presented in Table 2.

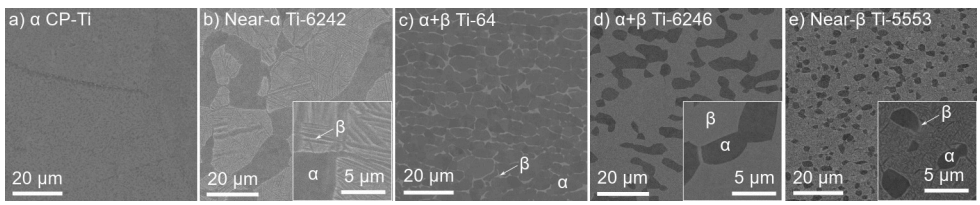


**Fig. 11** SEM-BSE microstructure images of titanium alloys. (a) α-phase CP-Ti [**IX**]. (b) Near-α Ti-6242 [**III**]. (c) α+β Ti-64 [**I**, **II**, **VII**, **VIII**, **X**, **XI**]. (d) α+β Ti-6246 [**III**]. (e) Near-β alloy Ti-5553 [**III**, **VII**, **IX**].

**Table 1** Chemical composition of Ti alloys in wt.%.

| | | Al | V | Sn | Zr | Mo | Si | Fe | Cr | Y | O | C | N | H | Res. | Ti |
|---|---|---|---|---|---|---|---|---|---|---|---|---|---|---|---|---|
| α | CP-Ti | - | - | - | - | - | - | 0.05 | - | - | 0.13 | 0.01 | <0.01 | 0.001 | <0.40 | Bal. |
| Near- α | Ti-6242 | 6.00 | - | 2.00 | 4.01 | 2.01 | 0.095 | 0.25 | - | - | 0.15 | 0.08 | 0.05 | 0.01 | <0.40 | Bal. |
| α+β | Ti-64 | 6.03 | 4.05 | - | - | - | - | 0.17 | - | <0.005 | 0.141 | 0.021 | 0.006 | 0.0013 | <0.40 | Bal. |
| α+β | Ti-6246 | 6.00 | - | 2.00 | 4.01 | 6.01 | - | 0.15 | - | - | 0.15 | 0.04 | 0.04 | 0.01 | <0.40 | Bal. |
| Near-β | Ti-5553 | 5.28 | 4.78 | - | <0.005 | 4.58 | <0.030 | 0.32 | 3.02 | <0.001 | 0.16 | 0.021 | 0.007 | - | <0.30 | Bal. |

**Table 2** Heat treatment and mechanical properties of the Ti alloys included in the work.

| | | Heat treatment | Ultimate tensile strength [MPa] | 0.2% yield strength [MPa] | Elongation [%] | Reduction of area [%] |
|---|---|---|---|---|---|---|
| α | CP-Ti | Sub-transus annealed | 463–483 | 364–376 | 31–34 | 52–58 |
| Near- α | Ti-6242 | Sub-transus solution treated and aged | 1004 | 895 | 19 | 42 |
| α+β | Ti-64 | Mill-annealed | 955 | 858 | 19 | 37 |
| α+β | Ti-6246 | Sub-transus solution treated and aged | 1214 | 1118 | 13 | 37 |
| Near-β | Ti-5553 | Sub-transus solution treated and aged | 1271 | 1210 | 7.5 | 23 |

### 3.2.2 Cast iron

The four most used types of cast iron are grey cast iron (GCI), ductile or nodular cast iron, malleable iron, and compacted graphite iron (CGI) [9]. Their machining behavior varies because of their different compositions and microstructures [61].

#### *3.2.2.1 Compacted graphite iron (CGI)*

Compacted graphite iron (CGI) started to be produced as an engineering material in the 1960s [10]. Compared to other cast irons, CGI has a high thermal conductivity, high resistance to thermal shock, and lower oxidation at elevated temperatures [9]. CGI has at least 75% higher tensile strength, 45% higher stiffness, 30–50% better wear resistance, and about double the fatigue strength of conventional grey cast iron [73, 74]. CGI is used in applications like diesel engine blocks, exhaust manifolds, gearbox housings, brake discs for high-speed trains, and flywheels [9, 10].

CGI is intermediate between grey cast iron and ductile iron as regards ductility and thermal conductivity [9, 10, 75]. The tensile strength and yield strength of CGI are similar to those in ductile iron, but higher than in grey cast iron [9]. Therefore, CGI is used in applications where the mechanical properties of grey cast iron are insufficient and those of ductile iron are redundant [10, 75]. These properties of CGI provide opportunities to improve design compared to conventional grey cast iron, like reduced wall thickness at operating loads and weight reductions. Increased operating loads allow the possibility of increasing power with an existing component design [73–75]. Additionally, the higher ductility offers reduced brittle failure in production and service [73–75]. The possibilities of weight reduction and power increases means that automotive manufacturers could benefit by changing from conventional grey cast iron to CGI, with results in line with the higher demands on specific engine performance by the European commercial vehicle sector and stricter emission legislation [73].

The graphite in CGI has a vermicular shape with rounded edges and irregular bumpy surfaces that provides strong adhesion between the graphite and the iron matrix [9, 10]. Graphite flakes in grey cast iron have natural cleavage paths that reduce fracture resistance, whereas the vermicular graphite in CGI inhibits crack initiation and growth and thus gives higher strength and stiffness [9, 73, 74]. Less than 20% of the graphite may exist as nodules that enhance strength, stiffness, and ductility [9, 73, 75]. ISO16112:2016(E) divides CGI into five grades ranging from ferritic to pearlitic and alloyed. Increased pearlite content raises tensile strength and hardness, which negatively affects machinability, while ferritic matrixes have lower strength and higher ductility [9, 74].

The chemistry of CGI is more complex than that of other cast iron types because the composition of alloying additives must be controlled to produce a microstructure with vermicular graphite and a limited degree of nodularity. The formation of pearlitic or ferritic matrixes is induced by heat treatment, which prevents flake

graphite formation [9]. Vermicular graphite is stable at low sulfur and oxygen levels. Additions of Mg and Si consume oxygen by forming magnesium silicate MgO and $SiO_2$ inclusions. Mg additionally forms MgS inclusions, which is different from grey cast iron where S is bonded to Mn forming lubricative MnS [74]. Higher Mg levels are attained by adding 0.1–0.2% Ti, which also results in the formation of abrasive TiC or Ti(C,N) inclusions [10, 73–75]. Other inclusions in CGI are oxides, nitrides, sulfides, or intermetallic inclusions with a size range of 0.1–10 μm [74]. CGI is more difficult to machine than conventional grey cast iron because its higher strength and stiffness require more power when cutting. The lack of lubricating MnS and the presence of abrasive inclusions also results in higher tool wear rates than grey cast iron [10, 75]. However, CGI has better machinability than ductile iron due to its higher thermal conductivity and lower elastic modulus [75].

The pearlitic GJV-450 grade of CGI was used in the work reported in this thesis. This is one of the more difficult-to-machine grades, and is commonly machined industrially under down face milling conditions. Its microstructure with inclusions is shown in Fig. 12a–c. Its chemical composition and mechanical properties are presented in Table 3 and Table 4 respectively. This CGI grade is 90–95% pearlite, 5–10% ferrite, and 5–10% nodularity. Analysis with SEM-XEDS shows the presence of MgO, $SiO_2$, (Ti, V, Nb, Cr) carbide or carbonitride inclusions, and local enrichments of Sn, Mn, and P. The recommended tooling for machining CGI includes CVD-coated cemented carbide of steel cutting grade (with small amounts of TiC and TaC hard phases) as these have demonstrated low wear rates and tolerate high cutting speeds [6].

#### *3.2.2.2 Grey cast iron (GCI)*

Grey cast iron (GCI) is the most cast material [76] and is used in a variety of applications including smaller cylinder blocks, cylinder heads, pistons, clutch plates, brake drums, and transmission cases [6, 9]. Its popularity is based on its high strength to cost ratio, castability, damping capacity, and high machinability [9, 69]. The high machinability is characterized by a low tool wear rate, high metal removal rate, low cutting forces, and low power consumption [6].

In grey cast iron, the carbon exists as graphite flakes in a pearlite and ferrite matrix [69]. Common elements in grey cast iron are the graphite forming Si and Ni, and fluidity improver P [69]. When machining GCI, cracks easily propagate along the flake graphite. However, the addition of carbide formers Cr and Mo can improve the limited strength and ductility by reducing the flake size and refining the pearlite [69]. MnS inclusions lubricate the tool surfaces and contribute to the high machinability [69]. GCI is a short-chipping material which results in easy chip evacuation and short contact length on the rake face [6].

Grey cast iron is also known for going through an aging process of up to 40 days after casting. As aging progresses, nitrides precipitate and the tensile strength

increases by up to 13%, the hardness increases by up to 10%, and the impact energy increases by up to 9% [77, 78]. Machining freshly cast GCI in a non-aged state often results in high tool wear rates and a poor surface finish [77, 79]. The alternative can be to absorb the prolonged storage cost and wait until the material attains the high machinability GCI is known for. The aging status can be checked by non-destructive impact testing [80]. Other options are to decrease the aging time by including extra Mn, N, and S in the alloying, or to accelerate the aging process by annealing the cast part [81]. The machining performance of aged GCI can be controlled by varying the cutting speed [82]. However, the tool wear rate is not improved by reducing the cutting speed when using otherwise high-performing pcBN tooling [79].

In the research work reported here, grey cast iron grade GG25 was used in the turning of industrial flywheels. It has a mostly pearlitic microstructure with MnS inclusions, less than 2% of which contain a core $Al_2O_3$ platelet, as shown in the microstructure image in Fig. 12d–e. There is also minor presence of steadite ($Fe_3P$) and abrasive (Ti,V)C inclusions of 1–2 µm size. The chemical composition and the mechanical properties are presented in Table 3 and Table 4 respectively. Recommended tooling when machining GCI includes coated cemented carbide, cermets, and pcBN [6, 51]. Although pcBN has a higher cost than cemented carbide, it exhibits superior performance at higher cutting speeds which, when combined with its high abrasion resistance and resistance to reacting with the ferrous material, makes it an economical choice [6].

**Table 3**
Chemical composition of CGI GJV-450 and GCI GG25 in wt.%.

| | C | Si | Mg | Cu | Sn | Mn | S | Cr | Ti | Al | Mo | Ni | Fe |
|---|---|---|---|---|---|---|---|---|---|---|---|---|---|
| CGI-450 | 3.62 | 2.18 | 0.0065 | 0.86 | 0.08 | 0.161 | 0.008 | 0.03 | 0.0032 | - | - | - | Bal. |
| GCI GG25 | 3.52 | 1.97 | - | - | - | 0.58 | 0.11 | 0.19 | 0.03 | 0.05 | 0.06 | 0.05 | Bal. |

**Table 4**
Mechanical properties of CGI GJV-450 and GCI GG25.

| | Tensile strength [MPa] | 0.2% yield strength [MPa] | Elongation [%] | Hardness |
|---|---|---|---|---|
| CGI-450 | 452 | 360 | 1.7 | 242 HB or 255 HV |
| GCI GG25 | 250 | 230 | <1 | 215 HB or 222 HV |

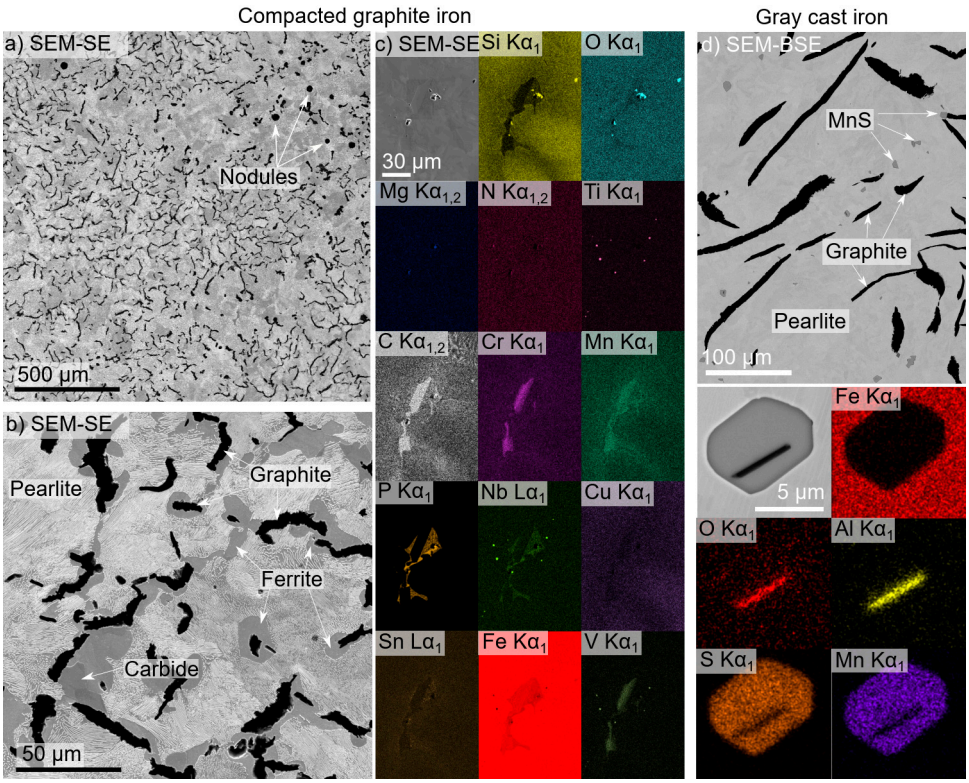


**Fig. 12** Microstructure and inclusions of cast irons. (a–b) SEM-SE microstructure images of 1% Nital etched CGI and (c) XEDS maps of non-etched region with inclusions [**IV**, **V**]. (d) SEM-BSE image of GCI microstructure and (e) XEDS maps of MnS inclusion with $Al_2O_3$ platelet [**VI**].

## 3.3 Conclusions

This section has introduced the tool and workpiece materials employed in this work. The tool materials include uncoated and coated cemented carbide in straight or steel cutting grades with differing Co content depending on the machining application. Coatings include CVD-applied Ti(C,N)-$Al_2O_3$ and PVD-applied $Ti_{0.45}Al_{0.55}N$ with and without a NbN overlayer. Ultra-hard PCD and pcBN are also employed. Workpiece materials include Ti alloys that range from α CP-Ti, near-α Ti-6242, common α+β Ti-64, α+β Ti-6246, to the gradually more popular near-β Ti-5553 with increasing β-phase fraction that reduces the machinability. Compacted graphite iron of GJV-450 grade is used, as well as grey cast iron in non-aged and aged state. Knowing the materials in their state prior to machining is crucial to understand the changes undergone due to tool wear. When selecting sample preparation methods and characterization techniques with suitable settings, it is helpful to know the materials beforehand. The machining performance can in some parts also be understood by knowing the material properties and microstructures.

# 4 Basics of tool wear and characterization techniques

*"Where relative motion takes place between surfaces, wear can never be completely eliminated, although in some circumstances it may be reduced to an insignificant level"* [52].

The cutting tool experiences extreme loads and temperatures during the machining process as the workpiece material is fractured or plastically deformed and sheared off and flows over the contact surfaces of the tool. The tool must be able to withstand such extreme conditions created by the metal cutting action for a given time. The wear resistance of a tool is not a unique property like hardness, for it depends on the interaction between the tool and the workpiece material, their geometrical relationship, the cutting conditions, and the environment [6, 52]. Tool wear limits the effective time a tool can be used in machining and thus restricts tool life. It cannot be avoided, but it may be reduced by adjusting the tool material and the cutting conditions. However, knowing what adjustments will reduce the wear rate requires an understanding of the active wear mechanisms and what controls them [6, 51, 52]. The main contributing wear mechanism may also change over time as the tool is gradually worn and the contact conditions change, which means that the wear rate may not be constant [52].

## 4.1 Basic tool wear and wear mechanisms

Tool wear is a loss of tool material or its deformation that occur during a machining operation [6, 51]. Material is removed either by massive fracturing on a macroscale, by smaller fragments or grains on a micro- or nanoscale, or by atomic loss [6, 51]. The wear changes the geometrical shape of the tool which affects the machined part's geometry, tolerance, and surface finish [6]. After some time, the tool no longer cuts efficiently or fails. The tool's deterioration is indicated by a rising cutting temperature, higher cutting forces, increased noise and vibrations, dimensional errors, and a poorer surface finish [6]. Common tool wear by loss of material takes the form of cratering and flank wear on the rake and flank sides

respectively as illustrated in Fig. 13 on an as-worn tool (Fig. 13a) and its cross-section (Fig. 13b). Another type of tool deterioration that changes the geometry of the tool without the loss of tool material is plastic deformation as illustrated in Fig. 13c [6, 51]. Plastic deformation occurs when the tool cannot withstand the high loads and contact stresses induced by the cutting action. It usually occurs at high temperatures when the hardness and strength of the tool are typically reduced [6, 51]. Tool material loss due to tool wear can be caused by a variety of wear mechanisms: mechanical, diffusional, or chemical. The wear mechanisms applicable in this work are explained below. Identification of the wear mechanism based on an as-worn tool morphology is often ambiguous and it is thus important to determine the actual wear mechanisms causing the wear morphology in order to understand the cause of the tool degradation.

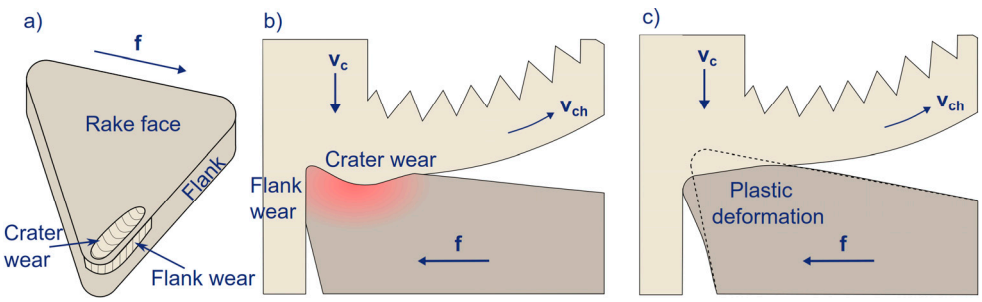


**Fig. 13** (a) Crater and flank wear in an as-worn tool and (b) cross-sectioned view of the cutting action and wear morphologies. (c) Visualization of plastic deformation in a cross-sectioned tool.

Tool wear can be monitored during production and wear-induced errors can be compensated for by adjusting the position of the tool. The time at which the tool needs to be replaced depends on the specific operation. In a testing or R&D environment, it is common practice to use the standards for tool life testing like ISO 3685:1993 for single point turning tools or ISO 8688-1:1989 and ISO 8688-2:1989 for milling operations. It is common to use either the flank wear criterion VB, for instance VB = 300 µm, or crater depth criterion KT, which is usually around 0.05–0.15 mm but depends on the feed rate. In some cases, the two criteria are combined. Flank wear influences the generated surface roughness and geometric accuracy, while cratering can result in tool failure [51]. Complete failure is not used as a tool life criterion as it can cause production stops and can seriously damage the machined part, tool holder, or machine [51].

### 4.1.1 Mechanical wear and adhesion

Abrasive wear occurs when hard particles like inclusions or precipitates in the workpiece material remove tool material as they slide over the tool surface [6, 51, 52, 61]. Attrition occurs when mechanically weakened grains in the tool material are removed by the chip flow, and is more common at lower cutting speeds [6, 51]. Adhesion occurs when workpiece material attaches to the tool and the bonding between the two becomes stronger than the local fracture strength of the tool material, resulting in repeated breaking off of tool material [51, 61]. Chipping or flaking occurs when tool fragments break off, usually because of mechanical shock caused by large force fluctuations like those in milling [51]. Fracturing or catastrophic failure can occur at different stages. Early-stage fractures may be due to incorrect tool geometry, cutting conditions, or tool defects. Final stage fracture may be due to thermal or mechanical stress fatigue [51, 61]. Another wear mechanism related to coatings is delamination, which can occur due to insufficient bonding between coating and substrate or due to mechanical loads being too high [52].

### 4.1.2 Diffusion

Diffusion and chemical reactions between workpiece and tool material occurs at elevated cutting temperatures in the range of 700–900 °C or higher and are thus more likely at higher cutting speeds [6, 48]. Atoms diffuse in the opposite direction of the concentration gradient, for example from the tool material into the workpiece material or vice versa [48, 61]. Interstitial diffusion occurs when atoms move in between an existing crystal lattice and occupy an interstitial position. This type of diffusion takes place with atoms in the smaller size range, like carbon, boron, nitrogen, and oxygen [69]. Substitutional diffusion or vacancy diffusion occurs when atoms take the place of an already existing atom in a lattice, moving from one site to another [69]. Its prevalence depends on the probability that the site is vacant and that the atom has the activation energy for the transit. Movements like this are more likely around defects and grain boundaries [69].

When atoms from the tool material diffuse into the workpiece material, they will eventually be transported away by the chip or workpiece flow [6, 48]. When atoms from the workpiece material diffuse into the tool material, the integrity and properties of the tool are altered, which may cause an increase in the wear rate. The diffusion wear rate depends not only on the temperature and flow rate of the workpiece material, but also on the combination of the solubility and mobility of the material constituents of the tool and workpiece [6], which is sometimes referred to as their permeability [83]. Diffusion wear commonly results in craters and flank wear [6]. The workpiece material flows more slowly around the edge line and the stagnation zone where the temperature tends to be slightly lower and therefore the

tool tends to be less worn [6]. Diffusional loss often undermines the integrity of the cutting tool material, leaving it more exposed to mechanical wear by processes such as adhesion, attrition, or abrasion [6].

### 4.1.3 Chemical reactions

Tools may wear due to reactions with the environment or with the workpiece material, facilitated by high cutting temperatures [6, 51]. Oxidation of tool material is one way in which the tool integrity may weaken. For cemented carbides, oxidation is already occurring at 600 °C and becomes rapid at 900 °C [6]. Phase changes can occur for PCD or pcBN tooling when diamond graphitizes and cBN undergoes a hBN transformation. These transformations are temperature and pressure dependent. Graphitization occurs above around 700 °C at 3 GPa [84] and cBN transforms to hBN above 1300 °C at common cutting pressures [85]. Both graphite and hBN are easily removed by the chip flow. Chemical reactions between the tool and workpiece material can occur spontaneously at the interface or may be due to an enrichment of elements at the interface due to diffusion. Reaction products may be more easily removed by the chip flow due to their weak mechanical properties, or may locally protect the underlying material from wear, in which case they form what is called a tool protection layer [86].

## 4.2 Investigation of tool-chip/workpiece interaction

Tool wear and wear mechanisms can be investigated in tools used in machining or in samples from imitational experiments. Due to the dynamic nature of the process, it is difficult or even impossible to study tool wear *in-operando* during the actual cutting operation. It is easier to study a tool that has been removed from the cutting process. Tool wear occurs where the tool and workpiece interact and this region can be studied using multiscale characterization techniques ranging from the macro-, micro- and nanoscale to the atomic scale. The evolution of wear can be followed by studying the tool at varying engagement times.

### 4.2.1 As-worn tools and their cross-sections

As-worn tools display the overall wear morphology, and large-scale wear mechanisms like abrasive score marks, chipping or flaking, fracturing, fatigue, and coating delamination are easily detected. Attrition and adhesive wear can be detected on an as-worn tool but sometimes the workpiece material adheres to the wear regions and covers the worn tool beneath. Such adhesion layers can be removed by using etchants, but there is a risk of removing chemical reaction

products at the same time. Fig. 14 displays two as-worn tools and their cross-sections, where the first tool (Fig. 14a–b) is a coated carbide used in milling CGI-450 that exhibits cratering, flank wear, and adhered CGI along the edge line. The other tool is an uncoated cemented carbide used in turning Ti-64 (Fig. 14c–d) that has almost the entire wear region covered by adhered workpiece material. Plastic deformation, attrition, and adhesive wear are easier to detect and verify as active wear mechanisms in cross-sections of the tool at selected locations across the interface. Wear mechanisms like diffusion and chemical reactions are not detectable by studying an as-worn tool.

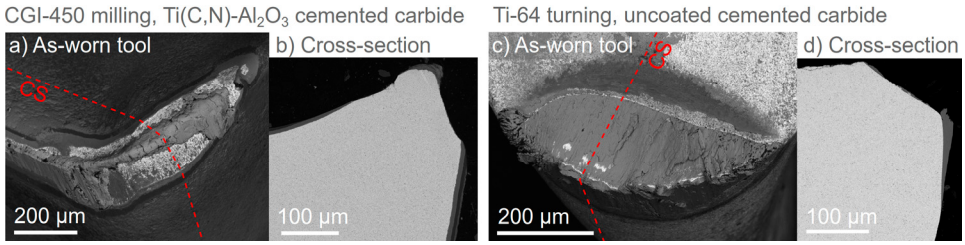


**Fig. 14** SEM-BSE images of as-worn tools and their cross-sections. (a–b) After milling CGI-450 with Ti(C,N)-$Al_2O_3$ coated carbide [**V**]. (c–d) After turning Ti-64 with uncoated cemented carbide [**II**].

A cross-section reveals the shape of the wear region on the macroscale and the microscale wear at the tool contact regions. If there is adhered workpiece material, the interaction between workpiece material and tool material can be investigated and reveal information on mechanical wear, diffusional wear, or chemical reactions. Given the vast range of available tool geometries, depths of cut and feed rates, the process of preparing a cross-section may need to be adapted to suit the situation. The sample preparation methods for taking cross-sections in cases applicable in this work are presented in Fig. 15 and include the cross-section method for a turning insert with low depth of cut and a milling insert with high depth of cut.

It is important to avoid clamping on the worn regions of the tool. However, if this cannot be avoided, as with a milling insert where both edges are used and need inspection, rubber padding can be placed over the area while taking care not to overtighten the clamp. When clamping the tool for grinding, it is important that it remains clamped through steps II–IV so as to be able to correctly program the final position after referencing in step II. The tool tip is cut off to make sure that the center of gravity is so placed that the tool piece can balance on the ground area and not fall over during hot mounting in a conductive resin. A third cut in step V may be needed for a milling insert to reduce its thickness.

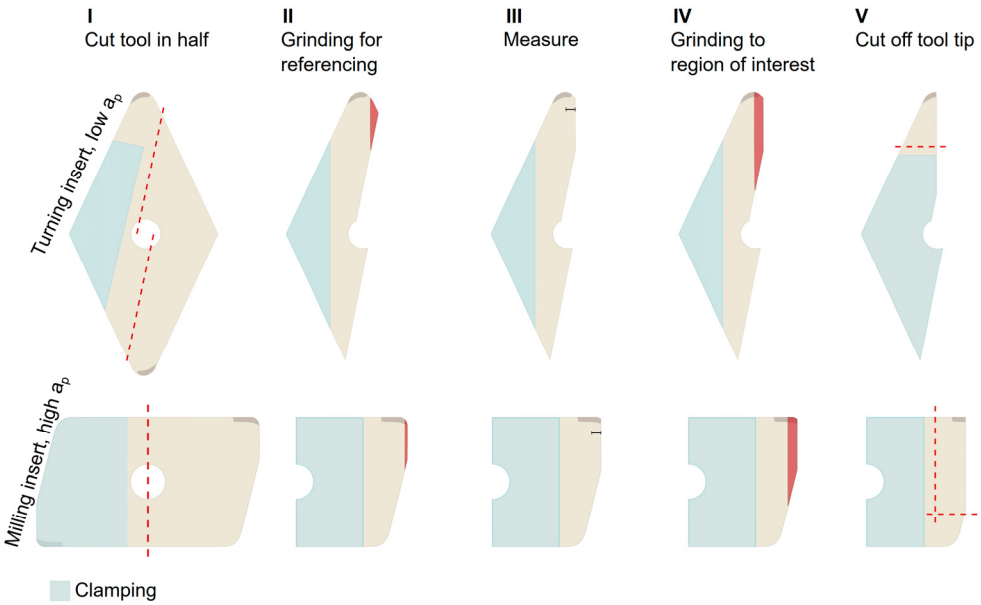


**Fig. 15** Two methodologies to prepare cross-sections of as-worn tools. The upper row shows a method for a turning insert with a low depth of cut, and the bottom row shows a method for a milling insert with a high depth of cut.

The tool-chip/workpiece material interaction can be studied using the quick-stop method described in section 2.4. The level of wear can be controlled by using a pre-worn tool and then performing the quick stop operation. By introducing a pre-cut in the tool, by cutting it with a diamond disc, a crack can be produced during machining. The cutting edge may remain in the cutting region due to the adhesive force between tool and workpiece material after disengagement of the toolholder, as explained in Fig. 6. This allows the whole tool-chip/workpiece interaction to be studied, as displayed in Fig. 16a–b. The cross-section in Fig. 16c displays the tool-chip/workpiece material contact.

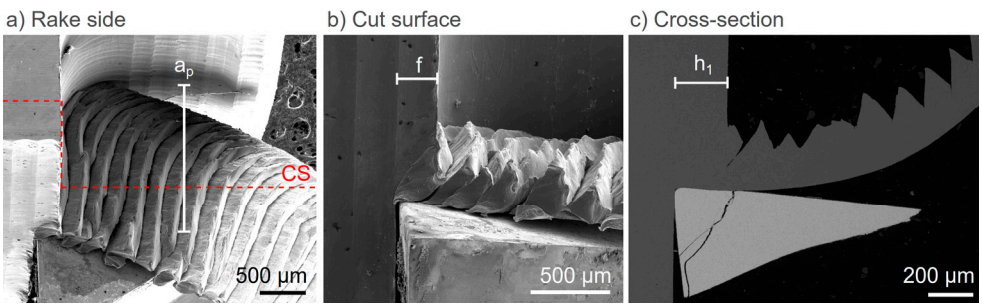


**Fig. 16** Quick stop experiment with tool edge that is attached to the cutting zone, seen from (a) the rake side, (b) shifted 90° from the previous view facing the radial direction of the workpiece, and (c) the cross-section in the same plane as in (b) [**IX**].

Preparing and preserving a successful quick stop sample is a delicate process. Fig. 17 shows a method for preparing a cross-section of a tool attached to the workpiece. The first step involves extracting a piece of the machined metal or alloy without damaging the tool and chip. This can be done by using wire electrical discharge machining or by manual sawing. The former method gives a bulkier and square sample that is easier to handle in the coming preparation steps. The ends of the sample are cut off to make it fit during hot mounting. The sample is then glued on an adjustable holder or a goniometer stage that allows adjustments around two axes. The cross-section is revealed by cutting using a diamond disc when the tool is cemented carbide and the workpiece is non-ferrous. Cutting is initially done at the lowest feed rate (0.005 mm/min), going from the metal and into the chip and tool to avoid the risk of tool removal. The sample is removed from the holder with acetone that dissolves the glue, mounted in conductive resin and polished.

Titanium and cemented carbide have different hardness. To produce a flat sample, harder polishing cloths are used with as few polishing steps as possible. The following recipe in a Struers Tegramin-30 semi-automatic polisher and Struers consumables has been successful:

1) rough grinding using either 220–500 grit MD-Piano at 15 N for about 30 seconds (stop every 10 seconds to rotate sample to avoid a tilted interface),
2) polishing using 9 µm diamond DiaPro Allegro Largo suspension on an MD-Plan cloth at 10 N for 3 minutes,
3) 3 µm diamond DiaDuo-2 suspension on an MD-Dac cloth at 10 N for 5 minutes,
4) 1 µm diamond DiaDuo-2 suspension on an MD-Nap cloth at 10 N for 5 minutes,
5) colloidal silica OP-U NonDry on an MD-Chem cloth at 5 N for 5–10 minutes.

Using co-counter rotation has worked well and gives slightly faster removal rates. The rotational speed for polishing disc and sample holder were both 150 rpm. The samples, holder, and support board were cleaned with water and dish soap between polishing steps, while the final sample was rinsed in ethanol and stored.

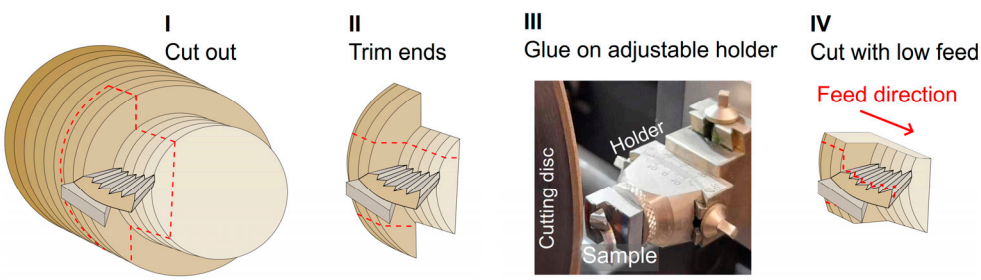


**Fig. 17** A methodology to prepare a cross-section from a quick stop experiment.

### 4.2.2 Diffusion couple method

Diffusion and chemical wear can be artificially produced by using the diffusion couple method. This is done by establishing a static contact between tool and workpiece material and applying a temperature and pressure similar to a cutting operation for a given time, followed by rapid cooling or quenching to preserve the reaction products. The dynamic flow of workpiece material is lost with this method and the diffusion couple is encapsulated and protected from the environment. Fig. 18 shows a schematic of the diffusion couple cell [33]. If good contact is established across the interface, the distribution and occurrence of reaction products can be estimated. The reaction products or interaction volume are usually larger than in an as-worn tool which makes it easier to detect and characterize reaction products or diffusion.

This method can complement actual machining when the major wear mechanisms are diffusional dissolution and chemical wear, as when machining titanium or other difficult-to-cut materials at high-speed conditions. The diffusion couple method offers economic benefits, enabling costly machining trials to be kept to a minimum or even avoided, and allows investigation of larger materials systems. The method can be used in testing the design of new tool materials and alloys that might, for example, promote the formation of tool protection layers that extend tool life. Alternatively, it can be used to identify what temperatures and thus cutting conditions promote the formation of diffusion barriers or tool protection layers and also to indicate negative interactions like diffusional loss. The reactions identified can be used to validate thermodynamic and diffusion models and simulations [27, 87, 88].

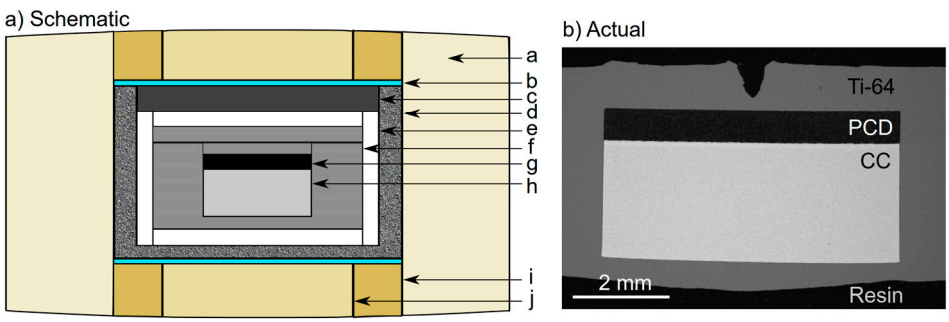


**Fig. 18** The diffusion couple cell adapted from Olsson et al. [33] (a) with its schematic constituents a: limestone container, b: metallic current lead disc, c: graphite lid, d: tubular graphite heater, e: electrical insulation gasket, f: workpiece material (Ti-64) capsule, g: PCD, h: cemented carbide substrate, i: pyrophyllite ring, j: axial graphite heater, and (b) a cross-sectioned diffusion couple after removal of protective capsule material.

### 4.2.3 Focused Ion Beam (FIB) lift-out

The tool-chip/workpiece interaction can be studied at a nano to atomic scale by extracting a micrometer sized sample using the FIB lift-out technique. The sample is usually less than 200 nm thick to enable electron transmission. Chemical reaction products and diffusion wear can be more confidently characterized by studying this size of sample. The location of the extracted sample can be somewhere on the contact region of an as-worn tool. For instance, an interesting location can be the center of the crater where the wear rate has been highest. The extracted sample can also be along the tool/workpiece material interface in a cross-sectioned as-worn tool or diffusion couple, in which interesting phenomena are clearly seen compared to an as-worn tool with adhered workpiece material.

Fig. 19a displays an example of how FIB extractions were done across the interface of a cross-sectioned as-worn cemented carbide tool. Fig. 19b displays a FIB extraction at the center of the rake contact zone of a PCD tool. In both cases the tool was used in turning Ti-64. In the latter case, the as-worn tool was etched to reveal the wear morphology of the PCD tool without the visual block of adhered Ti alloy, but a FIB sample was extracted prior to etching to spare a part of the tool-chip interface. The FIB used in this work was an FEI Nova NanoLab 600 dual FIB-SEM.

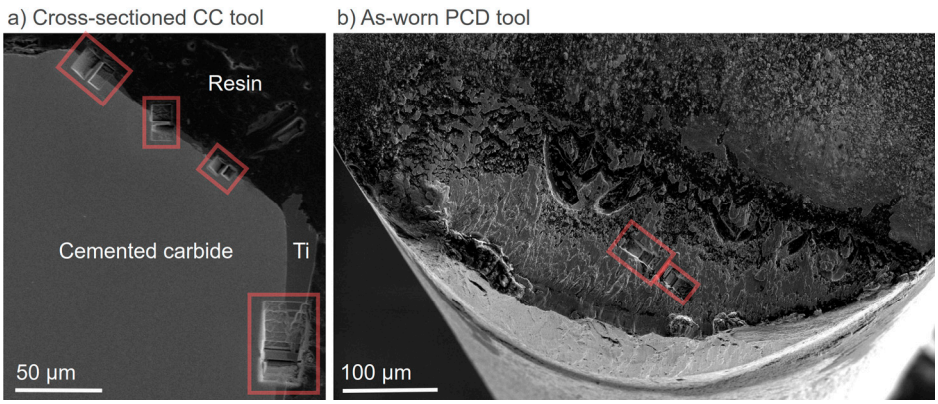


**Fig. 19** FIB-extractions from (a) across the interface of a cross-sectioned as worn cemented carbide tool and (b) an as-worn PCD tool. Both were used in turning Ti-64 [**I**].

The lift-out process for site-specific TEM-samples is well described in [89] but is simplified in Fig. 20 with examples from different samples. Initial deposition of a protective metal like Pt (Fig. 20a) is followed by ion milling on either side making trenches (Fig. 20b). This is followed by thinning the section to a smaller thickness of the sample and then milling away material in a U-shape, in so-called undercutting (Fig. 20c). The probe is inserted and fastened to the sample using Pt deposition, and the lamella is cut loose (Fig. 20d). The lamella is then attached to e.g., a Cu-half-grid using the Pt deposition. The probe is then cut off (Fig. 20e). The lamella is polished to its final thickness of less than 200 nm (Fig. 20f).

Ion milling with $Ga^+$ can lead to its implantation in the sample, causing microstructural and topographical disruptions, but most artifacts created in FIB prepared samples are due to redeposition and not to interaction of ions and sample. However, recent research shows that large lattice distortions form when using FIB even at low ion doses that were previously thought negligible [90]. The sample extracted with FIB also represents a very small portion of the overall contact region. It is difficult to say how well it correlates with the whole tool wear region. This unknown must be balanced against the insights obtainable from the FIB sample and the time and cost investment required to make several FIB lamellae from the same tool.

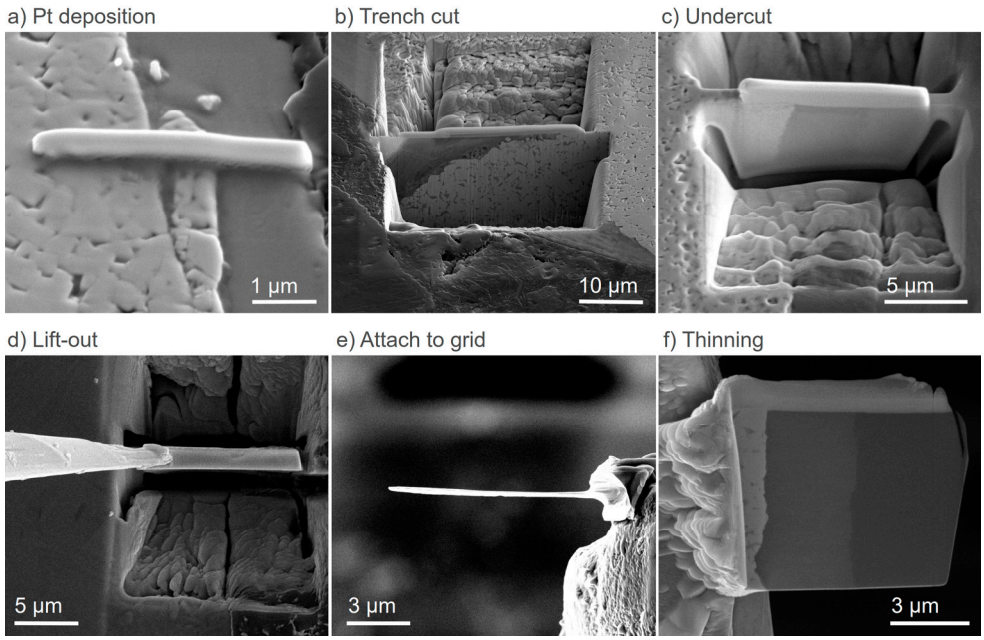


**Fig. 20** The FIB lift-out procedure with examples from different samples. (a) Deposition of protective Pt. (b) Ion milling of a trench pattern on either side of the deposited Pt. (c) Ion milling undercut of the lamella. (d) Lift-out by ion milling the remaining attachments after fastening of the probe with deposited Pt. (e) Attachment of the lamella to the grid. (f) Thinning with ion beam to a suitable thickness.

## 4.3 Microscopy methods

The interface between tool and workpiece material where the wear mechanisms are active can be studied using a variety of microscopy methods and analysis techniques ranging in scale from mm, µm, nm, to atomic scale. Williams and Carter wrote *"know the forest before you start looking at the veins in the leaves on the trees"* [91] and this approach is suited to investigating wear mechanisms. The techniques used in this work are light optical microscopy, SEM, XEDS, EBSD, ICCI, (S)TEM, and XRD which combined offer both good sampling and resolution of the wear regions. These methods are briefly introduced here. More in-depth information can be found in the references.

### 4.3.1 Light optical microscopy (LOM)

Light optical microscopy is used to measure the evolution of flank wear during tool life testing (Fig. 21a) and when preparing cross-sections (Fig. 21b). The microscope used was an Olympus SZX7 optical stereo microscope. Especially in turning or milling titanium alloys and cast iron, adhered metal covers the contact regions and blocks the actual tool wear regions, affecting the measurement of the tool-chip/workpiece contact. The actual tool wear can be measured by removing the adhered metal by etching, but the downside is the potential removal of reaction products and the alteration of the conditions the tool experienced if it was being used in continuous machining.

3D-scanning of as-worn tools was done using an Alicona Infinite Focus 3D optical microscope. Geometric changes like crater depth and tool volume loss can be estimated by scanning and comparing a new and an as-worn tool (Fig. 21c–d). Adhered workpiece material may cause a divergence from the geometrical change of the tool, in which case removal of the adhered metal may be necessary.

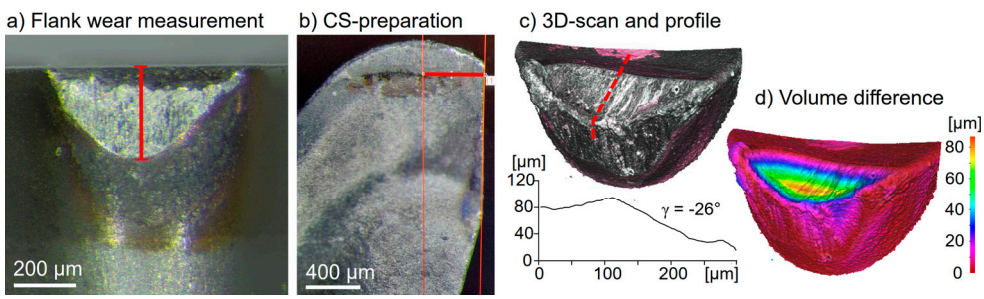


**Fig. 21** Examples of LOM applications. (a) Flank wear measurements in tool life testing. (b) Measuring how much tool material to grind away when preparing cross-sections of an as-worn tool. (c) 3D-scanning and profile contouring of an as-worn tool. (d) Volume difference measurement of an as-worn tool.

### 4.3.2 Scanning electron microscopy (SEM)

As-worn tools and their cross-sections, quick stop samples and their cross-sections, and diffusion couples were initially studied in a scanning electron microscope (SEM) at 10–15 kV (Fig. 14, Fig. 16, Fig. 18). The electron beam spot is about 2–10 nm and scans the surface in a raster [69, 92]. As-worn tools are preferably studied with a longer working distance (e.g., 15–30 mm) to focus over a longer depth, while flat samples like cross-sections and diffusion couples are studied at a smaller working distance (10–15 mm) with a smaller spot size (< 5 nm) for higher resolution when using the SEM Tescan Mira3 in this work. The same view was studied using SE and BSE detectors simultaneously.

The SE detector gathers all low energy electrons (2–5 eV [92]) that are ejected from the sample. These can be bent around corners, which means that the SE view can show details of topography as displayed in Fig. 22a [69]. The BSE detector gathers of high energy electrons (5–50 eV [92]) that returns from the sample (Fig. 22a) and displays atom density with the Z-contrast mechanism. A darker Z-contrast displays lighter elements and a brighter Z-contrast displays heavier elements relative to the overall composition [69]. Both detectors contribute to understanding wear morphology and composition, as can be seen in Fig. 22b–c, which show the same area as seen by the two detectors.

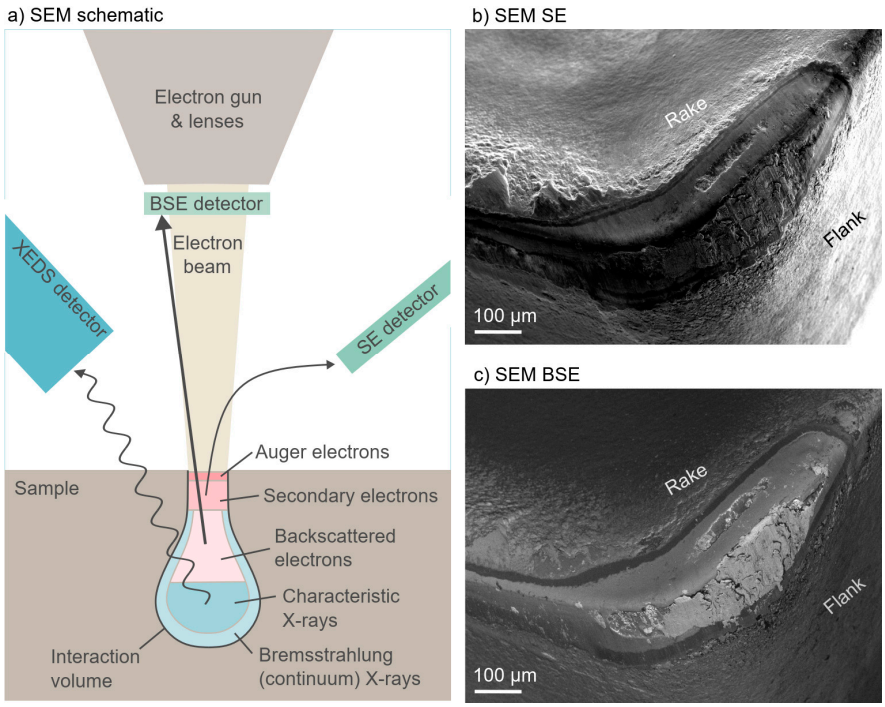


**Fig. 22** (a) Schematic of the SEM with SE-, BSE-, and XEDS detectors and the interaction volume in the sample. SEM images of an as-worn tool imaged with (b) SE detector and (c) BSE detector.

### 4.3.3 X-ray energy-dispersive spectroscopy (XEDS)

The elemental composition of a sample can be studied using X-ray energy-dispersive spectroscopy (XEDS) at standard settings for SEM of 15 kV and 15 mm working distance. This technique was used on as-worn tools, cross-sections, diffusion couples, and TEM lamellae. As the sample is bombarded with high energy electrons, it emits characteristic X-rays for the elements present in the excitation volume (Fig. 22a). The main advantage of XEDS is that a detector like the Si-Li detector [69, 91–93] can simultaneously collect the whole range of X-rays, rather than just the X-rays for one element at a time [69, 93]. It is easier to detect characteristic energies from elements above Z = 11 [69, 93]. Because of the excitation volume, XEDS resolution can be relatively poor [69, 93].

Bremsstrahlung or continuum X-rays form when incident electrons are decelerated as they interact with atomic nuclei. The energy of these X-rays can be as high as the beam energy [91–94]. The excitation volume goes some µm into the sample depending on the element density and the acceleration voltage [91–94], and may excite material underneath. This feature needs to be taken into consideration in the analysis. The generated XEDS spectrum in Fig. 23b from the linescan in Fig. 23a first needs to be qualitatively analyzed and the elements present in the region of interest need to be identified before doing a quantitative analysis like a map (Fig. 23c), linescan (Fig. 23d–e), or a quantification [91].

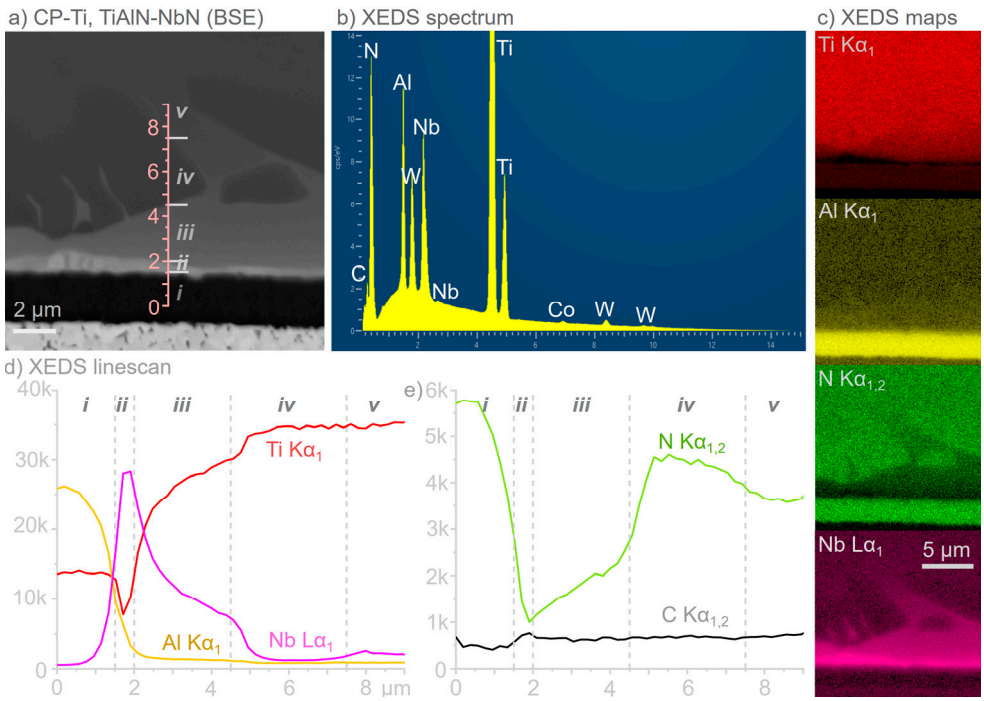


**Fig. 23** (a) SEM-BSE image and XEDS (b) spectrum, (c) maps, and (d–e) linescan [**IX**].

### 4.3.4 Electron backscatter diffraction (EBSD)

Electron backscatter diffraction (EBSD) is an SEM-based technique in which the sample is tilted at a steep angle (70° is common) to the incoming beam [95]. The surface of the sample needs to be very flat for EBSD to give useful information on crystallography [96]. The Bragg diffracted electrons that have interfered with the sample impinge on a fluorescent screen and form a Kikuchi diffraction pattern [95, 96]. The Kikuchi pattern pairs spatial positioning and intersecting angles that are unique to the crystal structure and grain orientation, and so provide information on the specific sample's crystal structure and orientation, phases, grain boundaries, crystal rotation, and dislocations [95, 96]. Modern EBSD programs use image recognition algorithms to automate analysis of Kikuchi patterns [95, 96].

The spatial resolution of EBSD is poorer than that of conventional SEM imaging and is governed by the excitation volume where the information depth is limited due to the high interface tilt [95]. The excitation volume and spatial resolution increases with lighter materials and higher beam voltage, which is typically 20 kV. Beam spots around 0.02–0.5 µm in diameter can be attained [95]. Fig. 24c–e shows the same region analyzed using different EBSD modes including band contrast or pattern quality (Fig. 24c), phase map (Fig. 24d), and inverse pole figure (IPF) (Fig. 24e), which indicates the crystallographic poles aligned with a specific sample direction [95]. In this work a Tescan Mira3 SEM with Oxford EBSD detector and Zeiss Sigma VP SEM with Nordlys Max2 Oxford EBSD detectors were used for EBSD investigations.

### 4.3.5 Ion channeling contrast imaging (ICCI)

Ion channeling occurs in crystalline materials when ions penetrate crystals with different orientations and gives a varying contrast in secondary electron images which allow identification of individual grains, their size and distribution [89]. Ion channeling contrast imaging (ICCI) of a single crystal gives a darker contrast when its alignment approaches a low index direction that decreases the number of emitted secondary electrons [89]. The relative channeling contrast between grains in different materials depends mainly on the interatomic planar distances and the atomic density. For example in an hcp material, elements with higher atomic density like Al or Au will have stronger channeling contrast while lower atomic density Si will have less contrast [89]. Ion channeling contrast images show the grain contrast without needing to etch the sample [89]. Fig. 24b shows an image obtained using ICCI. Individual grains of $Ti_{0.45}Al_{0.55}N$ coating are evident, compared to the very dark Z-contrast in SEM-BSE image (Fig. 24a). In this work a FEI Nova NanoLab 600 dual FIB-SEM was used to obtain ICCI.

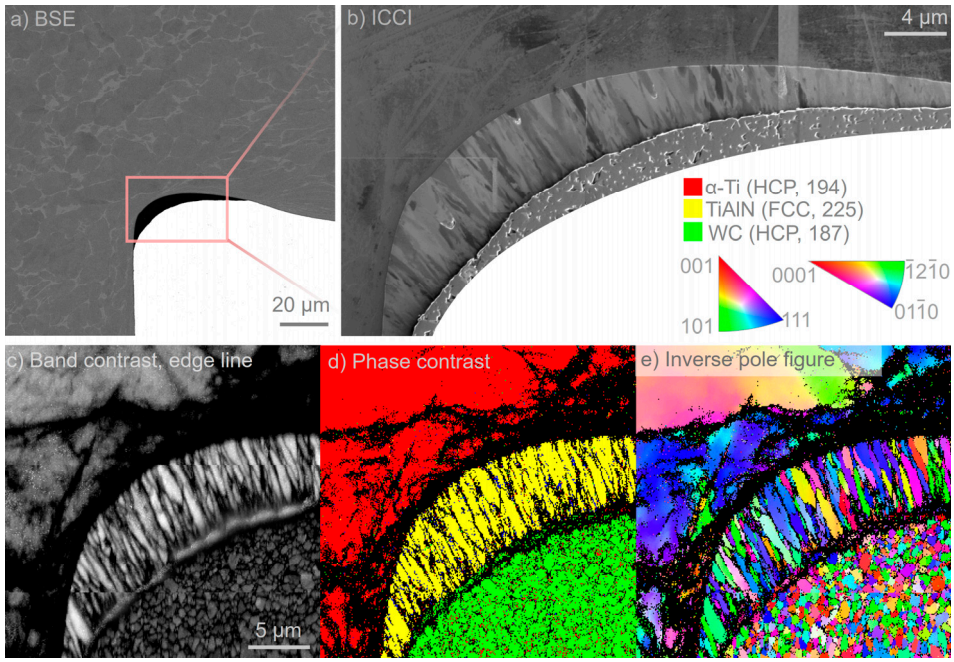


**Fig. 24** The edge line of a quick stop sample in turning Ti-64 with $Ti_{0.45}Al_{0.55}N$ coated WC-6%Co imaged with (a) SEM-BSE, (b) ICCI, and (c–e) EBSD [**IX**].

### 4.3.6 Transmission electron microscopy (TEM)

In the transmission electron microscope (TEM), electrons are transmitted through an extremely thin sample (<200 nm) [69]. Today, it is possible to achieve 1 Å image resolution [69, 92–94]. The electrons are emitted from an electron gun and the beam column consists of several magnetic lenses in an enclosed column in vacuum [69, 93]. The TEM is composed of an illumination system, a condenser lens system, an objective lens system, a magnification system, and a data recording system [92–94]. Condenser lenses above the sample stage collimate the beam and projector lenses below the sample stage magnify the image view up to more than 1 500 000 times [69]. There are more than 40 combinations of modes for forming an image, a diffraction pattern (DP), or a spectrum that yield different types of information on the sample [91].

The TEM provides both image and diffraction information from the same part of the sample [69, 93]. The diffraction pattern is displayed when the back focal plane is projected on the camera [69]. The DP from a selected part of the sample (selected area electron diffraction, SAED) is obtained by inserting an aperture in an image plane that blocks the beam emitted from the surrounding sample [69, 93]. Nanobeam diffraction (NBD) is done by using a beam probe in the nanometer scale to obtain DP from regions smaller than those possible with SAED [93]. Fig. 25d shows a

diffraction pattern from a TiAlN coating obtained with SAED. A diffraction pattern from an fcc, bcc, or hcp sample can be indexed by measuring the lattice spacing d from the central spot to each diffracted spot and calculating their proportions and angles relative to each other. This is compared to already indexed DP with known orientations relative the beam. If the DP fits well with the already indexed one, the cell lengths can be calculated using the interplanar spacing equations for cubic or hexagonal structures.

In TEM mode, a small aperture inserted in the back focal plane blocks the diffracted ray and makes the image become a contrast shown on a bright background. This is bright-field (BF) imaging (Fig. 25a). Dark-field (DF) imaging on a dark background (Fig. 25e) occurs when the diffracted ray goes through an aperture [69, 94]. In this work, TEM-DF imaging was used to highlight the phases identified with diffraction in different locations. Superimposing those images enabled an overview of the phase distribution as in Fig. 25e.

Scanning transmission electron microscopy (STEM) is done by forming a fine probe of the beam that scans the sample in a raster [91, 93, 94]. The detectors that pick up electrons that are scattered at low angles are called low angle annular dark-field (LAADF) detectors. Electrons scattered at higher angles are detected by the high angle annular dark-field (HAADF) detector [91, 94]. A dark-field detector is inserted to create STEM-HAADF images, which gives mass thickness contrast or Z-contrast (Fig. 25b) [94]. STEM-LAADF gives another contrast that more resembles grain contrast (Fig. 25c). By combining these modes, different information on the same region of interest can be attained, as shown in Fig. 25a–c. XEDS analysis of the lamella is possible in STEM mode. The TEM used in this work was a JEOL 3000F Field Emission Electron Microscope operating at 300 kV.

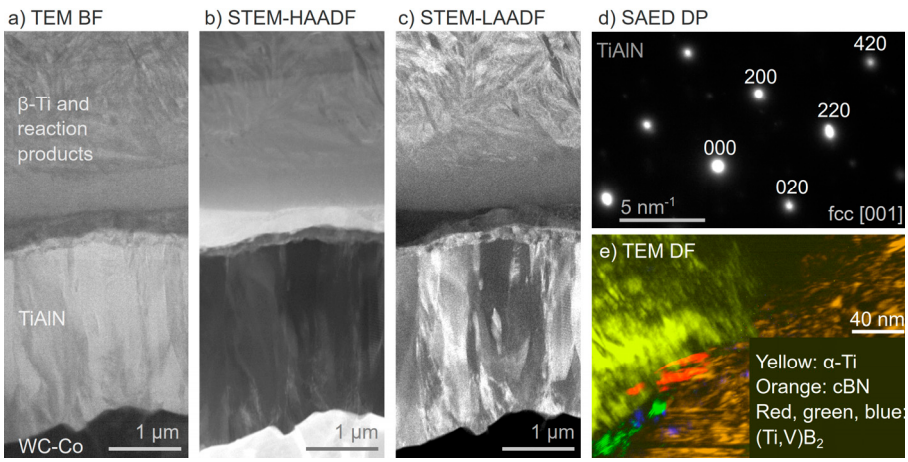


**Fig. 25** Examples of TEM modes showing the same region of interest but imaged using (a) TEM BF, (b) STEM-HAADF, and (c) STEM-LAADF [**IX**]. (d) The diffraction pattern obtained from the $Ti_{0.45}Al_{0.55}N$ coating using SAED [**IX**]. (e) Five superimposed TEM-DF images that include several reflections from the identified phases [**I**].

### 4.3.7 X-ray diffraction (XRD)

In X-ray diffraction (XRD), a divergent beam of monochromatized radiation is aimed at the surface of a sample that rotates around its own axis as the sample tilt changes gradually [69]. The intensity of the diffracted beam is recorded for the various angles (2θ), as is the distance between lattice planes d according to Bragg's law and the interplanar spacing relationship. This creates a spectrum like the one in Fig. 26 [69]. The diffracted peak position can be matched to peaks from a standard sample or by calculation [94]. The interplanar spacing is calculated using $2d \sin\theta = \lambda$. For cubic crystals the lattice parameter a can be calculated using $d_{hkl} = a/\sqrt{h^2 + k^2 + l^2}$ while non-cubic crystals require iterations to calculate lattice parameters and angles [94]. Another method is to use the fingerprint method where the spectrum peaks are compared against diffraction patterns from databases with previously indexed peaks with interplanar spacings, hkl-index, and relative intensity [94]. In this work the XRD method was used to study the reaction products at the interface of a diffusion couple of cemented carbide and Ti-64 using an XRD STOE Darmstadt diffractometer with Cu-Kα source.

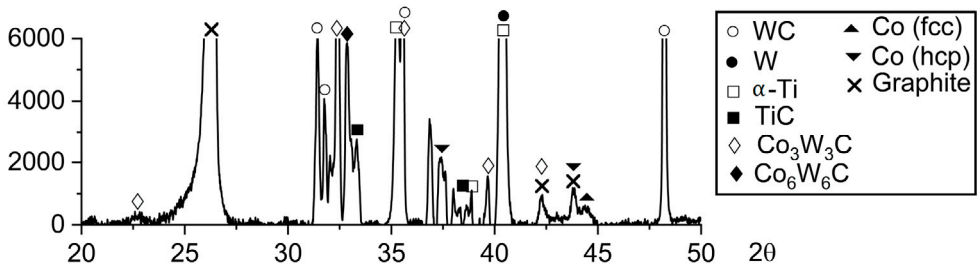


**Fig. 26** XRD spectrum from the interface region of a diffusion couple with cemented carbide and Ti-64 [**VIII**].

## 4.4 Conclusions

This section introduced the changes in tool geometry due to tool material loss and plastic deformation. Tool material loss is caused by tool wear mechanisms, and the mechanical, adhesive, diffusional, and chemical wear mechanisms were introduced. The types of samples in which the interaction between tool and workpiece material can be studied were presented and included as-worn tools and quick stop samples with the tool attached to the workpiece and their cross-sections. A method of preparing cross-sections of as-worn cutting tools and samples obtained in quick stop experiments was briefly introduced, as well as how such samples can be polished.

Imitational experiments like diffusion couples can also be used to investigate the interaction between tool and workpiece material. Using FIB, thin lamellae can be extracted from selected locations across the interface regions or the as-worn tool for exploration at a higher magnification in a TEM. This method is especially useful when it is difficult to make cross-sections, as is the case with ultra-hard tooling, or when adhered material covers the wear morphology in worn tools. In these cases, FIB extraction is useful to save the tool-chip/workpiece interaction before etching that may reveal the morphology but may also remove reaction products. The types of samples used in this work allow studies at a macro or mm scale down to a higher resolution at the nano scale. The analysis of wear mechanisms takes the form of an inverted cone, allowing studies of "*the forest before the veins of the leaves of the trees*" [91].

The microscopy methods employed to explore the wear mechanisms and their contribution to the wear morphology were introduced. LOM was used to measure flank wear, when preparing cross-sections, and for measuring crater depth and estimating tool material loss. SEM was used to study as-worn tools, quick stop samples and their cross-sections and diffusion couples. SEM, XEDS, and EBSD were additional methods that provided information on chemical composition and phase presence. ICCI was done in FIB-SEM and provided information on the crystal orientation of grains and potential plastic deformation in coatings. The combination of modes to form an image, diffraction pattern, or spectrum in TEM allows for more than 40 ways of getting information from a sample. The techniques used were done at nm resolution. XRD is done at larger resolutions than SEM and was used to identify reaction products in diffusion couples where the volumes were larger than in as-worn tools.

# 5 Tool wear mechanisms

In this chapter the tool wear mechanisms identified in the selected materials systems and the state of the art in the research field are presented. Tooling used in turning and milling Ti alloys includes commercial PCD, pcBN, uncoated and $Ti_{0.45}Al_{0.55}N$ with and without NbN overlayer coated cemented carbide. Commercial Ti(C,N)-$Al_2O_3$ coated carbide was used in milling CGI, and commercial pcBN in turning GCI. The tool wear mechanisms were studied in controlled variability, process freezing, and imitational experiments, and by modeling and simulations at industrially similar cutting conditions. Ways to decrease the tool wear rate are suggested based on the identified wear mechanisms.

## 5.1 PCD and Ti-64

Reported wear morphologies and mechanisms in PCD tooling when machining Ti alloys include cratering, flank wear, notching, cracking, chipping, and catastrophic tool failure. Diamond graphitization has also been observed in diffusion couples [97] and in tools used in machining [98, 99]. Formation of TiC in the crater has been suggested [49, 98] and experimentally verified in as-worn tools using advanced microscopy techniques [100]. Attrition wear by adhered Ti alloy is a suggested wear mechanism [101, 102], but there is no experimental evidence for it, and the diamond-diamond bonding may be too strong to permit it. Cratering is common and is often correlated with diffusional dissolution, but there is little evidence for this mechanism in the cutting tool [103]. More details on wear mechanisms of PCD tooling when machining Ti-64 are reported in **Paper I**.

When turning Ti-64 at high-speed conditions, rake cratering with the shape of a chamfer occurred due to the short rake contact width. Although massive adhesion of Ti alloy covered the contact surfaces of the tool (Fig. 27a), there was no evidence of adhesive wear as no grain pluck-out was observed on the worn tool surface after etching (Fig. 27c). Channel and ridge-like features formed at the end of tool-chip contact zones on the rake (Fig. 27b) where diamond grains in the channels had a smoother appearance than the Co binder, indicating that they were the target of wear. The low pressure and high temperature in the regions of these features match the conditions that cause graphitization [98]. Graphite would be easily removed by the coolant jets that create smooth surfaces in the channels and could therefore not

be detected. Etching or diamond burn-out in the presence of oxygen is also a likely mechanism causing the channels, as etch rates can be close to those of graphitization [104].

Formation of (Ti,V)C occurred in the presence of Co binder at the interface to the adhering Ti-64 (Fig. 27d–e) and was likely facilitated by diffusional dissolution of carbon. This may also be an active wear mechanism of diamond, as there was larger material loss on diamond grains directly exposed to Ti-64 than on grains separated by the (Ti,V)C reaction product. This carbide acts as a diffusion barrier for carbon and is thus a tool protection layer. The (Ti,V)C layer was not uniform and there were several crystallites within the Co matrix, indicating that the (Ti,V)C spontaneously crystallized on solidification of liquid Co. Co liquefies above 1020 °C [105], which is lower than the temperature detected in turning (Fig. 7c) and explains why Co stretches over neighboring diamond grains. Decreasing the grain size and increasing the binder content increases tool life as protective caps of (Ti,V)C can merge and form a continuous tool protection layer. Another study similarly showed that a submicron grain size with high Co content gave high machining performance for Ti-5553 [100].

Intermetallic $Co_3W_3C$ formed in the binder pool on top of the Ti alloy as a result of C diffusing in Co and dissolved W from the cemented carbide substrate. The same phase was observed in [99]. Because it forms between Co and diamond grains, this phase can potentially delay the graphitization of diamond, which is expected to graphitize in the same locations [99]. This intermetallic phase could also reduce the dissolution rate of C in Co and thus act as a tool protection layer.

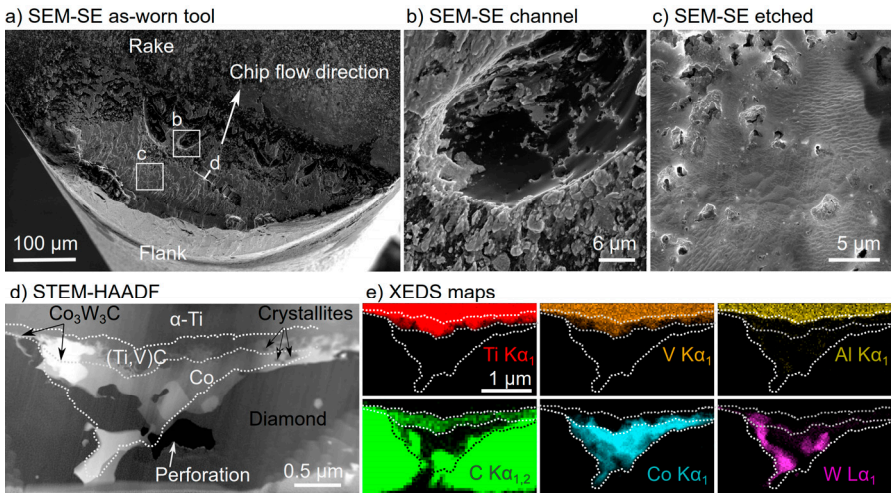


**Fig. 27** Investigation of wear mechanisms in PCD tool used in turning Ti-64 [**I**]. (a) SEM-SE image of the as-worn PCD tool with highlighted regions for investigations. (b) SEM-SE image of a channel formed in the PCD material. (c) SEM-SE image of the surface of the worn PCD tool after removal of the Ti alloy with etchant. (d) STEM-HAADF image of a TEM lamella from the rake showing reaction products. (e) XEDS maps highlighting reaction products.

Diffusion couples showed that the (Ti,V)C reaction product forms above 1000 °C and increases in volume with temperature. The (Ti,V)C is characterized in Fig. 28a–d using STEM-XEDS and SAED to verify the reaction product. Co between the grains of (Ti,V)C (Fig. 28b) indicate its outward diffusion through the (Ti,V)C tool protection layer, indicating that diffusional loss of Co can weaken the grain bonding of PCD in machining and lead to their potential pluck-out if the grain does not have diamond-diamond bonding to another grain. An extreme reaction between PCD and Ti-64 occurs in a diffusion couple subjected to 1300 °C as displayed in Fig. 28e–g, where Co has liquefied and gone through the extra thick TiC or (Ti,V)C layer and alloyed the original α-phased titanium (Fig. 28c) into the β-phase (Fig. 28g). Aluminum is not an interactive element in the formation of reaction products in either as-worn PCD tools or their diffusion couples. Formation of TiC or (Ti,V)C is found in as-worn tools, diffusion couples, and simulations. Liquefaction of Co drastically increases the carbon transport leading to a massive (Ti,V)C layer. Further evidence and details are reported in **Paper VIII**.

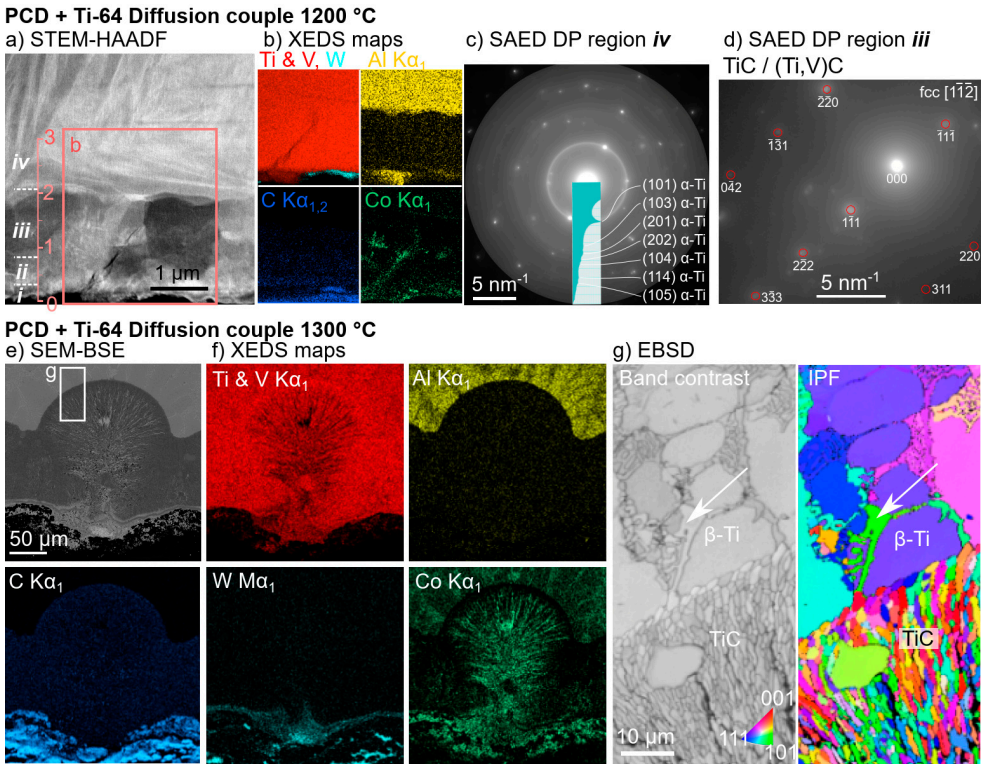


**Fig. 28** Investigation of wear mechanisms in diffusion couple of PCD and Ti-64 at (a–d) 1200 °C and (e–g) 1300 °C [**VIII**]. (a) STEM-HAADF image of interface region. (b) XEDS maps of the interface region. (c) Diffraction pattern of α-Ti. (d) Diffraction pattern of TiC or (Ti,V)C reaction product. (e) SEM-BSE image of interface region. (f) XEDS maps of interface region. (g) EBSD band contrast and IPF of TiC reaction product and the mix of α- and β-phased Ti.

## 5.2 PcBN and Ti-64

In machining Ti alloys with pcBN tools, reported wear morphologies and mechanisms include cratering, flank wear, notching, cracking, chipping, and catastrophic tool failure. Adhesive tests show strong bonding between Ti alloy and cBN that creates a failure junction in the cBN which indicates that adhesive wear in machining could occur [39]. Transformation from cBN to hBN has been found in notch regions of as-worn tools, where hBN is easily removed by the chip flow [98]. Reaction products of TiN, TiB, or $TiB_2$ have been suggested without experimental validation, and cratering has been suggested to be due to adhesive wear [98]. Reaction products formed during friction stir welding Ti-64 are reported to be $TiB_2$ and TiB and diffusional dissolution of B and N that stabilize the α-Ti [106].

In the research reported here, PCD outperformed the pcBN grade by 2–5 times in tool life as the wear rate of pcBN was higher. Catastrophic tool failure due to cracking and fractures were observed in pcBN when turning Ti-64 at high speeds. Before failure, the wear morphology was rake cratering in the form of a chamfer due to the short tool-chip contact length. Despite strong adhesion of Ti-64 to pcBN (Fig. 29a–b), adhesive wear was not an active mechanism as no grain pluck-out was observed after etching (Fig. 29c). Compared to PCD, pcBN does not form channels or ridges. This can be related to the significantly higher temperature level of the cBN to hBN transformation. That occurs above 900 °C, while the graphitization of diamond occurs at 600 °C at ambient pressures [107, 108]. The oxidation resistance has a similar trend, which occurs at 680 °C for diamond while cBN oxidizes at 1190 °C [109]. This excludes the possibility of oxidation wear of pcBN, while it is probable for PCD.

The primary wear mechanism in pcBN when turning Ti-64 at high speeds was the diffusional dissolution of B, N, and binder elements, as indicated in Fig. 29d–e. Diffusional loss causes the major tool material loss that results in cratering and flank wear. The diffusion also results in chemical reactions between tool and workpiece material (Fig. 29e). Diffusional dissolution of B and N is observed in XEDS maps that show their gradually declining concentration in the Ti alloy (Fig. 29e). The maps also show the absence of Al at the pcBN-Ti interface. This further confirms its absence as a reactive element, as is also in the case when machining with PCD. Combining advanced microscopy techniques further verified the formation of nanometric (30–50 nm thick) $(Ti,V)B_2$ layer at the interface between cBN and Ti-64 (Fig. 29e–f), while the presence of Cr binder resulted in formation of a $(Ti,V,Cr)B_2$ reaction product. Both can work as a diffusion barrier. This finding shows that a Cr-based binder can better withstand diffusional attack and contribute to the creation of tool protection layers in pcBN tooling. Because diboride reaction products form in the contact of both cBN and binder sites, a continuous protective layer can form over the tool surface, whereas the tool protection layer in PCD is

limited to binder sites only. More details on the wear of pcBN tooling used in turning Ti-64 are found in **Paper I**.

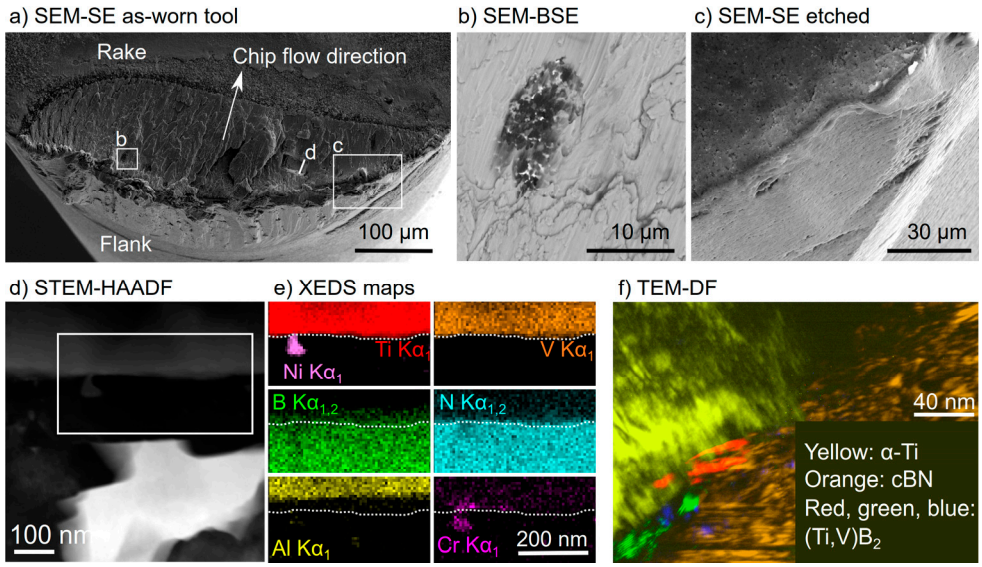


**Fig. 29** Investigation of wear mechanisms in pcBN tool used in turning Ti-64 [**I**]. (a) SEM-SE image of the as-worn pcBN tool with highlighted regions for investigations. (b) SEM-BSE image of exposed pcBN material. (c) Surface of the worn pcBN tool after removal of the Ti alloy with etchant. (d) STEM-HAADF image of interface region. (e) XEDS maps of the interface region. (f) Superimposed TEM-DF images of the interface region highlighting grains of α-Ti, cBN, and $(Ti,V)B_2$ reaction product.

In diffusion couples (Fig. 30), reaction product formation is already observed at 1000 °C, compared to 1100 °C for PCD, which shows the higher dissolution rate that explains the higher wear rate of pcBN. Increased temperatures increase the diffusional loss of B and N where N stabilizes the α-phase of Ti (Fig. 30a–e). Increased temperatures in diffusion couples also show the accumulation of binder elements like Ni, Co, Cr, Mo, and W at the interface due to the loss of B and N and the limited solubility of binder elements in Ti (Fig. 30b–d). The observed wavy interface indicates that the accumulation of binder can locally reduce the diffusion rate. Mo and W are not typical binder elements; the former originates from the Mo sintering cell and the latter from the cemented carbide substrate [110]. These two elements have higher concentrations than Ni, Co, and Cr at the interface, which shows that they are the main diffusion barriers. Ni and Co binder elements have diffused into the Ti alloy (Fig. 30c) which decreases the grain bonding. During machining this could potentially lead to adhesive wear and grain pluck-out. Mo and W have limited solubility in Ti [111, 112] and their addition to the binder mix could result in the formation of a thicker and more stable layer on top of the cBN grains. Such a layer could reduce the outward diffusion of B and N and thus reduce the

wear rate, while simultaneously reducing outward diffusion of the binder elements Co, Ni, and Cr.

In diffusion couples, a layer of Ti(C,N) is formed above the binder layer due to diffusion of N from cBN grains and C from the cemented carbide that travel through the binder in pcBN. This phase is observed in a diffusion couple treated at 1300 °C and is not observed in tools used in machining where such high temperatures are unlikely. Formation of $Cr_2N$ reaction product at the binder layer is observed (Fig. 30c,e) and this phase, like Ti(C,N), is a diffusion couple artifact. However, $(Ti,V)B_2$ reaction product is characterized at the border of Ti-64 and cBN in the diffusion couple, and this reaction product is also observed in as-worn tools used in machining. Its absence in EBSD characterization can be explained by a fine grain size. The order of cBN, binder layer, Ti(C,N), $(Ti,V)B_2$, and α-Ti in the diffusion couple at 1300 °C can be explained by the high permeability of B giving an instantaneous formation of non-diffuse borides that limit the N diffusion, leading to precipitation of Ti(C,N) and $Cr_2N$. Diffusion simulations show formation of borides, nitrides, and α-Ti, which agrees well with what was observed in diffusion couples, although binder elements of Mo, Cr, Ni, and W could not be included in the simulations. More detailed information on the diffusion couple experiments can be found in **Paper VIII**.

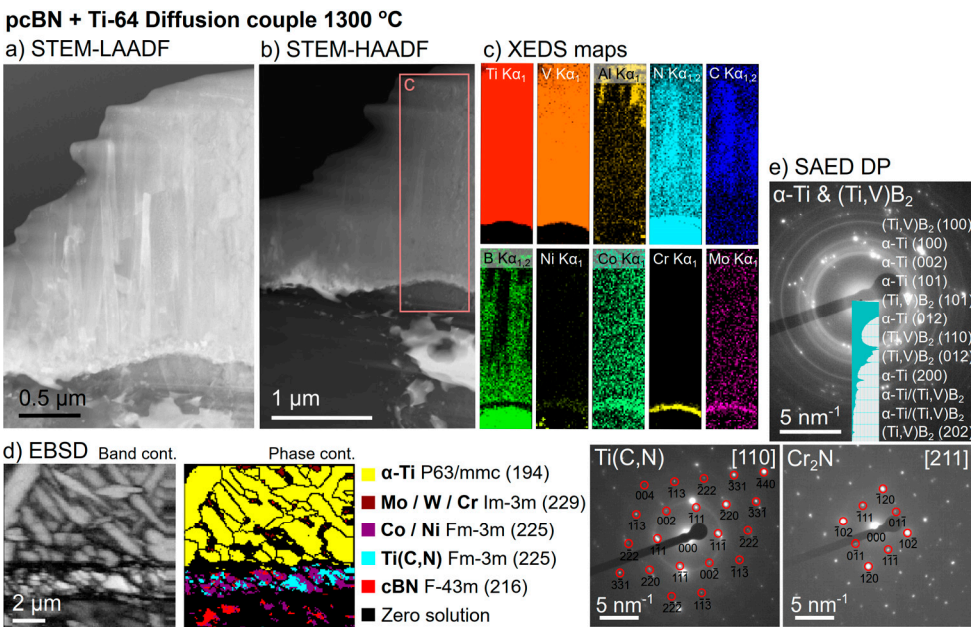


**Fig. 30** Investigation of wear mechanisms in diffusion couple of pcBN and Ti-64 at 1300 °C [**VIII**]. (a) STEM-LAADF image of interface region. (b) STEM-HAADF image of interface region. (c) XEDS maps of the interface region. (d) EBSD band contrast and phase contrast of the interface region showing the presence of α-Ti, binder elements, cBN, and Ti(C,N) reaction products. (e) Diffraction patterns of α-Ti and $(Ti,V)B_2$, Ti(C,N), and $Cr_2N$ reaction products.

## 5.3 Cemented carbide and Ti alloys

In machining Ti alloys using cemented carbide tooling, commonly reported wear modes and mechanisms include cratering, flank wear, chipping, and plastic deformation while less common modes are notch wear, flaking, and catastrophic tool failure. These wear modes may be caused by mechanically induced, chemical, or diffusional wear mechanisms. Some studies report mechanical wear mechanisms like attrition that are linked to the higher shear stresses brought by hcp α-Ti due to its lower number of slip systems than β-Ti, which is more ductile [104]. A mix of attrition, abrasion, and adhesive wear are also reported [113]. However, there are no hard abrasive inclusions in Ti alloys. Other studies suggest adhesive wear as a dominant wear mechanism because failure junction tests show that fractures occur in the cemented carbide due to strong adhesion to the Ti alloy [39, 114].

More studies report diffusion and chemical reactions as responsible for tool material loss. Outward carbon diffusion from WC grains is a main contributor that if accumulated to 35 at.% leads to formation of TiC or (Ti,V)C, as Ti is a strong carbide former [32, 115–119]. Due to carbon loss, residual W remains at the interface because of its low solubility in Ti [32, 118–122], as has been observed in as-worn tools and diffusion couples [30–32, 115, 122–124]. Outward diffusion of Co has also been suggested [31, 32, 115, 123] in which depleted regions can be filled with Ti [31, 120]. It has been suggested that η-phase $Co_3W_3C$ or $Co_6W_6C$ form as reaction products, but this phase is observed only in diffusion couples [30, 114, 122, 125, 126]. Many of the studies in which these were observed used mm to µm sized resolution techniques like SEM-XEDS, or XRD that have no spatial resolution, and can indicate the presence of reaction products. A few studies used advanced microscopy techniques at nano to atomic scale resolution like TEM to experimentally verify the presence of reaction products.

The research reported in this thesis shows that when turning at high speeds, Ti-64 adheres to and covers the worn surfaces of the cemented carbide tool. More details on the wear mechanisms in cemented carbide tooling in turning Ti-64 are found in **Paper II**. The cross-section in Fig. 31a–b reveals that the thickness of the covering Ti alloy can vary from 30 µm to less than 1 µm. At the end of tool life, surface WC grains are fractured and have lost the grain bonding about 5 µm into the tool, and damaged WC grains are removed by the chip flow (Fig. 31a–b). Decarburization due to outward C diffusion is noted as a brighter Z-contrast rim of W on surface WC grains. STEM-XEDS reveals the stronger concentration of W, and SAED further confirms its presence (Fig. 31c–f). The W layer is brittle and is gradually removed by the chip flow. The W may locally stabilize the β-phase of Ti in which the substitutionally diffusing elements like Co have higher mobility, leading to a higher wear rate. However, the presence of (Ti,V)C reaction product at the interface due to outward carbon diffusion locally reduces the diffusion rate and works as a tool protection layer. As when turning Ti-64 with PCD and pcBN, the Al in Ti-64 does

not contribute to the formation of reaction products and does not progress into the cemented carbide, which means that Al is not a participating element in the wear.

Outward Co diffusion is visible as empty binder sites at the interface where Ti has taken its place (Fig. 31c–f). The formation of intermetallic $TiCo_2$ works as a diffusional block to further Co diffusion. The Co in near-surface regions has the fcc structure high-temperature phase, showing the quenching effects of the coolant at the end of machining. Loss of Co binder results in reduction or loss in grain bonding that enables the removal of WC grains by the chip flow. Additionally, more Ti alloy can surround the exposed WC grains and accelerate the diffusional wear of WC. Formation of intermetallic $Co_3W$ in near-surface regions is confirmed in turning Ti-64 and Ti-5553 using similar WC-6%Co tooling as explained in detail in **Papers II** and **VII**. This intermetallic phase works as a diffusional block for Co. Its formation is preceded by C diffusion through Co into the Ti alloy. The released W with lower mobility in Co accumulates together with the already dissolved W in the binder from sintering and forms intermetallic $Co_3W$. Formation of $TiCo_2$ can work as a diffusion barrier to Co (Fig. 31g).

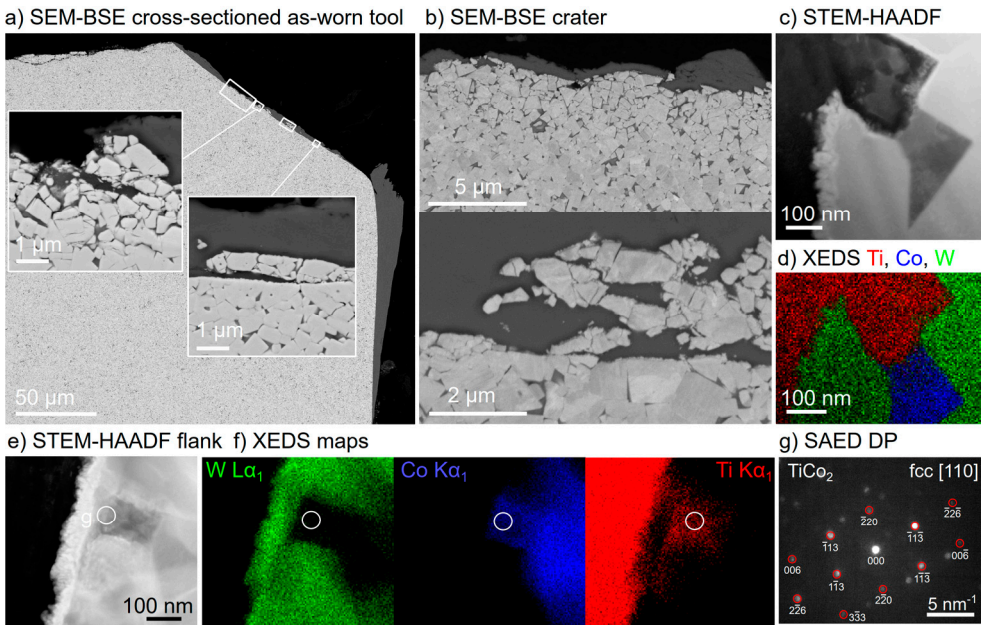


**Fig. 31** Investigation of wear mechanisms in a WC-6%Co tool used in turning Ti-64 [**II**]. (a) SEM-BSE image of the cross-sectioned as-worn tool with highlighted regions. (b) SEM-BSE image of worn cemented carbide interface to the adhered Ti alloy at the center of the crater. (c) STEM-HAADF image of the interface. (d) Superimposed XEDS maps of interface region. (e) STEM-HAADF image of the interface from the flank region. (f) XEDS maps of interface. (g) Diffraction pattern of $TiCo_2$ reaction product.

High temperature at the center of the crater in combination with a high chip flow deplete the cemented carbide of C, W, and Co more intensely and result in massive

material loss (Fig. 31a). The conditions near the stagnation point have a similarly high temperature but lower or close to zero material flow. Thus, conditions in this region resemble the conditions in a diffusion couple in which outward diffusing elements can saturate and potentially form TiC or intermetallic phases.

A sub-beta transus (850 °C) heat-treated WC-6%Co tool with adhered CP-Ti chip after removal with the quick stop method in **Paper IX** showed exaggerated reaction products at the tool-chip interface (Fig. 32a). The absence of alloying elements in the Ti enables a straightforward understanding of the diffusional and chemical wear mechanisms of the cemented carbide. The combined results of machining using the quick stop method and diffusion couple method captures the common wear mechanisms (Fig. 32a). The interface region contains an enrichment of W segments at the interface due to the diffusional loss of C from WC grains, where C travels into the CP-Ti in such quantity that TiC forms (Fig. 32b–c). Outward Co diffusion into original α-Ti has transformed it into the β-phase as Co is a β-stabilizer.

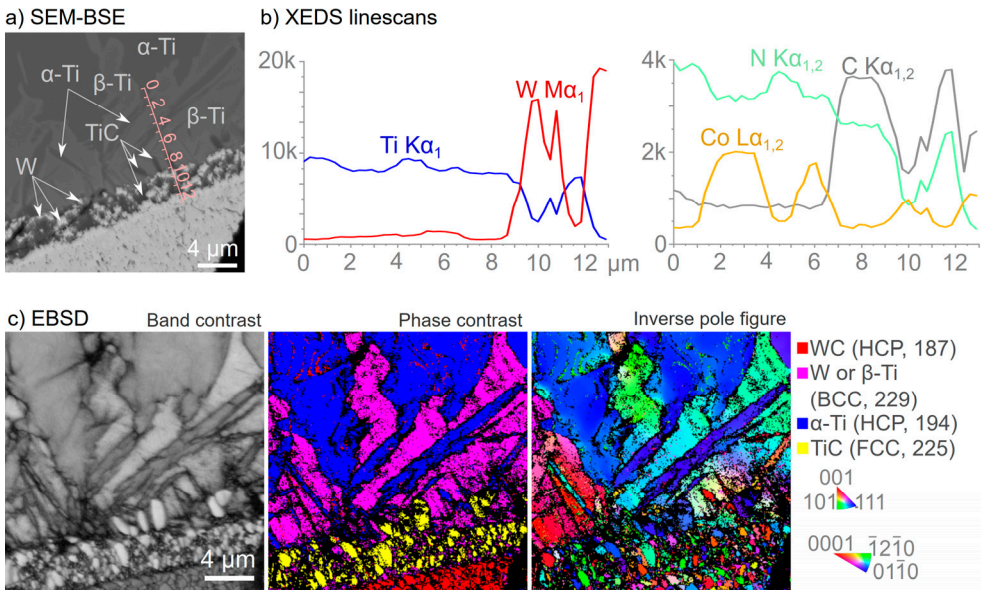


**Fig. 32** Investigation of wear mechanisms in WC-6%Co tool used in turning CP-Ti after a quick stop test and heat treated at sub-beta transus temperature [**IX**]. (a) SEM-BSE image of the cross-sectioned as-worn tool with highlighted phases and reaction products. (b) XEDS linescan of the interface region. (c) EBSD band contrast, phase contrast, and IPF showing the WC grains, α-Ti, and W, β-Ti, and TiC reaction products.

Diffusion couples in **Paper VIII** reveal the formation of TiC reaction product and W fragments at 1000 °C (Fig. 33a). With increasing temperature, the TiC layer and the amount of W increase due to diffusional loss of C whereas at 1300 °C the WC become rounded due to the higher diffusional loss of C. At this high temperature, partial melting of Co accelerates the C transport which facilitates massive C loss

leading to grain rounding. Formation of TiC is confirmed by using STEM-XEDS mapping, EBSD, and SAED (Fig. 33b–e). EBSD shows the polycrystalline TiC layer in which outward diffusing elements like C and Co need to go around grain boundaries indicating that the TiC layer effectively reduces their diffusion rate.

XRD analysis of the interface region after treatment at 1200 °C reveals the likely formation of η-phase $Co_3W_3C$ and $Co_6W_6C$ (Fig. 26). This is a brittle phase that if formed during machining might be removed by the chip flow or might act as a diffusion barrier. Diffusion couples further confirms Al as a non-interactive element (Fig. 33c). Diffusion simulations confirm the reaction products TiC, β-Ti, and η-phases, while it is unclear whether the predicted intermetallic $Co_7W_2(Co,W)_4$ formation can nucleate.

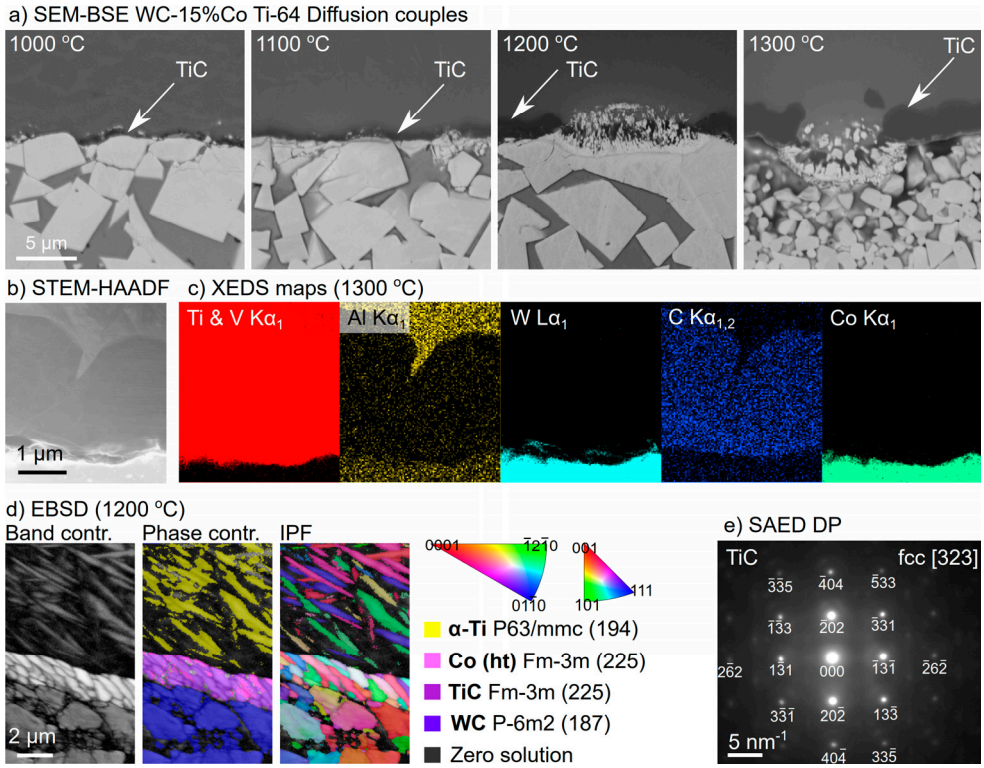


**Fig. 33** Investigation of wear mechanisms in diffusion couple of WC-15%Co and Ti-64 at 1000–1300 °C [**VIII**]. (a) SEM-BSE images of the interface region with increasing temperature with highlighted TiC reaction product. (b) STEM-HAADF image of interface region. (c) XEDS maps of interface region. (d) EBSD band contrast, phase contrast, and IPF of interface with α-Ti, Co binder, WC grains, and TiC reaction product. (e) Diffraction pattern of TiC reaction product.

Chemical wear with oxidation of cemented carbide is not observed in as-worn tools used in turning Ti alloys, but it is an active mechanism in milling as further detailed in **Paper III**. The cyclic engagement and exit of the tool in the workpiece material

allow oxygen to access the hot and worn regions of the tool. This is not the case when the tool is continuously in cut during turning, as oxygen ingress is limited. Diffusional dissolution of WC grains and outward Co diffusion are active wear mechanisms in milling Ti alloys ranging from near-α, α+β, to near-β. The diffusion results in weaker WC grains in the surface regions, and lack of dampening Co binder results in fracturing of WC grains and their removal with the chip flow. Voids in the Co phase near the interface are due to either plastic deformation or Kirkendall porosity. In milling these Ti alloys, extensive cracking that propagates between WC grains in the Co binder results in flaking and chipping. The stochastic behavior of crack occurrence results in varying tool life when repeating the same cutting operation.

The oxidation is higher when milling in α+β Ti-6246 and present but to a lesser extent when milling near-α Ti-6242. It was not observed when milling near-β Ti-5553 at a 25% lower cutting speed, where the oxidation onset temperature was likely not reached. The strength of these alloys is the highest for near-β Ti-5553, followed by α+β Ti-6246, and then near-α Ti-6242. The highest wear rate was found when milling α+β Ti-6246, followed by near-β Ti-5553. Near-α Ti-6242 had the lowest wear rate due to the combination of the strength of the machined alloy and the level of oxidation. The ingress of the oxidation reached several μm into the WC-12%Co tool (Fig. 34a) and resulted in the formation of $CoWO_4$ phase (Fig. 34b–c) that precipitated as smaller grains than the original Co that allowed crack propagation. The formation of $CoWO_4$ is likely at the expense of diffusional dissolution or oxidation of WC shown as rounder WC grains near the $CoWO_4$ phase. The Co binder regions are transformed from the original fcc to hcp due to deformation caused by the cyclic loading.

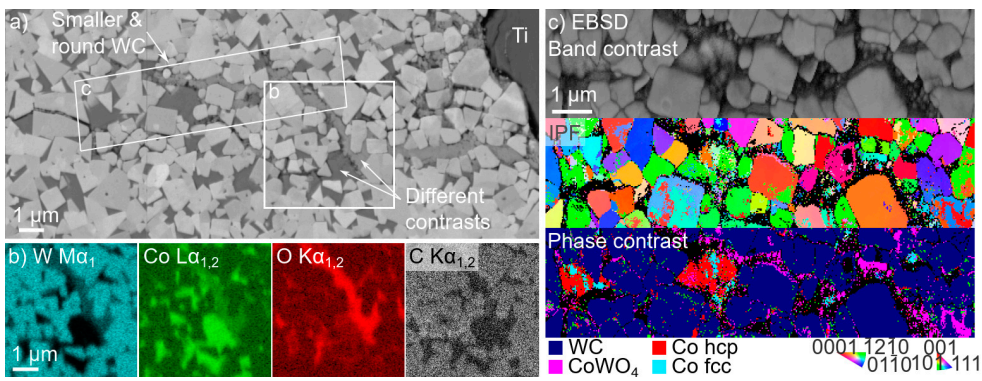


**Fig. 34** Investigation of wear mechanisms in a WC-12%Co tool used in milling Ti-6246 [**III**]. (a) SEM-BSE image of cemented carbide with the adhered Ti alloy on the right side and highlighted regions of investigation. (b) XEDS maps of oxidized binder region. (c) EBSD band contrast, IPF, and phase contrast with WC grains, original fcc Co, $CoWO_4$ reaction product, and deformed hcp Co.

## 5.4 $Ti_{0.45}Al_{0.55}N$ coatings with and without NbN overlayer and Ti alloys

It is a challenge to find suitable coatings for cemented carbide in machining Ti alloys due to the high chemical reactivity of Ti. Common TiN or Ti(C,N) coatings have shown no appreciable advantage over uncoated cemented carbide in machining Ti alloys and thus remains the traditional choice in Ti machining. A PVD-applied $Ti_xAl_{1-x}N$ coating with stoichiometry ratio x = 0.4–0.7 is commonly recommended for machining Ti and Ni based alloys [13, 127] because it has a lower friction coefficient than TiN, lower residual stress and cracks than CVD-applied coatings, and high oxidation resistance and hot hardness [128–131].

Delamination, crack nucleation, and abrasion are reported in machining Ti alloys and steels with $Ti_xAl_{1-x}N$ [132–134]. Oxidation of $Ti_xAl_{1-x}N$ forms a diffusion barrier of $Al_2O_3$ at temperatures above 800 °C [128–130]. An extra NbN overlayer is beneficial because it has higher hardness than other binary nitrides [135] and is thus becoming increasingly popular in milling Ti alloys and steels. Mechanical wear like flaking, chipping, and delamination are reported [136–138], while the formation of a protective oxide film based on Al, Cr, or Nb reduces frictional energy and the wear rate [139, 140]. This oxide film is unlikely to form during turning operations because of the limited ingress of oxygen to the wear zones.

Initial wear of $Ti_{0.45}Al_{0.55}N$ with and without NbN in turning α+β Ti-64 and near-β Ti-5553 is based on diffusional dissolution and mechanical wear. Diffusional dissolution is more intense in turning Ti-64 and mechanical wear takes over when turning Ti-5553 due to the higher strength of this Ti alloy. However, Fig. 35a–b shows that the $Ti_{0.45}Al_{0.55}N$ on the tool edge in turning Ti-5553 is worn by the outward Al and N diffusion. The same image shows a crack. Cracks are observed more frequently in turning Ti-5553 than α+β Ti-64 due to the higher yield and tensile strength and hardness of Ti-5553, which imposes higher stress on the tool edge. The combination of a higher β-phase fraction in the Ti-5553 in contact with the coated surface contributes to a higher diffusion rate of the Al and N, as their mobility is higher in β- than α-phased titanium.

The combination of higher strength, hardness, and mobility for β-Ti explains why there are more coating fractures when turning Ti-5553 than when turning Ti-64. Diffusional dissolution of the $Ti_{0.45}Al_{0.55}N$ coating weakens its integrity and can act as a catalyst for fracturing along the tool-chip contact surfaces. Diffusion couples with CP-Ti, and thus no interfering alloying elements, further reveal the outward diffusion of Al and N. Diffusion of Al and N stabilize α-Ti at the interface (Fig. 35c–e) in which substitutionally diffusing elements have lower mobility. The loss of Al forms a TiN layer at the interface toward the CP-Ti.

$Ti_{0.45}Al_{0.55}N$ in the crater and flank region wear rapidly and are removed within less than one minute of engagement time for the cutting conditions in the study, but the coating remains around the edge line for longer. The geometry of the edge line is retained by the protection of the coating, and the crater and flank wear grow until the point of collapse due to the geometrical change. However, once the coating on the edge line is removed, cemented carbide wears rapidly, which can result in massive tool material loss, as shown in Fig. 31a. Spinodal decomposition of $Ti_{0.45}Al_{0.55}N$ is promoted at the active cutting pressures and temperatures which results in a volume increase that induces cracks and reduces its hardness and wear resistance [141]. This can contribute to the wear in flank and crater regions. It has also been demonstrated that plastic deformation of the $Ti_{0.45}Al_{0.55}N$ coating is not an active wear mechanism (Fig. 24), but common droplet defects seen in Fig. 35a become mechanical failure points. Further details on the wear of $Ti_{0.45}Al_{0.55}N$ with and without NbN in turning are presented in **Paper IX**.

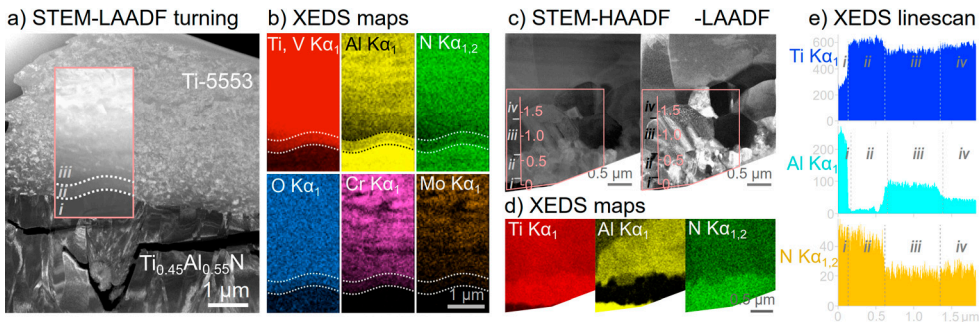


**Fig. 35** Investigation of wear mechanisms in $Ti_{0.45}Al_{0.55}N$ coated carbide in (a–b) turning Ti-5553 and in (c–e) diffusion couple with CP-Ti at 1200 °C [**IX**]. (a) STEM-LAADF image of interface region. (b) XEDS maps of interface region. (c) STEM-HAADF and -LAADF images of interface region. (d) XEDS maps of interface region. (e) XEDS linescan of interface region.

Ingress of oxygen to the contact regions is limited in continuous turning which limits or prevents oxidization. However, milling with cyclic engagement and exit of the tool from the workpiece allows oxidation of the contact regions. Formation of tribo-oxides of the NbN overlayer is likely in milling, but in turning other wear mechanisms are expected. The extra NbN layer delays the diffusion wear of $Ti_{0.45}Al_{0.55}N$ by reducing the diffusion rate of substitutionally diffusing Al that moves around NbN grain boundaries. However, Al diffusion is restricted but not stopped, and its diffusion results in a 200 nm thin TiN layer below NbN. Simultaneous outward diffusion of Nb stabilizes β-Ti, which makes it easier for Al to move away from the interface once it has passed through the NbN layer. Once Nb has diffused, so should N; it moves interstitially and travels a longer distance from the interface. Outward diffusing Nb and Al sporadically form intermetallic $Nb_3Al$ above the NbN layer and locally block further diffusional dissolution of NbN

and $Ti_{0.45}Al_{0.55}N$. The intermetallic $Nb_3Al$ has a high brittleness of $K_{1c}$ = 1.1 $MPa^{1/2}$ [142] and may thus be easily removed by the chip flow.

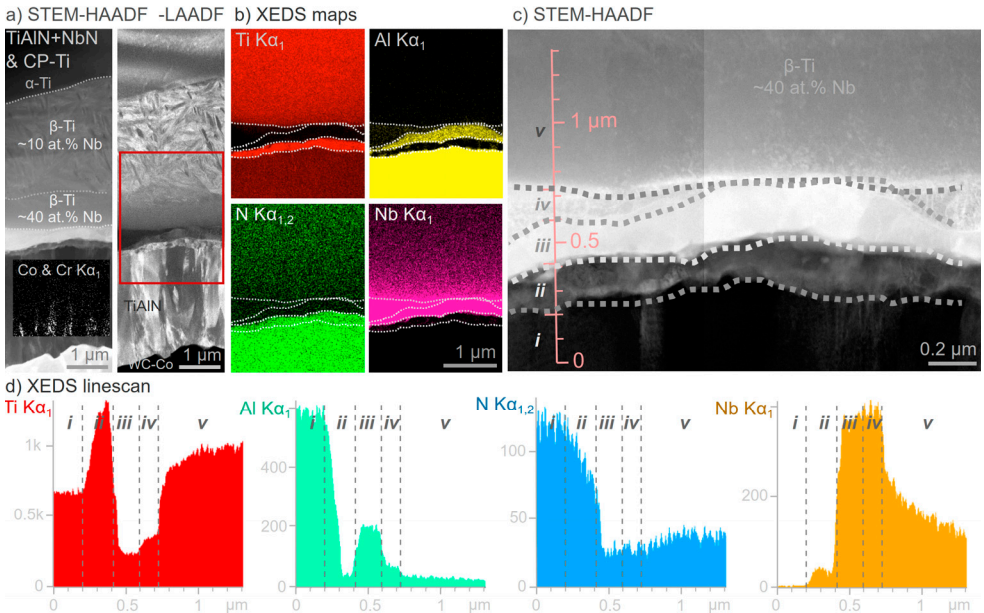


**Fig. 36** Investigation of wear mechanisms in $Ti_{0.45}Al_{0.55}N$-NbN coated carbide in diffusion couple with CP-Ti at 1200 °C [**IX**]. (a) STEM-HAADF and -LAADF images of interface region with highlighted phases and an inset XEDS map of Co and Cr. (b) XEDS maps of interface region. (c) STEM-HAADF image of near-interface region with highlighted areas of reaction products. (d) XEDS linescan of the interface region.

**Paper III** investigates wear mechanisms of $Ti_{0.45}Al_{0.55}N$-NbN when milling Ti alloys ranging from near-α Ti-6242, α+β Ti-6246, and near-β Ti-5553 at moderate cutting speeds. The paper reports rapid coating wear in the near-edge region after only 5 seconds of total engagement with the workpiece material. The main wear mechanism in the coating when milling these alloys is crack formation within the bulk of the coating, or smaller microfractures that are removed by the chip flow. There are no thermal cracks or delamination, but diffusional dissolution of the coating is not excluded and may be present to a small extent. However, the extensive mechanical wear points to the need for a more robust coating formulation.

## 5.5 Ti(C,N)-$Al_2O_3$ coated carbide and CGI

CVD-coated Ti(C,N)-$Al_2O_3$ cemented carbide is recommended for increased machining performance in CGI. However, MgO inclusions in steels react with the $Al_2O_3$ coating during turning forming $MgAl_2O_4$ spinel that is easily removed by the chip flow [143]. Other wear modes and mechanisms like abrasion, crack nucleation and propagation, delamination, and detachment between coating layers are reported in turning steels with Ti(C,N)-$Al_2O_3$ [134]. In turning or milling CGI with the same coatings, reported wear mechanisms are either adhesive or abrasive wear or a combination of these [144–148], but thermal cracks and chipping have also been reported [145, 149]. Adhesion of CGI to the coating is common and is more intense when it occurs to the exposed cemented carbide once the coating is removed [144–146, 150–152].

In milling CGI, a 20% longer tool life can be attained by using sustainable machining conditions with minimum quantity lubrication (MQL) compared to dry conditions. During milling, there is rapid wear of substrate cemented carbide once the coating layers are removed as CGI tends to adhere to the exposed cemented carbide (Fig. 37a). Because cemented carbide wears faster than the coating, erosion of the cemented carbide can undermine the coating and cause its mechanical failure. Oxidation of the exposed cemented carbide occurs sporadically in notch regions. At a lower cutting speed of $v_c$ = 150 m/min, there is an equal mix of cratering and flank wear, while at a medium cutting speed of $v_c$ = 250 m/min, flank wear dominates. At a higher cutting speed of $v_c$ = 330 m/min, cratering tends to dominate due to the higher cutting temperature and higher flow rate of abrasive inclusions. Mechanically induced delamination of both $Al_2O_3$ and Ti(C,N) occurs sporadically (Fig. 37b), and plastic deformation of the tool edge can occur and mechanically induce cracks on the flank.

Ti(C,N) on the rake face is worn by diffusional dissolution and abrasion, while on the flank it is worn by debonding, abrasion, and micro-fracturing. Fractures can be seen in Fig. 37c, which are filled with oxidized CGI elements that can transform the coating to $TiO_2$ rutile as reported in other studies [44, 153]. As the fractures contract and expand during the cyclic cutting, they amplify mechanical and thermal stresses that trigger delamination. Plastic deformation of Ti(C,N) is known to occur [154], but its absence in present work is explained by the small grain size. Mg is present on top of the $Al_2O_3$ layer. TEM-based investigation points to the likely formation of an Fe and Mn doped (Mg,Fe,Mn)$Al_2O_4$ spinel that is easily removed by the chip flow, creating scratch marks (Fig. 37d). Because of the larger number of slip planes in spinel than $Al_2O_3$, the spinel is more easily superficially sheared and worn by abrasive inclusions present in the CGI.

In regions of exposed cemented carbide without adhered CGI, deposition of MgO and $SiO_2$ inclusions works as adhesion blockers that partly protect the cemented

carbide from diffusion wear because contact with CGI is limited. Exposed cemented carbide with adhered CGI is worn by the diffusional dissolution of WC grains, making them rounder. In addition, outward diffusion of Co binder reduces grain bonding and enables cracking in the surface cemented carbide that is removed by adhesive wear (Fig. 37b). At stable adhesive conditions, outward C and Co diffusion results in their reaction to Fe forming $(Fe_x,Co_{1-x})_3C$, which is found to periodically fracture and delaminate (Fig. 37e).

Oxidation has a positive effect when adhered CGI oxidizes to form tool protection layer $Fe_2SiO_4$ ceramic (Fig. 37e). It is similar to other oxide protective layers forming *in-situ* like $\gamma$-$Al_2O_3$ and $(Al,Fe,Cr)_3O_4$ or $(Al,Cr,Ti)_3O_4$ spinel [47, 155-157]. This expands on the family of known oxide tool protection layers. Local inward diffusion of Fe to binder sites accompanied by its oxidation results in the formation of complex oxides $FeWO_4$ and $CoWO_4$ that speed up the oxidative stress on WC and Co. This results in the formation of cracks on the rake (Fig. 37f) as the oxidized Co in CoO and $CoWO_4$ has a larger volume than Co. This expansion widens the cracks, creating a positive feedback loop for further O ingress. These cracks weaken tool integrity and results in spontaneous tool failure. Details of wear of Ti(C,N)-$Al_2O_3$ coated carbide in milling CGI are found in **Papers IV** and **V**.

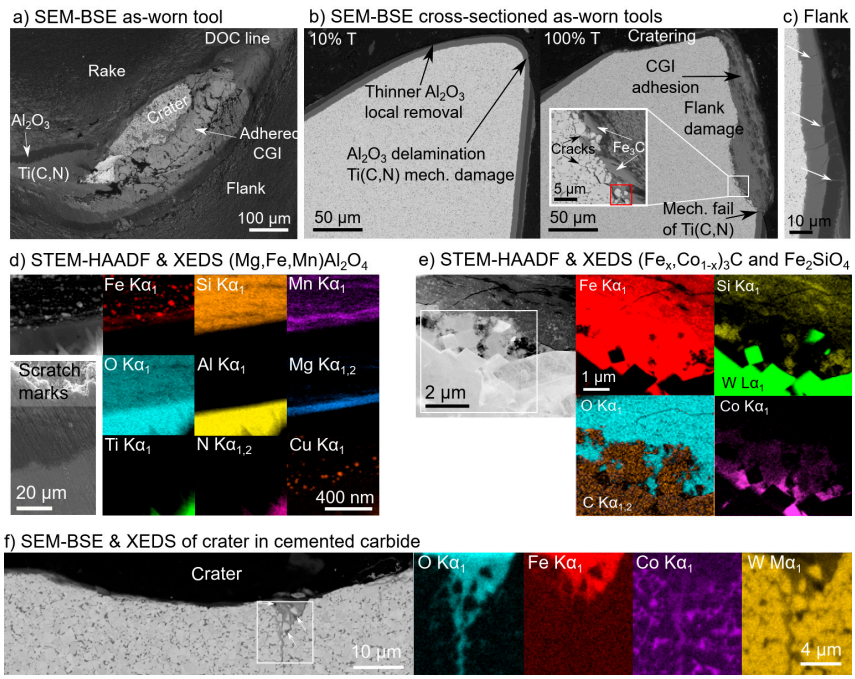


**Fig. 37** Investigation of wear mechanisms in Ti(C,N)-$Al_2O_3$ coated carbide tools used in milling CGI-450 [**IV**, **V**]. (a) SEM-BSE image of an as-worn tool, (b) cross-sectioned as-worn tools at 10% and 100% engagement time, and (c) cracks within the coating. (d) STEM-HAADF and XEDS maps of interface between $Al_2O_3$ and adhered CGI with possible formation of $(Mg,Fe,Mn)Al_2O_4$ and (e) $(Fe_x,Co_{1-x})_3C$ and $Fe_2SiO_4$ reaction products. (f) SEM-BSE image and XEDS of oxidized binder.

## 5.6 PcBN and GCI

The poor machining performance of non-aged GCI (less than 6 days since the GCI material was cast) is caused by excessive flank wear, but it can be compensated for by adjusting the cutting speed. An optimal cutting speed of $v_c$ = 1200 m/min was identified (Fig. 38a). Tools used for machining at this speed had minimal tool wear due to deposition of protective $Al_2O_3$ and MnS (Fig. 38b). This speed is higher than the industrial standard and offers higher efficiency both in material removal rate and reduced costs related to storage and logistics. The higher cutting speed has been successfully implemented in industry for the last four years [158].

The low tool wear due to protective deposits in machining non-aged GCI is related to process temperature. Lower cutting speeds up to the industrially common $v_c$ = 900 m/min generate lower tool temperatures, resulting in a lack of protective deposits, but still sufficient for diffusional dissolution that causes tool degradation. Cutting speeds higher than the optimum identified in the previous paragraph result in deposition of weaker $(Fe,Mn)_2SiO_4$ and (Fe,Mn)O with cBN oxidation that drives tool wear. Tools used to machine non-aged GCI can partially be worn by self-abrasion of loose cBN grains, but additional micro-grooves on individual cBN grains on the worn flank region are either oriented with or contrary to the material flow direction, which contradicts abrasion by (Ti,V)C inclusions. The micro-grooves are likely a result of diffusional dissolution of cBN. Further evidence of the protective oxides and their relation to performance is presented in **Paper VI**.

Infrared thermography measurements reveal that tool temperatures up to 170 °C higher are reached when machining aged GCI due to its higher hardness and strength in the aged state. The higher temperatures ensure stable protection by deposition of mainly $Al_2O_3$, $SiO_2$, and MnS on tools used to machine aged GCI. The higher friction and temperature occur because the friction coefficient between $Al_2O_3$ and ferrous materials is μ = 0.49 [159] while it is μ = 0.31 for pcBN [160].

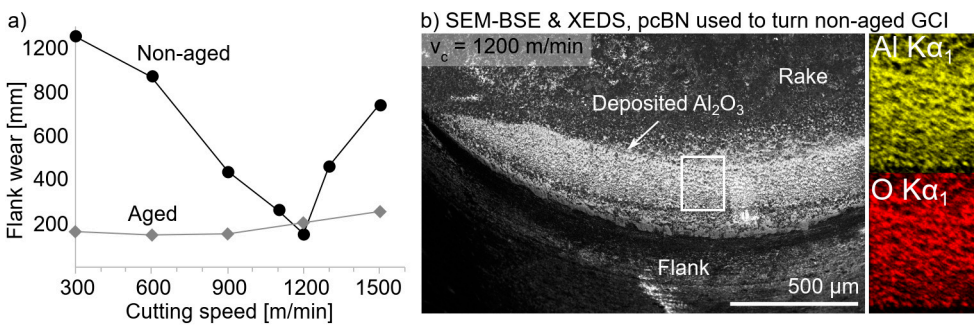


**Fig. 38** (a) Tool flank wear at varying cutting speeds in turning both non-aged (less than 6 days from casting) and completely aged GCI with local optimum of $v_c$ = 1200 m/min in non-aged GCI. (b) SEM-BSE and XEDS maps of etched pcBN tool used to turn non-aged GCI with $Al_2O_3$ deposit [**VI**].

## 5.7 Modeling and simulation of wear mechanisms

Thermodynamic modeling and diffusion simulations are cost-efficient ways of understanding and predicting the diffusional and chemical wear that are common when cutting difficult-to-machine materials like Ti alloys. This method can also be used in the development of new tool material solutions. It can, for example, be used to screen or broaden promising material systems without having to perform tool life testing and subsequent experimental tool wear analysis on a full test matrix. It thus makes for greater sustainability by minimizing workpiece material consumption and the energy and costs related to machining, sample preparation, and microscopy. The method can also be used to design tool materials or alloys that promote the formation of diffusion barriers or tool protection layers that prolong efficient tool life.

Experimental tool wear analysis is important for understanding and verifying the actual wear mechanisms that serve as input data and for setting boundary conditions in modeling and simulations. In this initial work, experimental data were used as input for thermodynamic modeling using ThermoCalc software and diffusion simulations using DICTRA software to show that it is possible to create reliable models that can be used in similar materials systems without the need for costly machining trials and microscopy investigations, as presented in **Papers III**, **VII**, and **VIII**.

Simulations of the PCD-Ti system described in **Paper VIII** showed the formation of Al-based reaction products, which is unlikely as Al has been experimentally shown to be a non-interactive element. However, the simulations were accurate as regards the other reaction products. This result shows the need for knowledge of material combinations so as to be able to critically analyze simulation results. The simulation also showed a thicker reaction layer than the experimental observations. The simulations shed light on the similar permeabilities of Co and C over short distances. Co diffuses substitutionally at a lower mobility rate than C, but has higher solubility in Ti than C. C diffuses interstitially at a higher mobility rate, but has lower solubility in Ti than Co, which explains the formation of TiC at the interface with stabilized β-Ti by Co that occurs further from the interface than TiC.

For the pcBN-Ti system in **Paper VIII**, the complexity of the binder necessitated simplification of the boundary conditions and simulations were inconclusive due to numerical difficulties. This result shows the limitations of the method, for the need for simplification means that it cannot completely represent the original composition. However, the initial wear mechanisms could be simulated and the thickness of reaction products at the interface was accurate. About half of the suggested reaction products were found experimentally, and permeability simulations did explain the order of formed reaction products.

For the cemented carbide-Ti system in **Paper VIII**, the simulated reaction products were similar to those found in diffusion couples, but not all are found in as-worn

tools (e.g. $M_6C$ and $M_{12}C$). A different intermetallic phase was indicated by the simulations, but it is unclear whether it can nucleate. Simulations in **Paper VII** show the stability of $Co_3W$ up to 1130 °C, and indicate that the saturation of W in Co binder leads to its formation. Intermetallic $Co_3W$ is found closer to the interface in the flank region rather than the crater in experimental samples, and can be explained by interstitial C diffusion through Co, which is enabled at lower temperatures than substitutional diffusion of Co and W.

Thermodynamic calculations in **Paper III** showed initial oxidation of Cr followed by the formation of $CoCr_2O_4$, $CoWO_4$, and CoO. The calculations also showed that $Co_3O_4$ can form when complete oxidation of the Co binder occurs when milling Ti alloys. The dissolved W in the binder is enough to form $CoWO_4$. The rounder WC grains near the oxide product (Fig. 34) could be explained by their oxidation or earlier diffusional dissolution.

The analysis of the phases formed and the diffusion process at the tool-chip/workpiece interface can be complex due to the large number of elements present. Therefore, the STEM-XEDS images from the cemented carbide used in turning Ti-64 were also evaluated using principal component analysis (PCA) to find chemical correlations and help separate signals from the phases present. This is described in more detail in **Paper X**. PCA can aid XEDS analysis by de-noising the spectra and finding chemical correlations by using simulated spectra. The results confirmed the presence of W at the interface and ruled out the intermediate $W_2C$ phase, indicating the direct transformation to W after outward diffusion of C. PCA can thus be used as an extra step in the analysis of XEDS imaging and complements SAED when studying the presence of phases.

## 5.8 Tool performance

Wear mechanisms drive the rate of tool degradation and the loss of tool material, and directly affect tool life and tooling performance. Three machining methods are explored in the machining of the selected workpiece materials, namely continuous turning (section 2.1), down face milling (section 2.2), and external circular milling (section 2.3). The selected wear criterion was the flank wear VB, which was measured incrementally until reaching or exceeding the predefined value. The wear criterion varied between 200 μm to 300 μm depending on the selected insert geometry and the shape of the workpiece materials, as related to industrial practices of attainable product quality. These criteria are within the recommended values in the ISO standards introduced in section 4.1.

Basic continuous turning was initially used to explore the performance and wear mechanisms of commercial PCD, pcBN, and cemented carbide in the common α+β Ti-64. In a PCD tool with multimodal grain size, a (Ti,V)C cap formed in the

presence of binder. By changing to another PCD grade with a smaller grain size (1 µm) and higher binder content, the protective carbide could merge and form a continuous protective layer that reduced the outward diffusion of C from diamond to Ti-64. The effect of the formation of this layer and the reduction in diffusion wear can be observed in Fig. 40a , which shows the longer tool life obtained. Commercial PCD and pcBN turning Ti-64 demonstrate significant tool life at the cutting conditions in Fig. 40b. The potential attractiveness of PCD is demonstrated by its having a 2–5 times longer tool life than pcBN due to the higher diffusion rate in pcBN.

Commercial uncoated cemented carbide is used when machining at lower cutting speeds than with ultra-hard tooling, and Fig. 40c shows a less than 5 minute tool life at cutting speeds above $v_c$ = 200 m/min. A longer tool life of above 20 minutes is obtained by reducing the cutting speed and using a higher coolant pressure. This additionally shows the effect of cooling on the wear rate as it effectively reduces the rate of diffusional dissolution. The lower usable cutting speed with cemented carbide compared to high-performing PCD can still be cost effective due to the lower cost of cemented carbide. Fig. 39 shows an 8% longer cycle time and lower material removal rate when using cemented carbide (Fig. 39a), but the higher price of PCD also increases the cost of the part. PCD and cemented carbide become cost neutral at a long tool life of 30 minutes (Fig. 39b).

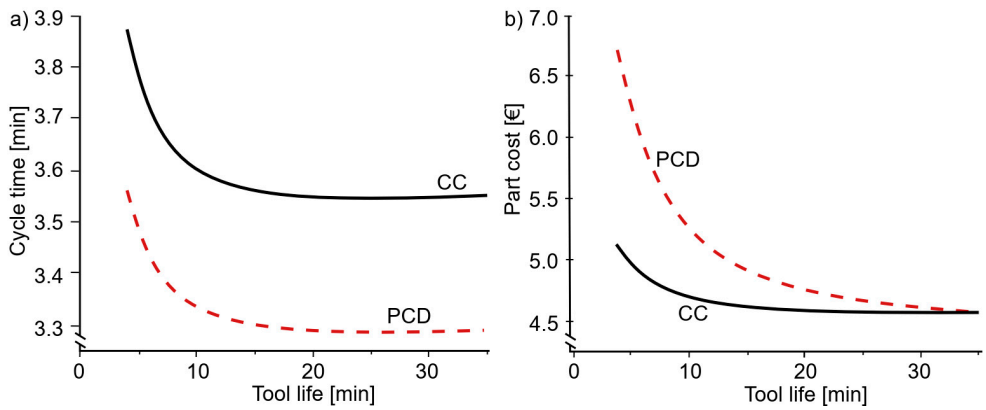


**Fig. 39** Cost performance ratio estimations for uncoated cemented carbide and PCD in turning Ti-64 displayed as (a) cycle time and (b) the part cost as a function of tool life when removing 10 $cm^3$ of work material [**XI**].

In milling Ti alloys (Fig. 40d–f), both commercial uncoated cemented carbide and PVD-coated $Ti_{0.45}Al_{0.55}N$-NbN tools were evaluated. External circular milling was employed to make the most use of the cylindrical bars. Rapid coating removal and stochastic formation of crack networks within the cemented carbide explain the variation in tool life. The highest wear rate was found when milling α+β Ti-6246 (Fig. 40e), followed by a moderate wear rate of near-β Ti-5553 (Fig. 40f). The lowest wear rate of the three alloys was obtained for near-α Ti-6242 (Fig. 40d) owing to the high oxidation wear that enables deep crack formation, the high diffusional dissolution, and the moderate strength of α+β Ti-6246. Higher strength and diffusional dissolution drive the wear rate in near-β Ti-5553. The lower wear rate in near-α Ti-6242 is explained by its lower strength and lower diffusional dissolution and oxidation.

Common down face milling was employed in machining CGI-450, with the test bars designed to resemble the geometries of engine blocks or cylinder heads. Commercial CVD Ti(C,N)-$Al_2O_3$ cemented carbide of steel-cutting grade demonstrated the lowest wear rate during sustainable machining conditions with environmentally friendly rapeseed oil supplied at MQL, which provided a 17–23% longer tool life than dry conditions. When using oil mixed with graphite nanoparticles, an 8% longer tool life was obtained compared to dry conditions (Fig. 40). The same low wear rate was also obtained when using the lowest cutting speed in the cutting data set. Some important wear mechanisms can be identified at lower cutting speeds, and their intensity increases with temperature, which is highly controlled by the cutting speed.

Face turning of GCI in a completely aged state and a non-aged state with pcBN cutting tools was done at cutting speeds ranging from $v_c$ = 300 m/min to $v_c$ = 1500 m/min (Fig. 38a). Tool flank wear was low when machining the aged material due to the protective deposits while an optimal cutting speed of $v_c$ = 1200 m/min was identified for the non-aged GCI due to the deposition of protective oxides. This cutting speed is higher than the industrial standard and provides opportunities for increased productivity and management of the lower machinability in non-aged GCI.

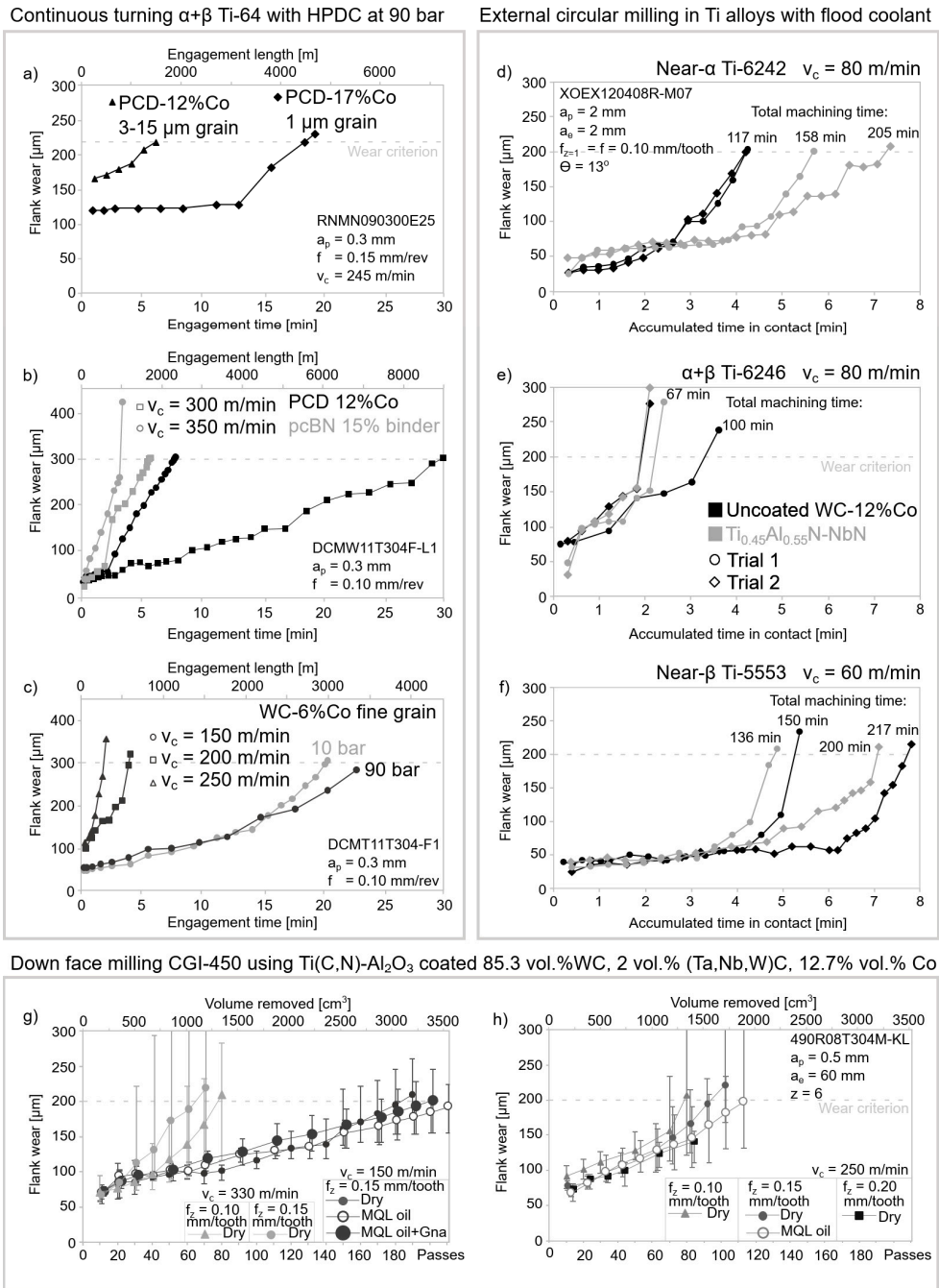


**Fig. 40** Cutting performance. (a–c) Continuous turning in Ti-64 with HPDC using PCD, pcBN, and cemented carbide tooling. (d–f) External circular milling in Ti alloys with flood coolant using uncoated and PVD coated $Ti_{0.45}Al_{0.55}N$-NbN cemented carbide. (g–h) Down face milling in CGI-450 at dry and MQL oil conditions using CVD Ti(C,N)-$Al_2O_3$ coated cemented carbide [**I**–**V**].

## 5.9 Conclusions

This section presents the identified wear mechanisms in the selected tooling at the specific conditions used to machine the workpiece materials. Because it is impossible to study the wear mechanisms as they progress at the tool-chip/workpiece contact regions, different experimental methods were employed to explore the process and qualitatively examine wear mechanisms. These methods included working with as-worn tools and their cross-sections after controlled variation in machining conditions, process freezing experiments with the quick stop method where the cross-sections include the tool edge attached to the workpiece material, imitational experiments with the diffusion couple method, heat treatment of tool-chip interfaces, and finally modeling and simulations. The wear rate or tool performance was evaluated quantitatively, and the rate or performance was then explained with reference to qualitatively identified wear mechanisms.

PCD and pcBN cost more than conventional cemented carbide in Ti machining, and should thus demonstrate higher material removal rates. At these rates, diffusional dissolution is an active wear mechanism for both materials. Diffusional dissolution of diamond grains can be reduced or stopped by selecting a grade with smaller grains and higher Co binder content to create a more coherent layer of (Ti,V)C reaction product that acts as the tool protection layer. For pcBN, higher performance can be obtained by modifying the binder content by the addition of W and Mo, which have been shown to work as diffusion barriers. Protective $(Ti,V)B_2$ or its Cr-doped version at binder sites forms at cBN-Ti interfaces. This is the opposite of PCD, where formation of (Ti,V)C reaction product is limited to binder sites. However, the higher dissolution rate in pcBN tooling makes PCD the more performing tool material of the two. Given the lower performance but lower price of uncoated cemented carbide, PCD needs to demonstrate a long tool life to be competitive.

The wear mechanisms in cemented carbide in machining Ti alloys can vary depending on the machining application and the alloy being machined. The intensity of diffusional dissolution increases with temperature and chip flow at higher cutting speeds. However, diffusion of C is not necessarily negative, because it can form a protective (Ti,V)C or TiC reaction product. Additional diffusion of Co and loss of it as the binder facilitates removal of WC grains by the chip flow. Oxidation of Co and WC is another wear mechanism identified in milling, causing formation of $CoWO_4$ several µm into the cemented carbide, which promotes crack formation. PVD-applied $Ti_{0.45}Al_{0.55}N$-NbN was rapidly removed by mechanical damage. However, in turning, similarly rapid mechanical damage was present in combination with diffusional dissolution of the coating that remained local and protected the edge line.

Modeling and simulations supported the findings on wear mechanisms for the materials, although some artifacts occur. The intensity of the wear mechanisms is

reflected in the performance, where diffusional and chemical reactions are driven by temperature and speed of chip flow. These two factors are directly related to cutting speed. Their effect can be altered by cooling but primarily by selecting optimal cutting parameters.

Wear mechanisms in CVD-applied Ti(C,N)-$Al_2O_3$ coating while milling CGI-450 include mechanical wear of the coating by debonding, cracking, abrasion, and micro-fracturing, as well as diffusional dissolution. Potential formation of (Mg,Fe,Mn)$Al_2O_4$ spinel on the $Al_2O_3$ layer increases the removal rate. Exposed cemented carbide is worn by diffusional dissolution resulting in the formation of brittle $(Fe_x,Co_{1-x})_3C$ unless there are protective MgO and $SiO_2$ deposits. Additional oxidation wear results in the formation of protective $Fe_2SiO_4$, while formation of $FeWO_4$ ($Fe_2WO_6$) and $CoWO_4$ causes cracking. Increased performance can be achieved by using sustainable vegetable oil lubrication with MQL.

Wear of pcBN tooling in machining GCI reveals low wear rates in aged state GCI due to deposits of protective oxides and sulfides, while large variations in tool wear in machining non-aged GCI at varying cutting speeds are due to more complex wear phenomena. At the optimal cutting speed, protective $Al_2O_3$ and MnS deposits prevent diffusional dissolution. Diffusional dissolution and instable formation of such deposits occurs at lower speeds with lower process temperature. The formation of $(Fe,Mn)_2SiO_4$ at higher temperatures provides weaker protection for the tool material and (Fe,Mn)O drives cBN oxidation. By managing the cutting speed, the poorer machinability of non-aged GCI can be handled, contributing to higher efficiency and potential cost savings as the optimal cutting speed is higher than the industrial standard.

# 6 Conclusions and outlook

This chapter summarizes the appended papers and the major conclusions that can be drawn from the work, and presents the response to the research questions and suggestions for future work. The main aim of the work was to explore wear mechanisms in commercial tooling in the machining of difficult-to-cut Ti alloys and CGI, including the variance in machinability of non-aged GCI, and to contribute to the knowledge of wear rate and tooling performance.

## 6.1 Summary of publications

**Paper I** *Performance and Wear Mechanisms of PCD and PcBN Cutting Tools during Machining Titanium Alloy Ti6Al4V*

Tooling performance and wear mechanisms were studied in high-speed turning of Ti-64 using commercial PCD and pcBN. Wear evolution, cutting forces, and surface roughness were recorded, as was the temperature of the PCD tool. PCD had superior performance to pcBN, which failed by cracking and fracturing but provided favorable surface roughness evolution. Rake cratering, a high edge temperature (1100 °C), and a short contact length were shown to result in a new chamfer-shaped edge geometry that negatively affected surface roughness and cutting forces. There was no sign of adhesive wear, but channel formation was observed in PCD, caused by the likely combination of diamond burn-out and graphitization. PCD is worn by diffusional dissolution of C while its reaction with Ti and V at the interface forms (Ti,V)C caps that function as a diffusion barrier. This phenomenon is facilitated by the presence of Co. Longer tool life can be achieved by using a PCD grade with a smaller grain size and larger Co content, which allows protective caps of (Ti,V)C to merge into a continuous tool protection layer. Diffusional dissolution of B, N, and binder elements are active in pcBN. A tool protection layer consisting of $(Ti,V)B_2$ and $(Ti,V,Cr)B_2$ forms at the cBN and binder interface to Ti-64, respectively.

**Paper II** *Performance and Wear Mechanisms of Uncoated Cemented Carbide Cutting Tools in Ti6Al4V Machining*

Tooling performance and wear mechanisms were studied in high-speed turning of Ti-64 using commercial cemented carbide. Changes in the cutting speed and coolant pressure gave the expected tool life trends, and the flank wear evolutions were

shown to be predictable. Cratering negatively affected the surface roughness, but there was no plastic deformation. Strong adhesion of Ti alloy to the worn regions facilitated the removal of dislodged WC grain clusters with the chip flow. The contact of Ti alloy with the cemented carbide resulted in outward diffusion of C and Co, with the loss of Co decreasing grain bonding. Studying several locations at the crater and flank interface showed that the intensity of diffusion wear is largest at the center of the crater. Outward C diffusion results in a residual W layer at the interface that stabilizes the β-phase of Ti, while enough C saturation forms protective TiC. Intermetallic $TiCo_2$ and $Co_3W$ form at surface binder sites due to inward diffusion of Ti and loss of C that travels through the Co binder. Both products work as diffusion barriers that locally retard material loss.

**Paper III** *On the Wear Mechanisms of Uncoated and Coated Carbide Tools in Milling Titanium Alloys*

Tooling performance and wear mechanisms were studied in external circular milling of near-α Ti-6242, α+β Ti-6246, and near-β Ti-5553 using commercial uncoated or PVD $Ti_{0.45}Al_{0.55}N$-NbN cemented carbide. Rapid coating removal due to cracking points to the need for a more robust coating formulation. Massive tool material loss was due to extensive flaking and chipping, as well as crack networks within the cemented carbide. Diffusional loss of C produces rounder WC grains. Outward diffusing Co binder results in easier removal of surface WC grains by the chip flow, and loss of dampening Co results in damage to the diffusionally weakened WC grains. Voids in surface Co regions can be explained by Kirkendall porosity or by plastic deformation of the binder. Oxidative wear results in the formation of $CoWO_4$ several μm into the tool, in which cracks easily propagate. The intensity of the oxidation is highest in milling α+β Ti-6246, which explains why it has the highest wear rate. Neighboring Co to oxide product has an hcp structure indicating its deformation.

**Paper IV** *Degradation of Multi-Layer CVD-Coated Cemented Carbide in Finish Milling Compacted Graphite Iron*

The wear mechanisms and basic performance of commercial multilayer CVD-coated Ti(C,N)-$Al_2O_3$ cemented carbide were evaluated in finish face milling of CGI-450 with 90–95% pearlite content and 5–10% nodularity. The $Al_2O_3$ reacts with MgO inclusions potentially forming $(Mg,Fe,Mn)Al_2O_4$ spinel that is easily removed by superficial shear and abrasion by hard inclusions. Ti(C,N) is worn by abrasion, debonding, and microfractures, and on the rake it also experiences diffusional dissolution. Deposition of MgO and $SiO_2$ inclusions on exposed cemented carbide inhibits adhesion of CGI. Where adhesion occurs, it causes rapid wear due to outward diffusion of C, W, and Co forming an iron-based carbide at the interface. Decreased grain bonding causes periodic removal with adhesive wear.

**Paper V** *Wear Mechanisms in Ti(C,N)-$Al_2O_3$ Coated Carbide during Sustainable Machining CGI*

The wear mechanisms and basic performance of commercial multilayer CVD-coated Ti(C,N)-$Al_2O_3$ cemented carbide were explored and evaluated in finish face milling CGI-450 at sustainable dry and MQL conditions. A 20% longer tool life was achieved when using MQL rapeseed oil compared to dry conditions. The formation of easily removed (Mg,Fe,Mn)$Al_2O_4$ spinel was an expected reaction product but was not confirmed in the TEM lamella, likely due to its location. Plastic deformation of the tool edge induces coating cracks where oxidized CGI accelerates delamination. Advanced microscopy methods verified the protective mechanism of oxide inclusions as well as the outward diffusion of C, W, and Co. New findings include that the C and Co diffusion at stable conditions reacts with Fe, forming a $(Fe_x,Co_{1-x})_3C$ iron carbide diffusion barrier. Local inward diffusion of Fe accompanied by its oxidation in Co regions speeds up oxidation of W and Co, resulting in cracks on the rake side. The positive effects of oxidation in CGI result in a $Fe_2SiO_4$ oxide ceramic tool protection layer.

**Paper VI** *Effect of Ageing on Machining Performance of Grey Cast Iron and Its Compensation by Cutting Speed Management*

The machining performance and wear mechanisms for pcBN tooling used to machine GCI in the non-aged state (less than six days after casting) and in the aged state were investigated. It was found that wear can be minimized by adjusting the cutting speed, and an optimal speed was identified. This speed is higher than the industrial standard and provides increased efficiency and potential cost savings. Protective $Al_2O_3$ and MnS deposits are active when machining aged GCI, and the same deposits are present at the optimal cutting speed, preventing diffusional dissolution of pcBN, which is active at lower cutting speeds due to the lack of protective deposits. At cutting speeds above the optimum, the formation of weaker $(Fe,Mn)_2SiO_2$ replaces $Al_2O_3$ and oxidation accelerates degradation.

**Paper VII** *A Combined Experimental and Modelling Approach to Understand Chemical Wear in Titanium Turning*

Two TEM lamellae from cemented carbide tools used in turning Ti-64 and Ti-5553 were studied. The formation of intermetallic $Co_3W$ was identified in both samples near the interface to the Ti alloy. Its formation is enabled by the outward diffusion of C from WC grains through Co that release W. $Co_3W$ works as a diffusion barrier in local Co regions. Boundary conditions for simulations were established based on experimental knowledge. The simulation suggests that intermetallic formation occurs because the fcc Co becomes supersaturated with W, giving a mix of fcc with low W content and $Co_3W$, after which Co attains the hcp structure on cooling.

**Paper VIII** *Predicting Wear Mechanisms of Ultra-Hard Tooling in Machining Ti6Al4V by Diffusion Couples and Simulation*

Imitational experiments with diffusion couples and diffusion simulations were used to study and predict chemical and diffusion wear mechanisms. Known temperature, pressure, and time in contact served as input data for the simulations. The results were verified against known wear mechanisms in commercial PCD, pcBN, and cemented carbide tooling used in machining conventional Ti-64. TiC or (Ti,V)C formation in PCD and cemented carbide was shown. Liquefaction of Co facilitates diamond graphitization and accelerates C transport and thus diffusional wear. Loss of C in cemented carbide gives W clusters at the interface that inhibit formation of protective TiC. Brittle $Co_3W_3C$ was shown to form, but has not yet been found in used tools. In pcBN, Ti(C,N) and $Cr_2N$ were artifacts while the formation of $(Ti,V)B_2$ was correctly predicted. Wear resistance in pcBN can be improved by increasing Mo and W volume in the binder, as they work as diffusion barriers.

**Paper IX** *On Wear of TiAlN Coated Tools with and Without NbN Overlayer in Machining Titanium Alloys*

Wear mechanisms in $Ti_{0.45}Al_{0.55}N$ coating with and without NbN overlayer and substrate cemented carbide were explored with controlled variability experiments, process freezing experiments with quick stop, and imitational experiments with the diffusion couple method in the machining of α CP-Ti, α+β Ti-64, and near-β Ti-5553. The coating wears mechanically by cracking and by diffusional dissolution of Al and N. The NbN overlayer reduces the Al diffusion rate, but the NbN itself is diffusionally worn where Nb stabilizes the interface β-Ti, which increases diffusion rates of substitutionally diffusing elements. The formation of intermetallic $Nb_3Al$ works as a diffusion barrier for $Ti_{0.45}Al_{0.55}N$, but could be easily removed in machining due to its brittleness. The findings highlight that any new coating design for Ti machining should combine high mechanical integrity and resistance to diffusional dissolution. The wear rate of cemented carbide is faster than that of the coating due to diffusional dissolution of C and Co. This may be reduced by formation of a TiC reaction product. The presence of a coating on the edge line is crucial for protecting the tool from edge failure.

**Paper X** *Characterisation of Worn WC Tool using STEM-EDS Aided by Principal Component Analysis*

Principal component analysis (PCA) was used on STEM-XEDS images of the interface between cemented carbide and Ti-64 after turning Ti-64. PCA aided XEDS analysis by de-noising the spectra and found chemical correlations by using simulated spectra. PCA confirmed SAED's identification of the presence of a rim of W on WC grains facing Ti-64 as a remnant of C diffusion. Intermediate $W_2C$ was ruled out, which indicated direct transformation to W. The PCA method can be used when XEDS is difficult to interpret, or as a complement or substitute for SAED to identify phases present.

**Paper XI** *Assessment of Metal Cutting Tools using Cost Performance Ratio and Tool Life Analyses*

Conventional uncoated cemented carbide was compared to more cost-intensive commercial PCD tooling, which can be efficient at high-speed conditions. Cost performance and productivity were evaluated using a combination of Colding tool life modeling, which is based on real tool life data for the two tool materials in turning Ti-64, and a model for cost performance ratio that included part cost calculations. The higher productivity of PCD provided an 8% faster cycle time than cemented carbide, but the cemented carbide had a lower part cost and better cost performance. It would require at least 30 minutes of tool life for PCD to become cost neutral, and that long a running time is associated with risks like unexpected tool failure. The study shows the importance of considering both tool cost and machining performance.

## 6.2 Conclusions

This thesis reported on experimental and characterization techniques that enable exploration of wear mechanisms in cutting tools used in machining. Because it is not yet possible to study wear progression *in-operando*, the methods used to explore tool wear mechanisms and related phenomena across the tool-chip/workpiece interfaces were controlled variability experiments, process freezing experiments, imitational experiments, and modeling and simulations (Fig. 1). The controlled variability experiments investigated different machining methods, varying cutting parameters, the use of coolant or lubricants, and changes in tool material grades and workpiece materials. The intensity of diffusional dissolution and chemical wear mechanisms, and thus the wear rate, increases with the higher temperatures induced by increasing the cutting speed and feed, while cooling allows for higher cutting data parameters. Sustainable MQL in CGI machining reduced the wear rate by minimizing the tool-chip/workpiece contact. Process freezing included the quick stop method that retains the tool-chip/workpiece contact and allows study of their actual interface. Preparation techniques to enable studies of the interfaces in as-worn tools from controlled variability experiments, from process freezing quick stop, and from imitational experiments including diffusion couples were introduced. The **first research question** is answered by selecting and combining the microscopy techniques used to capture the wear mechanisms and related phenomena from a macro to nano range. These techniques included SEM, XEDS, EBSD, ICCI, TEM, and XRD.

The range of tooling included ultra-hard PCD and pcBN, uncoated cemented carbide, and its coated versions including PVD-applied $Ti_{0.45}Al_{0.55}N$ and $Ti_{0.45}Al_{0.55}N$-NbN and CVD-applied Ti(C,N)-$Al_2O_3$. These were used to machine a

range of Ti alloys from CP-Ti, near-α Ti-6242, α+β Ti-64, α+β Ti-6246 to near-β Ti-5553, as well as CGI-450 and GCI, making for many combinations of materials and wear mechanisms. The identified wear mechanisms included diffusional and chemical wear that directly or indirectly cause tool material loss or the formation of tool protection layers. Mechanical wear was predominant for PVD coatings and tool bulk in Ti machining. The exploration of these wear mechanisms across multiple length scales answers the **second research question**.

Diffusional loss of C from diamond and WC grains, as well as B and N from cBN grains, are major contributors to the wear of PCD, pcBN, and cemented carbide. Protective reaction products include (Ti,V)C or TiC when machining Ti alloys with PCD and cemented carbide. The (Ti,V)C forms a more continuous layer as the Co binder content increases, and when using a smaller grain size in PCD. Protective $(Ti,V)B_2$ or $(Ti,V,Cr)B_2$ forms when machining Ti alloy with pcBN. This knowledge has resulted in two patents [161, 162]. The formation of the protective phase can be accelerated by artificially adding nucleation sites to the binder. Protective $Ti_2Co$ and $Co_3W$ form in near-surface binder regions of cemented carbide when machining Ti alloys. They can reduce outward diffusion of Co, as Co loss reduces grain binding, making surface WC grains prone to removal with the chip flow.

Chemical wear by oxidation occurs in cemented carbide when milling Ti alloys and CGI, leading to the formation of brittle $CoWO_4$. The formation of $FeWO_4$ ($Fe_2WO_6$) is limited to CGI milling, and cracks propagate along the formed oxides. The positive effects of oxidation in CGI milling include the formation of $Fe_2SiO_4$ and $(Fe_x,Co_{1-x})_3C$ diffusion barriers. In machining non-aged GCI, diffusional dissolution of pcBN is active. At higher cutting speeds, additional oxidation and formation of mechanically weak $(Fe,Mn)_2SiO_2$ contribute to its degradation. Formation of protective $Al_2O_3$ prevents diffusional dissolution in aged GCI, but also occurs at an optimal cutting speed in non-aged GCI. This speed is higher than the current industrial standard and thus hints at improved machining efficiency and related cost savings.

Tooling performance expectedly demonstrates shorter tool life at higher cutting speeds and feeds for all tool and workpiece combinations. The observation can be explained by the higher cutting temperatures that increase the diffusional and chemical wear that are major wear mechanisms in the conditions used in this work. This answers the **third research question**. Lower wear rates can be attained by decreasing the cutting speed or feed and applying coolant at high pressures. Lubrication has a similar effect in CGI machining because it decreases the contact between tool and workpiece material. In machining Ti alloys the highest performance is achieved with PCD followed by pcBN. This is due to the lower diffusion rate of diamond compared to cBN and the more extensive formation of tool protection layers. Increasing Mo and W in the binder for pcBN could result in a more continuous tool protection layer which could increase tool life. By carefully

selecting the PCD grade, the protective layers can merge and form a more coherent layer that extends tool life.

The wear rate of cemented carbide in Ti machining is higher than that of PCD and pcBN. The less expensive tool material justifies machining at lower speeds, which can cause lower cycle times in production. However, the more expensive PCD needs a longer tool life before it can become cost neutral to cemented carbide; therefore both cost and tool life need to be considered in an industrial machining setup. Oxidation wear that leads to cracking in cemented carbide could be avoided by decreasing the cutting temperature and thus the onset of oxidation. Another measure to increase the tool life of cemented carbide would be to engineer more robust and wear-resistant coating formulations for both turning and milling operations, as the coatings have been shown to fail mechanically and by diffusional dissolution.

## 6.3 Future work

The wear of cutting tools evolves as long as the tool is in contact with the workpiece material. The tool-chip/workpiece interface is shielded by the chip and workpiece material, and it is not yet possible to study the direct interaction as cutting proceeds. The methods identified in Fig. 1 in their own way resemble the wear mechanisms occurring during machining; however, there may be methods not identified in this work that could allow *in-operando* studies of the wear process. Future work could include studying wear mechanisms as they occur in real time using large-scale facilities with synchrotron or neutron spallation sources.

The characterization methods presented in section 4.3 serve as a foundation for exploring wear mechanisms. However, there are other available techniques like electron energy loss spectroscopy (EELS) that could be efficient to study lighter elements like C, B, O, and N with better resolution. Another useful characterization method is atom probe tomography (APT), which can image a sample in 3D and provide information on the distribution of elements at the atomic scale. This could be used to study diffusion of elements and reaction products at the interface, which would be helpful in understanding the initial diffusion and chemical reactions and their evolution. These methods could be used in future research to explore other combinations of tool and workpiece material systems.

I hope that the knowledge generated on active wear mechanisms and methods of exploring them in this work can be used to engineer future generations of tooling with improved wear resistance, including the formation of tool protection layers during cutting that prolong tool life. While the work done here has focused on wear mechanisms in the common machining methods of turning and milling, there are also other machining methods used in industry. The work needs to be expanded to address other methods like drilling or threading.

This work qualitatively confirmed the presence of certain wear mechanisms. However, it would be valuable to know quantitatively how much each wear mechanism contributes to the overall wear for a given set of machining conditions and a given tool-workpiece material combination. Such knowledge would allow effort to be efficiently directed where it is most needed.

While conditions at the cutting tool edge during machining can be understood based on methods using temperature and force measurements, there would be value in knowing the exact temperature and pressure distribution over the tool contact regions at the same time as the wear mechanisms are being explored. This would enable a direct link between those conditions and the intensity and presence of wear mechanisms.

The work reported on here could serve as a model and provide simulation input data for verification and validation of future sustainable research and development work. Such research could be used to find the settings at which certain phenomena occur, enabling tweaking of industrial setups to avoid the onset of wear mechanisms leading to rapid tool wear. Future sensor-based tooling in smart manufacturing systems can help provide such knowledge, which combined with suitable microscopy techniques and experimental methods to explore the tool-chip/workpiece interaction, can help manufacturing industry select the most efficient cutting data and tool-workpiece material combination to supplement the proposed cost performance ratio analyses.

# 7 References


[1] Statistikmyndigheten. "Svensk export" Accessed 2023-11-01, https://www.scb.se/hitta-statistik/sverige-i-siffror/samhallets-ekonomi/sveriges-export/.

[2] Svensk Gjuteriindustri, Svenska Gjuteriföreningen, Swerea SWECAST AB, Tekniska Högskolan Jönköping, Casting Innovation Centre, *Gjutna produkter i ett hållbart samhälle, för tillväxt och internationell konkurrenskraft i samverkan 2013-2030*, 2013-04-26.

[3] Ekonomifakta. "Industriproduktionens sammansättning" Accessed 2023-11-14, https://www.ekonomifakta.se/Fakta/makroekonomi/Produktion-och-Investeringar/Industriproduktionens-sammansattning/.

[4] SCB, *Industrins varuproduktion 2021 NV19 – Näringslivets struktur 2023:1*, 2023.

[5] G. E. Dieter, *Mechanical Metallurgy – SI Metric Edition*: McGraw-Hill Higher Education, 1988.

[6] P. K. Wright and E. M. Trent, *Metal Cutting 4th Edition*: Butterworth-Heinemann, 2000.

[7] United Nations Department of Economic and Social Affairs. "Transforming our world: the 2030 Agenda for Sustainable Development" Accessed 2023-10-30, https://sdgs.un.org/2030agenda.

[8] United Nations Environment Programme. "Emission Gap Report 2022: The Closing Window - Climate Crisis Calls for Rapid Transformation of Societies" Accessed 2023-10-30, https://www.unep.org/resources/emissions-gap-report-2022.

[9] W. D. Callister Jr., *Materials Science and Engineering – An Introduction (7th edition)*: John Wiley & Sons, Inc., 2007.

[10] M. König, "Literature Review of Microstructure Formation in Compacted Graphite Iron", *International Journal of Cast Metals Research*, vol. 23 (2010) pp. 185–192 https://doi.org/10.1179/136404609X12535244328378.

[11] Trafikanalys, *Styrmedel för tunga miljövänliga lastbilar – Rapport 2019:2*, 2019-03-01.

[12] Affärsvärlden. "Gjutet köp i verkstan" Accessed 2023-11-13, https://www.affarsvarlden.se/artikel/gjutet-kop-i-verkstan-6945098.

[13] R. M'Saoubi, D. Axinte, S. L. Soo, C. Nobel, H. Attia, G. Kappmeyer, S. Engin, and W.-M. Sim, "High Performance Cutting of Advanced Aerospace Alloys and Composite Materials", *CIRP Annals - Manufacturing Technology*, vol. 64 (2015) pp. 557–580 https://doi.org/10.1016/j.cirp.2015.05.002.

[14] K. Bobzin, "High-Performance Coatings for Cutting Tools", *CIRP Journal of Manufacturing Science and Technology*, vol. 18 (2017) pp. 1–9 https://doi.org/10.1016/j.cirpj.2016.11.004.

[15] J. Garcia, V. C. Cipres, A. Blomqvist, and B. Kaplan, "Cemented Carbide Microstructures: A Review", *International Journal of Refractory Metals and Hard Materials*, vol. 80 (2019) pp. 40–68 https://doi.org/10.1016/j.ijrmhm.2018.12.004.

[16] K. Schröter, *DRP 420.689: Sintered Hard Metal Alloy and Procedure for its Fabrication*, US1549615, 1923.

[17] H. M. Ortner, P. Ettmayer, and H. Kolaska, "The History of the Technological Progress of Hardmetals", *International Journal of Refractory Metals and Hard Materials*, vol. 44 (2014) pp. 148–159 https://doi.org/10.1016/j.ijrmhm.2013.07.014.

[18] "Celebrating 100 years of cemented carbide" Accessed 2023-06-20, https://www.sandvik.coromant.com/sv-se/press/celebrating-cemented-carbide.

[19] M. Grohol and C. Veeh, *Study on the Critical Raw Materials for the EU 2023 – Final Report*: Publications Office of the European Union, 2023.

[20] G. Li, M. Z. Rahim, W. Pan, C. Wen, and S. Ding, "The Manufacturing and the Application of Polycrystalline Diamond Tools - A Comprehensive Review", *Journal of Manufacturing Processes*, vol. 56 (2020) pp. 400–416 https://doi.org/10.1016/j.jmapro.2020.05.010.

[21] ECHA European Chemicals Agency. "Cobalt" Accessed 2023-11-01, https://echa.europa.eu/substance-information/-/substanceinfo/100.028.325.

[22] K. Houreld and A. Bashizi, "Despite reforms, mining for EV metals in Congo exacts steep cost on workers," *The Washington Post*, 2023.

[23] T. Mononen, S. Kivinen, J. M. Kotilainen, and J. Leino, *Social and Environmental Impacts of Mining Activities in the EU*, 2022.

[24] P. K. Philip, "Study of the Performance Characteristics of an Explosive Quick-Stop Device for Freezing Cutting Action", *International Journal of Machine Tool Design and Research*, vol. 11 (1971) pp. 133–144 https://doi.org/10.1016/0020-7357(71)90022-9.

[25] B. J. Griffiths, "A Fast Arrest and Freeze Wear Test - A New Tribological Testing Technique", *Tribology International*, vol. 23 (1990) pp. 277–284 https://doi.org/10.1016/0301-679X(90)90034-M.

[26] M. A. Seyyed Hamed and A. Ebrahim, "Analysis of Chip Removal Operations via New Quick-Stop Device", *Materials & Manufacturing Processes*, vol. 31 (2016) pp. 1782–1791 https://doi.org/10.1080/10426914.2015.1127959.

[27] J. Vleugels, T. Laoui, K. Vercammen, J. P. Celis, and O. Van der Biest, "Chemical Interaction Between a Sialon Cutting Tool and Iron-Based Alloys", *Materials Science and Engineering: A*, vol. 187 (1994) pp. 177–182 https://doi.org/10.1016/0921-5093(94)90345-X.

[28] H. Larsson and A. Engström, "A Homogenization Approach to Diffusion Simulations Applied to α+γ Fe–Cr–Ni Diffusion Couples", *Acta Materialia*, vol. 54 (2006) pp. 2431–2439 https://doi.org/10.1016/j.actamat.2006.01.020.

[29] S. Giménez, S. G. Huang, O. Van der Biest, and J. Vleugels, "Chemical Reactivity of PVD-Coated WC-Co Tools with Steel", *Applied Surface Science*, vol. 253 (2007) pp. 35473556 https://doi.org/10.1016/j.apsusc.2006.07.062.

[30] O. Hatt, H. Larsson, F. Giuliani, P. Crawforth, B. Wynne, and M. Jackson, "Predicting Chemical Wear in Machining Titanium Alloys Via a Novel Low Cost Diffusion Couple Method", *Procedia CIRP*, vol. 45 (2016) pp. 219–222 https://doi.org/10.1016/j.procir.2016.01.196.

[31] C. Ramirez, A. Idhil Ismail, C. Gendarme, M. Dehmas, E. Aeby-Gautier, G. Poulachon, and F. Rossi, "Understanding the Diffusion Wear Mechanisms of WC-10%Co Carbide Tools during Dry Machining of Titanium Alloys", *Wear*, vol. 390–391 (2017) pp. 61–70 https://doi.org/10.1016/j.wear.2017.07.003.

[32] L. von Fieandt, R. M'Saoubi, M. Schwind, and B. Kaplan, "Chemical Interactions Between Cemented Carbide and Difficult-to-Machine Materials by Diffusion Couple Method and Simulations", *Journal of Phase Equilibria and Diffusion*, vol. 39 (2018) pp. 369–376 https://doi.org/10.1007/s11669-018-0639-y.

[33] M. Olsson, F. Lenrick, R. M'Saoubi, H. Larsson, A. Markström, I. Petrusha, J-E. Ståhl, and V. Bushlya, "Study of Wear Mechanisms of Cemented Carbide Tools during Machining of Single-Phase Niobium", *Wear*, vol. 450–451 (2020) pp. 203244 https://doi.org/10.1016/j.wear.2020.203244.

[34] V. Bushlya, A. Bjerke, V. Z. Turkevich, F. Lenrick, I. A. Petrusha, K. A. Cherednichenko, and J-E. Ståhl, "On Chemical and Diffusional Interactions Between PCBN and Superalloy Inconel 718: Imitational Experiments", *Journal of the European Ceramic Society*, vol. 39 (2019) pp. 2658–2665 https://doi.org/10.1016/j.jeurceramsoc.2019.03.002.

[35] X. Liang, Z. Liu, and B. Wang, "Physic-Chemical Analysis for High-Temperature Tribology of WC-6Co Against Ti-6Al-4V by Pin-on-Disc Method", *Tribology International*, vol. 146 (2020) pp. 106242 https://doi.org/10.1016/j.triboint.2020.106242.

[36] W. Grzesik, J. Małecka, Z. Zalisz, K. Żak, and P. Niesłony, "Investigation of Friction and Wear Mechanisms of TiAlV Coated Carbide Against Ti6Al4V Titanium Alloy Using Pin-on-Disc Tribometer", *Archive of Mechanical Engineering*, vol. 63 (2016) pp. 114–127 doi: 10.1515/meceng-2016-0006.

[37] P. Sivaprakasam, T. Hailu, and Elias G., "Experimental Investigation on Wear Behavior of Titanium Alloy (Grade 23) by Pin on Disc Tribometer", *Results in Materials*, vol. 19 (2023) pp. 100422 https://doi.org/10.1016/j.rinma.2023.100422.

[38] M. K. Gupta, H. E. Etri, M. E. Korkmaz, N. S. Ross, G. M. Krolczyk, J. Gawlik, N. Yaşar, and D. Y. Pimenov, "Tribological and Surface Morphological Characteristics of Titanium Alloys: A Review", *Archives of Civil and Mechanical Engineering*, vol. 22 (2022) https://doi.org/10.1007/s43452-022-00392-x.

[39] F. Nabhani, "Wear Mechanisms of Ultra-Hard Cutting Tools Materials", *Journal of Materials Processing Technology*, vol. 115 (2001) pp. 402–412 https://doi.org/10.1016/S0924-0136(01)00851-2.

[40] J. Qu, P. J. Blau, T. R. Watkins, O. B. Cavin, and N. S. Kulkarni, "Friction and Wear of Titanium Alloys Sliding Against Metal, Polymer, and Ceramic Counterfaces", *Wear*, vol. 258 (2005) pp. 1348–1356 https://doi.org/10.1016/j.wear.2004.09.062.

[41] M. Long and H. J. Rack, "Friction and Surface Behavior of Selected Titanium Alloys During Reciprocating-Sliding Motion", *Wear*, vol. 249 (2001) pp. 157–167 https://doi.org/10.1016/S0043-1648(01)00517-8.

[42] J. Heinrichs, M. Olsson, I. Z. Jenei, and S. Jacobson, "Transfer of Titanium in Sliding Contacts - New Discoveries and Insights Revealed by In Situ Studies in the SEM", *Wear*, vol. 315 (2014) pp. 87–94 https://doi.org/10.1016/j.wear.2014.04.006.

[43] N. S. M. El-Tayeb, T. C. Yap, and P. V. Brevern, "Wear Characteristics of Titanium Alloy Ti54 for Cryogenic Sliding Applications", *Tribology International*, vol. 43 (2010) pp. 2345–2354 https://doi.org/10.1016/j.triboint.2010.08.012.

[44] O. A. Makgae, F. Lenrick, V. Bushlya, J. M. Andersson, R. M'Saoubi, and M. Ek, "Visualising Microstructural Dynamics of Titanium Aluminium Nitride Coatings under Variable-Temperature Oxidation", *Applied Surface Science*, vol. 618 (2023) pp. 156625 https://doi.org/10.1016/j.apsusc.2023.156625.

[45] Y. C. Chim, X. Z. Ding, X. T. Zeng, and S. Zhang, "Oxidation Resistance of TiN, CrN, TiAlN and CrAlN Coatings Deposited by Lateral Rotating Cathode Arc", *Thin Solid Films*, vol. 517 (2009) pp. 4845–4849 https://doi.org/10.1016/j.tsf.2009.03.038.

[46] N. Bertrand, C. Desgranges, D. Poquillon, M. C. Lafont, and D. Monceau, "Iron Oxidation at Low Temperature (260–500 °C) in Air and the Effect of Water Vapor", *Oxidation of Metals*, vol. 73 (2010) pp. 139–162 https://doi.org/10.1007/s11085-009-9171-0.

[47] A. Bjerke, A. Hrechuk, F. Lenrick, A. Markström, H. Larsson, S. Norgren, R. M'Saoubi, T. Björk, and V. Bushlya, "Thermodynamic Modeling Framework for Prediction of Tool Wear and Tool Protection Phenomena in Machining", *Wear*, vol. 484–485 (2021) pp. 203991 https://doi.org/10.1016/j.wear.2021.203991.

[48] T. N. Loladze, "Of the Theory of Diffusion Wear", *CIRP Annals*, vol. 30 (1981) pp. 71–76 https://doi.org/10.1016/S0007-8506(07)60898-1.

[49] P. D. Hartung, B. M. Kramer, and B. F. von Turkovich, "Tool Wear in Titanium Machining", *CIRP Annals*, vol. 31 (1982) pp. 75–80 https://doi.org/10.1016/S0007-8506(07)63272-7.

[50] A. Graves, A. Salmasi, S. J. Graham, W. Wan, C. Xiao, M. Jackson, H. Larsson, and S. Norgren, "An Experimental and Theoretical Investigation on Ti-5553/WC-Co(6%) Chemical Interactions during Machining and in Diffusion Couples", *Wear*, vol. 516–517 (2023) pp. 204604 https://doi.org/10.1016/j.wear.2022.204604.

[51] T.H.C. Childs, *Metal Machining: Theory and Applications*: Elsevier Science, 2013.

[52] I. Hutchings and P. Shipway, *Tribology: Friction and Wear of Engineering Materials, Second Edition*: Elsevier Ltd., 2017.

[53] N. A. Abukhshim, P. T. Mativenga, and M. Aslam Sheikh, "Heat Generation and Temperature Prediction in Metal Cutting: A Review and Implications for High Speed Machining", *International Journal of Machine Tools and Manufacture*, vol. 46 (2006) pp. 782–800 https://doi.org/10.1016/j.ijmachtools.2005.07.024.

[54] W. Liu, G. Li, Z. Shao, X. Wu, G. Ma, and F. Wang, "Advance in Experimental Research on Cutting Temperature of Titanium Alloys", *The International Journal of Advanced Manufacturing Technology*, vol. 126 (2023) pp. 1827–1844 https://doi.org/10.1007/s00170-023-11263-x.

[55] B. M. Pereira Guimarães, C. M. da Silva Fernandes, D. Amaral de Figueiredo, F. S. Correia Pereira da Silva, and M. G. Macedo Miranda, "Cutting Temperature Measurement and Prediction in Machining Processes: Comprehensive Review and Future Perspectives", *The International Journal of Advanced Manufacturing Technology*, vol. 120 (2022) pp. 2849–2878 https://doi.org/10.1007/s00170-022-08957-z.

[56] J. C. Heigel, E. Whitenton, B. Lane, M. A. Donmez, V. Madhavan, and W. Moscoso-Kingsley, "Infrared Measurement of the Temperature at the Tool-Chip Interface while Machining Ti-6Al-4V", *Journal of Materials Processing Technology*, vol. 243 (2017) pp. 123–130 http://dx.doi.org/10.1016/j.jmatprotec.2016.11.026.

[57] Q. Shi, L. Li, N. He, W. Zhao, and X. Liu, "Experimental Study in High Speed Milling of Titanium Alloy TC21", *The International Journal of Advanced Manufacturing Technology*, vol. 64 (2013) pp. 49–54 https://doi.org/10.1007/s00170-012-3997-3.

[58] A. Molinari, R. Cheriguene, and H. Miguelez, "Contact Variables and Thermal Effects at the Tool-Chip Interface in Orthogonal Cutting", *International Journal of Solids and Structures*, vol. 49 (2012) pp. 3774–3796 https://doi.org/10.1016/j.ijsolstr.2012.08.013.

[59] J. Saelzer, S. Berger, I. Iovkov, A. Zabel, and D. Biermann, "In-Situ Measurement of Rake Face Temperatures in Orthogonal Cutting", *CIRP Annals - Manufacturing Technology*, vol. 69 (2020) pp. 61–64 https://doi.org/10.1016/j.cirp.2020.04.021.

[60] R. M'Saoubi and H. Chandrasekaran, "Investigation of the Effects of Tool Micro-Geometry and Coating on Tool Temperature during Orthogonal Turning of Quenched and Tempered Steel", *International Journal of Machine Tools and Manufacture*, vol. 44 (2004) pp. 213–224 https://doi.org/10.1016/j.ijmachtools.2003.10.006.

[61] B. Mills, *Machinability of Engineering Materials*: Springer Netherlands, 2012.

[62] I. Konyashin and B. Ries, *Cemented Carbides*: Elsevier Science, 2022.

[63] A. Aditharajan, N. Radhika, and B. Saleh, "Recent Advances and Challenges Associated with Thin Film Coatings of Cutting Tools: A Critical Review", *Transactions of the IMF*, vol. 101 (2023) pp. 205–221 https://doi.org/10.1080/00202967.2022.2082154.

[64] N. Schalk, M. Tkadletz, and C. Mitterer, "Hard Coatings for Cutting Applications: Physical vs. Chemical Vapor Deposition and Future Challenges for the Coatings Community", *Surface and Coatings Technology*, vol. 429 (2022) pp. 127949 https://doi.org/10.1016/j.surfcoat.2021.127949.

[65] J-E. Ståhl, *Metal Cutting - Theories and Models*, Lund: Seco Tools AB, 2012.

[66] C. Artini, M. L. Muolo, and A. Passerone, "Diamond-Metal Interfaces in Cutting Tools: a Review", *Journal of Materials Science*, vol. 47 (2012) pp. 3252–3264 https://doi.org/10.1007/s10853-011-6164-6.

[67] M. W. Cook and P. K. Bossom, "Trends and Recent Developments in the Material Manufacture and Cutting Tool Application of Polycrystalline Diamond and Polycrystalline Cubic Boron Nitride", *International Journal of Refractory Metals and Hard Materials*, vol. 18 (2000) pp. 147–152 https://doi.org/10.1016/S0263-4368(00)00015-9.

[68] P. J. Heath, "Ultra-Hard Materials", *European Journal of Engineering Education*, vol. 12 (1987) pp. 5–20 https://doi.org/10.1080/03043798708939332.

[69] R. E. Smallman and A. H. W. Ngan, *Physical Metallurgy and Advanced Materials Engineering (7th Edition)*, Oxford: Butterworth-Heinemann, 2007.

[70] T. R. Bieler, R. M. Trevino, and L. Zeng, "Alloys: Titanium," *Encyclopedia of Condensed Matter Physics*, F. Bassani, G. L. Liedl and P. Wyder, eds., pp. 65–76, Oxford: Elsevier, 2005.

[71] P. J. Arrazola, A. Garay, L. M. Iriarte, M. Armendia, S. Marya, and F. Le Maître, "Machinability of Titanium Alloys (Ti6Al4V and Ti555.3)", *Journal of Materials Processing Technology*, vol. 209 (2009) pp. 2223–2230 https://doi.org/10.1016/j.jmatprotec.2008.06.020.

[72] A. Pramanik, "Problems and Solutions in Machining of Titanium Alloys", *The International Journal of Advanced Manufacturing Technology*, vol. 70 (2014) pp. 919–928 https://doi.org/10.1007/s00170-013-5326-x.

[73] S. Dawson, "Compacted Graphite Iron - A Material Solution for Modern Diesel Engine Cylinder Block and Heads", *China Foundry*, vol. 6 (2009) pp. 241–246.

[74] S. Dawson, I. Hollinger, M. Robbins, J. Daeth, U. Reuter, and H. Schulz, "The Effect of Metallurgical Variables on the Machinability of Compacted Graphite Iron", *Journal of Materials and Manufacturing*, vol. 110 (2001) pp. 334–352 https://doi.org/10.4271/2001-01-0409

[75] S. Dawson and T. Schroeder, "Practical Applications for Compacted Graphite Iron", *AFS Transactions*, vol. 112 (2004) pp. 1–9.

[76] "45th Census of World Casting Production", *Modern Casting*, vol. 12 (2011) pp. 16–19.

[77] S. N. Lekakh and V. L. Richards, "Aging and Machinability Interactions in Cast Iron", *AFS Proceedings*, vol. (2012) pp. 1–11.

[78] J. A. Teague, “Dependency of Machinability in Gray Cast Iron on Nitride-Induced Age Strengthening,” Missouri University of Science and Technology, 2010.

[79] R. K. Kountanya and P. Boppana, "Optimization of Machining of Automotive Components with Polycrystalline Cubic Boron Nitride", *Proceedings of the Institution of Mechanical Engineers, Part B: Journal of Engineering Manufacture*, vol. 222 (2008) pp. 797–805 https://doi.org/10.1243/09544054JEM1043.

[80] A. Vaucheret, F. Rossi, Q. Jean, and A. Eric, "Determination of Gray Cast Iron Age Strengthening by Nondestructive Methods: Effect of Alloying Elements", *Journal of Materials Engineering and Performance*, vol. 28 (2019) pp. 4026–4033 https://doi.org/10.1007/s11665-019-04180-2.

[81] J. Teague and V. Richards, "Age Strengthening of Cast Irons: Review of Research and Literature", *International Journal of Metalcasting*, vol. 4 (2010) pp. 45–57 https://doi.org/10.1007/BF03355465.

[82] P. Fiorini and G. Byrne, "The Influence of Built-Up Layer Formation on Cutting Performance of GG25 Grey Cast Iron", *CIRP Annals - Manufacturing Technology*, vol. 65 (2016) pp. 93–96 http://dx.doi.org/10.1016/j.cirp.2016.04.045.

[83] H. Larsson and L. Höglund, "Multiphase Diffusion Simulations in 1D using the DICTRA Homogenization Model", *Calphad*, vol. 33 (2009) pp. 495–501 https://doi.org/10.1016/j.calphad.2009.06.004.

[84] F. P. Bundy, H. P. Bovenkerk, H. M. Strong, and R. H. Wentorf Jr, "Diamond-Graphite Equilibrium Line from Growth and Graphitization of Diamond", *The Journal of Chemical Physics*, vol. 35 (1961) pp. 383–391 https://doi.org/10.1063/1.1731938.

[85] V. L. Solozhenko, V. Z. Turkevich, and W. B. Holzapfel, "Refined Phase Diagram of Boron Nitride", *The Journal of Physical Chemistry B*, vol. 103 (1999) pp. 2903–2905 https://doi.org/10.1021/jp984682c.

[86] J-E. Ståhl, "Requirements and Potential for High Performance Cutting Tools Based on Superhard Phases in New Applications", *Extended Abstract for keynote lecture at De Beers Diamond Conference 2016 hosted by Warwick University, UK, Conference number: 66*, (2016) pp. 1–3.

[87] J. Vleugels and O. Van Der Biest, "Chemical Wear Mechanisms of Innovative Ceramic Cutting Tools in the Machining of Steel", *Wear* vol. 225–229 (1999) pp. 285–294 https://doi.org/10.1016/S0043-1648(98)00362-7.

[88] J. Vleugels, P. Jacobs, J. P. Kruth, P. Vanherck, W. Du Mong, and O. Van der Biest, "Machining of Steel with Sialon Ceramics: Influence of Ceramic and Workpiece Composition on Tool Wear", *Wear*, vol. 189 (1995) pp. 32–44 https://doi.org/10.1016/0043-1648(95)06620-9.

[89] L. A. Giannuzzi, B. W. Kempshall, S. M. Schwarz, J. K. Lomness, B. I. Prenitzer, and F. A. Stevie, *Introduction to Focused Ion Beams: Instrumentation, Theory, Techniques and Practice*, Boston, MA: Springer US, 2005.

[90] F. Hofmann, E. Tarleton, R. J. Harder, N. W. Phillips, P.-W. Ma, J. N. Clark, I. K. Robinson, B. Abbey, W. Liu, and C. E. Beck, "3D Lattice Distortions and Defect Structures in Ion-Implanted Nano-Crystals", *Scientific Reports*, vol. 7 (2017) pp. 45993 https://doi.org/10.1038/srep. 45993.

[91] D. B. Williams and C. B. Carter, *Transmission Electron Microscopy Part 1: Basics (2nd Edition)*: Springer, 2009.

[92] L. Reimer and H. Kohl, *Transmission Electron Microscopy Physics of Image Formation (5th Edition)*: Springer, 2008.

[93] F. L. Deepak, A. Mayoral, and R. Arenal, *Advanced Transmission Electron Microscopy Applications to Nanomaterial*: Springer, 2015.

[94] B. Fultz and J. M. Howe, *Transmission Electron Microscopy and Diffractometry of Materials (3rd Edition)*: Springer, 2008.

[95] *Electron Backscatter Diffraction in Materials Science (2nd Edition)*: Springer New York, NY, 2009.

[96] R. E. Smallman and A. H. W. Ngan, *Modern Physical Metallurgy (8th Edition)*: Elsevier Ltd., 2014.

[97] W. König and A. Neises, "Wear Mechanisms of Ultrahard, Non-Metallic Cutting Materials", *Wear*, vol. 162–164 (1993) pp. 12–21 https://doi.org/10.1016/0043-1648(93)90479-6.

[98] N. Corduan, T. Himbart, G. Poulachon, M. Dessoly, M. Lambertin, J. Vigneau, and B. Payoux, "Wear Mechanisms of New Tool Materials for Ti-6Al-4V High Performance Machining", *CIRP Annals*, vol. 52 (2003) pp. 73–76 https://doi.org/10.1016/S0007-8506(07)60534-4.

[99] J. E. Westraadt, I. Sigalas, and J. H. Neethling, "Characterisation of Thermally Degraded Polycrystalline Diamond", *International Journal of Refractory Metals and Hard Materials*, vol. 48 (2015) pp. 286–292 https://doi.org/10.1016/j.ijrmhm.2014.08.008.

[100] M. I. Sadik, E. Coronel, and M. Lattemann, "Influence of Characteristic Properties of PCD Grades on the Wear Development in Turning of β-Titanium Alloy (Ti5Al5V5Mo3Cr)", *Wear*, vol. 426–427 (2019) pp. 1594–1602 https://doi.org/10.1016/j.wear.2019.01.012.

[101] D. J. Schrock, D. Kang, T. R. Bieler, and P. Kwon, "Phase Dependent Tool Wear in Turning Ti-6Al-4V using Polycrystalline Diamond and Carbide Inserts", *Journal of Manufacturing Science and Engineering*, vol. 136 (2014) pp. 041018 https://doi.org/10.1115/1.4027674.

[102] C. J. Pretorius, S. Leung Soo, D. K. Aspinwall, P. M. Harden, R. M'Saoubi, and A. L. Mantle, "Tool Wear Behaviour and Workpiece Surface Integrity when Turning Ti-6Al-2Sn-4Zr-6Mo with Polycrystalline Diamond Tooling", *CIRP Annals - Manufacturing Technology*, vol. 64 (2015) pp. 109–112 https://doi.org/10.1016/j.cirp.2015.04.058.

[103] Q. Lin, S. Chen, Z. Ji, Z. Huang, Z. Zhang, and B. Shen, "Atomic-Scale Interfacial Diffusion of Diamond into Titanium: Phase Transition and Layer Dependence", *Surfaces and Interfaces*, vol. 31 (2022) pp. 101993 https://doi.org/10.1016/j.surfin.2022.101993.

[104] T. Nguyen, P. Kwon, D. Kang, and T. R. Bieler, "The Origin of Flank Wear in Turning Ti-6Al-4V", *Journal of Manufacturing Science and Engineering*, vol. 138 (2016) pp. 121013 https://doi.org/10.1115/1.4034008.

[105] D. Bandyopadhyay, R. C. Sharma, and N. Chakraborti, "The Ti-Co-C System (Titanium-Cobalt-Carbon)", *Journal of Phase Equilibria and Diffusion*, vol. 21 (2000) pp. 179–185 https://doi.org/10.1361/105497100770340246.

[106] L. H. Wu, D. Wang, B. L. Xiao, and Z. Y. Ma, "Tool Wear and its Effect on Microstructure and Properties of Friction Stir Processed Ti-6Al-4V", *Materials Chemistry and Physics*, vol. 146 (2014) pp. 512–522 http://dx.doi.org/10.1016/j.matchemphys.2014.04.002.

[107] H. Sachdev, R. Haubner, H. Nöth, and B. Lux, "Investigation of the c-BN/h-BN Phase Transformation at Normal Pressure", *Diamond and Related Materials*, vol. 6 (1997) pp. 286–292 https://doi.org/10.1016/S0925-9635(96)00697-8.

[108] L. Jaworska, M. Szutkowska, P. Klimczyk, M. Sitarz, M. Bucko, P. Rutkowski, P. Figiel, and J. Lojewska, "Oxidation, Graphitization and Thermal Resistance of PCD Materials with the Various Bonding Phases of Up to 800 °C", *International Journal of Refractory Metals and Hard Materials*, vol. 45 (2014) pp. 109–116 http://dx.doi.org/10.1016/j.ijrmhm.2014.04.003.

[109] V. L. Solozhenko, O. O. Kurakevych, and Y. Le Godec, "Creation of Nanostuctures by Extreme Conditions: High-Pressure Synthesis of Ultrahard Nanocrystalline Cubic Boron Nitride", *Advanced Materials*, vol. 24 (2012) pp. 1540–1544 https://doi.org/10.1002/adma.201104361.

[110] M. Peicheng, C. Jiarong, Z. Zhe, C. Chao, P. Xiaoyi, X. Leyin, and L. Feng, "The Effect of cBN Volume Fraction on the Performance of PCBN Composite", *International Journal of Refractory Metals and Hard Materials*, vol. 100 (2021) pp. 105643 https://doi.org/10.1016/j.ijrmhm.2021.105643.

[111] M. Ångqvist, J. M. Rahm, L. Gharaee, and P. Erhart, "Structurally Driven Asymmetric Miscibility in the Phase Diagram of W-Ti", *Physical Review Materials*, vol. 3 (2019) pp. 073605 https://doi.org/10.1103/PhysRevMaterials.3.073605.

[112] S. Barzilai, C. Toher, S. Curtarolo, and O. Levy, "The Molybdenum-Titanium Phase Diagram Evaluated from Ab-Initio Calculations", *Physical Review Materials*, vol. 1 (2017) pp. 1–14 https://doi.org/10.1103/PhysRevMaterials.1.023604.

[113] R. A. Rahman Rashid, S. Palanisamy, S. Sun, and M. S. Dargusch, "Tool Wear Mechanisms Involved in Crater Formation on Uncoated Carbide Tool when Machining Ti6Al4V Alloy", *The International Journal of Advanced Manufacturing Technology*, vol. 83 (2016) pp. 1457–1465 https://doi.org/10.1007/s00170-015-7668-z.

[114] A. Ikuta, K. Shinozaki, H. Masuda, Y. Yamane, H. Kuroki, and Y. Fukaya, "Consideration of the Adhesion Mechanism of Ti Alloys Using a Cemented Carbide Tool during the Cutting Process", *Journal of Materials Processing Technology*, vol. 127 (2002) pp. 251–255 https://doi.org/10.1016/S0924-0136(02)00152-8.

[115] S. Zhang, J. F. Li, J. X. Deng, and Y. S. Li, "Investigation on Diffusion Wear during High-Speed Machining Ti-6Al-4V Alloy with Straight Tungsten Carbide Tools", *The International Journal of Advanced Manufacturing Technology*, vol. 44 (2009) pp. 17–25 https://doi.org/10.1007/s00170-008-1803-z.

[116] P. Olander and J. Heinrichs, "On Wear of WC-Co Cutting Inserts in Turning of Ti6Al4V - A Study of Wear Surfaces", *Tribology - Materials, Surfaces & Interfaces*, vol. (2020) pp. 1–12 https://doi.org/10.1080/17515831.2020.1830251.

[117] M. Latteman, E. Coronel, J. Garcia, and I. Sadik, "Interaction Between Cemented Carbide and Ti6Al4V Alloy in Cryogenic Machining", *Proceedings of the 19th Plansee Seminar, Reutte, Austria*, (2017) pp. 1–12.

[118] B. Kaplan, S. Odelros, M. Kritikos, R. Bejjani, and S. Norgren, "Study of Tool Wear and Chemical Interaction during Machining of Ti6Al4V", *International Journal of Refractory Metals & Hard Materials*, vol. 72 (2018) pp. 253–256 https://doi.org/10.1016/j.ijrmhm.2017.12.012.

[119] M. I. Sadik, M. Lattemann, and J. García, "Specific Carbide Substrate Design to Enhance Tool Performance in Machining of Ti5553", *Procedia CIRP*, vol. 77 (2018) pp. 598–601 https://doi.org/10.1016/j.procir.2018.08.203.

[120] P. Olander and J. Heinrichs, "Initiation and Propagation of Tool Wear in Turning of Titanium Alloys - Evaluated in Successive Sliding Wear Test", *Wear*, vol. 426–427 (2019) pp. 1658–1666 https://doi.org/10.1016/j.wear.2019.01.077.

[121] S. Saketi, S. Odelros, J. Östby, and M. Olsson, "Experimental Study of Wear Mechanisms of Cemented Carbide in the Turning of Ti6Al4V", *Materials*, vol. 12 (2019) pp. 2822 https://doi.org/10.3390/ma12172822.

[122] S. Odelros, B. Kaplan, M. Kritikos, M. Johansson, and S. Norgren, "Experimental and Theoretical Study of the Microscopic Crater Wear Mechanism in Titanium Machining", *Wear*, vol. 376 (2017) pp. 115–124 http://dx.doi.org/10.1016/j.wear.2017.01.104.

[123] D. Jianxin, L. Yousheng, and S. Wenlong, "Diffusion Wear in Dry Cutting of Ti-6Al-4V with WC/Co Carbide Tools", *Wear*, vol. 265 (2008) pp. 1776–1783 https://doi.org/10.1016/j.wear.2008.04.024.

[124] D. G. Bhat, V. A. Bedekar, and S. A. Batzer, "A Preliminary Study of Chemical Solubility of Ultra-Hard Ceramic AlMgB14 in Titanium: Reconciliation of Model with Experiment", *Machining Science and Technology*, vol. 8 (2004) pp. 341–355 https://doi.org/10.1081/MST-200038977.

[125] O. Hatt, P. Crawforth, and M. Jackson, "On the Mechanism of Tool Crater Wear during Titanium Alloy Machining", *Wear*, vol. 374–375 (2017) pp. 15–20 https://doi.org/10.1016/j.wear.2016.12.036.

[126] O. Hatt, Z. Lomas, M. Thomas, and M. Jackson, "The Effect of Titanium Alloy Chemistry on Machining Induced Tool Crater Wear Characteristics", *Wear*, vol. 408 (2018) pp. 200–207 https://doi.org/10.1016/j.wear.2018.05.020.

[127] S. Koseki, K. Inoue, K. Sekiya, S. Morito, T. Ohba, and H. Usuki, "Wear Mechanisms of PVD-Coated Cutting Tools during Continuous Turning of Ti-6Al-4V Alloy", *Precision Engineering*, vol. 47 (2017) pp. 434–444 http://dx.doi.org/10.1016/j.precisioneng.2016.09.018.

[128] W. Grzesik, J. Małecka, and W. Kwaśny, "Identification of Oxidation Process of TiALN Coatings Versus Heat Resistant Aerospace Alloys Based on Diffusion Couples and Tool Wear Tests", *CIRP Annals - Manufacturing Technology*, vol. 69 (2020) pp. 41–44 https://doi.org/10.1016/j.cirp.2020.04.024.

[129] S. PalDey and S. C. Deevi, "Single Layer and Multilayer Wear Resistant Coatings of (Ti,Al)N: A Review", *Materials Science and Engineering: A*, vol. 342 (2003) pp. 58–79 https://doi.org/10.1016/S0921-5093(02)00259-9.

[130] M. Zhang, Y. Li, Y. Feng, L. Xin, Y. Niu, J. Su, S. Zhu, and F. Wang, "Studies on Different Oxidation Behaviors of TiAlN on Titanium Alloy and Stainless Steel under Thermal Cycling", *Corrosion Science*, vol. 192 (2021) pp. 109865 https://doi.org/10.1016/j.corsci.2021.109865.

[131] M. Moreno, J. M. Andersson, R. Boyd, M. P. Johansson-Jöesaar, L. J. S. Johnson, M. Odén, and L. Rogström, "Crater Wear Mechanism of TiAlN Coatings during High-Speed Metal Turning", *Wear*, vol. 484–485 (2021) pp. 204016 https://doi.org/10.1016/j.wear.2021.204016.

[132] B. Wang, A. Li, and G. Liu, "Cutting Performance and Wear Mechanisms of TiAlN PVD-Coated Cemented Carbide Tool in High Speed Turning of Ti-5Al-2Sn-2Zr-4Mo-4Cr Alloy", *Journal of Mechanical Science and Technology*, vol. 34 (2020) pp. 2997–3006 https://doi.org/10.1007/s12206-020-0631-4.

[133] F. Wang, K. Ji, and Z. Guo, "Microstructural Analysis of Failure Progression for Coated Carbide Tools during High-Speed Milling of Ti-6Al-4V", *Wear*, vol. 456–457 (2020) pp. 203356 https://doi.org/10.1016/j.wear.2020.203356.

[134] D. Boing, A. J. De Oliveira, and R. B. Schroeter, "Evaluation of Wear Mechanisms of PVD and CVD Coatings Deposited on Cemented Carbide Substrates Applied to Hard Turning", *The International Journal of Advanced Manufacturing Technology*, vol. 106 (2020) pp. 5441–5451 https://doi.org/10.1007/s00170-020-05000-x.

[135] V. N. Zhitomirsky, "Structure and Properties of Cathodic Vacuum Arc Deposited NbN and NbN-Based Multi-Component and Multi-Layer Coatings", *Surface and Coatings Technology*, vol. 201 (2007) pp. 6122–6130 https://doi.org/10.1016/j.surfcoat.2006.08.125.

[136] T. Banda, K. Y. Ho, A. Akhavan Farid, and C. S. Lim, "Characterization of Tool Wear Mechanisms and Failure Modes of TiAlN-NbN Coated Carbide Inserts in Face Milling of Inconel 718", *Journal of Materials Engineering and Performance*, vol. 31 (2022) pp. 2309–2320 https://doi.org/10.1007/s11665-021-06301-2.

[137] V. Varghese, D. Chakradhar, and M. R. Ramesh, "Micro-Mechanical Characterization and Wear Performance of TiAlN/NbN PVD Coated Carbide Inserts during End Milling of AISI 304 Austenitic Stainless Steel", *Materials Today: Proceedings*, vol. 5 (2018) pp. 12855–12862 https://doi.org/10.1016/j.matpr.2018.02.270.

[138] V. Sivalingam, J. Sun, B. Yang, K. Liu, and R. Raju, "Machining Performance and Tool Wear Analysis on Cryogenic Treated Insert during End Milling of Ti-6Al-4V Alloy", *Journal of Manufacturing Processes*, vol. 36 (2018) pp. 188–196 https://doi.org/10.1016/j.jmapro.2018.10.010.

[139] L. Ning, S. C. Veldhuis, and K. Yamamoto, "Investigation of Wear Behavior and Chip Formation for Cutting Tools with Nano-Multilayered TiAlCrN/NbN PVD Coating", *International Journal of Machine Tools and Manufacture*, vol. 48 (2008) pp. 656–665 https://doi.org/10.1016/j.ijmachtools.2007.10.021.

[140] G. S. Fox-Rabinovich, K. Yamamoto, A. I. Kovalev, S. C. Veldhuis, L. Ning, L. S. Shuster, and A. Elfizy, "Wear Behavior of Adaptive Nano-Multilayered TiAlCrN/NbN Coatings under Dry High Performance Machining Conditions", *Surface and Coatings Technology*, vol. 202 (2008) pp. 2015–2022 https://doi.org/10.1016/j.surfcoat.2007.08.067.

[141] N. Norrby, "High Pressure and High Temperature Behavior of TiAlN," Licentiate thesis, comprehensive summary, Linköping Studies in Science and Technology. Thesis, Linköping University Electronic Press, Linköping, 2012.

[142] S. N. Yudin, A. V. Kasimtsev, A. V. Korotitskiy, T. A. Sviridova, G. V. Markova, S. S. Volodko, A. A. Nepapushev, and D. O. Moskovskikh, "Bulk $Nb_3Al$ Intermetallic Compound: Synthesis and High-Temperature Properties", *Materials Science and Engineering: A*, vol. 790 (2020) pp. 139715 https://doi.org/10.1016/j.msea.2020.139715.

[143] A. Bjerke, A. Hrechuk, F. Lenrick, R. M'Saoubi, H. Larsson, A. Markström, T. Björk, S. Norgren, J-E. Ståhl, and V. Bushlya, "Onset of the Degradation of CVD $\alpha$-$Al_2O_3$ Coating during Turning of Ca-Treated Steels", *Wear*, vol. 477 (2021) pp. 203785 https://doi.org/10.1016/j.wear.2021.203785.

[144] M. B. Da Silva, V. T. G. Naves, J. D. B. De Melo, C. L. F. De Andrade, and W. L. Guesser, "Analysis of Wear of Cemented Carbide Cutting Tools during Milling Operation of Gray Iron and Compacted Graphite Iron", *Wear*, vol. 271 (2011) pp. 2426–2432 https://doi.org/10.1016/j.wear.2010.11.030.

[145] S. Gabaldo, A. E. Diniz, C. L. F. Andrade, and W. L. Guesser, "Performance of Carbide and Ceramic Tools in the Milling of Compact Graphite Iron - CGI", *Journal of the Brazilian Society of Mechanical Sciences and Engineering*, vol. 32 (2010) pp. 511–517 https://doi.org/10.1590/S1678-58782010000500011.

[146] M. Chen, L. Jiang, G. Guo, and Q. An, "Experimental and FEM study of Coated and Uncoated Tools Used for Dry Milling of Compacted Graphite Cast Iron", *Transactions of Tianjin University*, vol. 17 (2011) pp. 235–241 https://doi.org/10.1007/s12209-011-1609-1.

[147] V. Nayyar, J. Kaminski, A. Kinnander, and L. Nyborg, "An Experimental Investigation of Machinability of Graphitic Cast Iron Grades; Flake, Compacted and Spheroidal Graphite Iron in Continuous Machining Operations", *Procedia CIRP*, vol. 1 (2012) pp. 488–493 https://doi.org/10.1016/j.procir.2012.04.087.

[148] V. Nayyar, G. Grenmyr, J. Kaminski, and L. Nyborg, "Machinability of Compacted Graphite Iron (CGI) and Flake Graphite Iron (FGI) with Coated Carbide", *International Journal of Machining and Machinability of Materials*, vol. 13 (2013) pp. 67–90 https://doi.org/10.1504/IJMMM.2013.051909.

[149] R. Su, C. Huang, L. Xu, B. Zou, H. Liu, Y. Liu, and C. Li, "Changes of Cutting Performance under Different Workpiece Removal Volume during Normal Speed and High Speed Milling of Compacted Graphite Iron", *The International Journal of Advanced Manufacturing Technology*, vol. 100 (2019) pp. 2785–2794 https://doi.org/10.1007/s00170-018-2848-2.

[150] J. Niu, C. Huang, R. Su, B. Zou, J. Wang, Z. Liu, and C. Li, "Study on Surface Integrity of Compacted Graphite Iron Milled by Cemented Carbide Tools and Ceramic Tools", *The International Journal of Advanced Manufacturing Technology*, vol. 103 (2019) pp. 4123–4134 https://doi.org/10.1007/s00170-019-03592-7.

[151] G. Grenmyr, A. Berglund, J. Kaminski, and C. M. Nicolescu, "Analysis of Tool Wear in CGI Machining", *International Multi-Conference on Engineering and Technological Innovation Proceedings*, vol. 1 (2008) pp. 34–39.

[152] G. Grenmyr, A. Berglund, J. Kaminski, and C. M. Nicolescu, "Investigation of Tool Wear Mechanisms in CGI Machining", *International Journal of Mechatronics and Manufacturing Systems*, vol. 4 (2011) pp. 3–18 https://doi.org/10.1504/IJMMS.2011.037996.

[153] V. Bushlya, F. Lenrick, J-E. Ståhl, and R. M'Saoubi, "Influence of Oxygen on the Tool Wear in Machining", *CIRP Annals - Manufacturing Technology*, vol. 67 (2018) pp. 79–82 https://doi.org/10.1016/j.cirp.2018.03.011.

[154] S. Koseki, K. Inoue, and H. Usuki, "Damage of Physical Vapor Deposition Coatings of Cutting Tools during Alloy 718 Turning", *Precision Engineering*, vol. 44 (2016) pp. 41–54 https://doi.org/10.1016/j.precisioneng.2015.09.012.

[155] V. Bushlya, F. Lenrick, A. Bjerke, H. Aboulfadl, M. Thuvander, J-E. Ståhl, and R. M'Saoubi, "Tool Wear Mechanisms of PcBN in Machining Inconel 718: Analysis Across Multiple Length Scale", *CIRP Annals - Manufacturing Technology*, vol. 70 (2021) pp. 73–78 https://doi.org/10.1016/j.cirp.2021.04.008.

[156] D. Nguyen, S. Tooptong, K. H. Park, and P. Kwon, "Formation Mechanism of Alumina Layer in Protecting Cubic Boron Nitride Inserts in Turning Cast Irons", *International Journal of Machine Tools and Manufacture*, vol. 153 (2020) pp. 103539 https://doi.org/10.1016/j.ijmachtools.2020.103539.

[157] O. Gutnichenko, V. Bushlya, J. Zhou, and J-E. Ståhl, "Tool Wear and Machining Dynamics when Turning High Chromium White Cast Iron with pcBN Tools", *Wear*, vol. 390–391 (2017) pp. 253–269 https://doi.org/10.1016/j.wear.2017.08.005.

[158] J-E. Ståhl, R. Lindvall, L. Magnusson Åberg, and C. Windmark, *Final Project Report - Competitive Grey Cast Iron for Sustainable Development*, Lund University, Vinnova, 2019.

[159] Y. Sert, L. Kara, T. Küçükömeroğlu, and H. Ghahramanzadeh, *The Wear Behavior of 52100 Steel against to $Al_2O_3$ and WC under Vacuum and Air Environment*: 9th International Conference on Tribology Proceedings, 2017.

[160] P. Klimczyk, P. Figiel, I. Petrusha, and A. Olszyna, "Cubic Boron Nitride Based Composites for Cutting Applications", *Journal of Achievements in Materials and Manufacturing Engineering*, vol. 44 (2011) pp. 198–204.

[161] R. Lindvall, A. Can, R. M'Saoubi, F. Lenrick, V. Bushlya, and J-E. Ståhl, *Polycrystalline cubic boron nitride material U.S. Patent No. 11,827,571*, 2023.

[162] R. Lindvall, A. Can, R. M'Saoubi, F. Lenrick, V. Bushlya, and J-E. Ståhl, *Polycrystalline cubic boron nitride material U.S. Patent No. 17/791,391*, 2023.

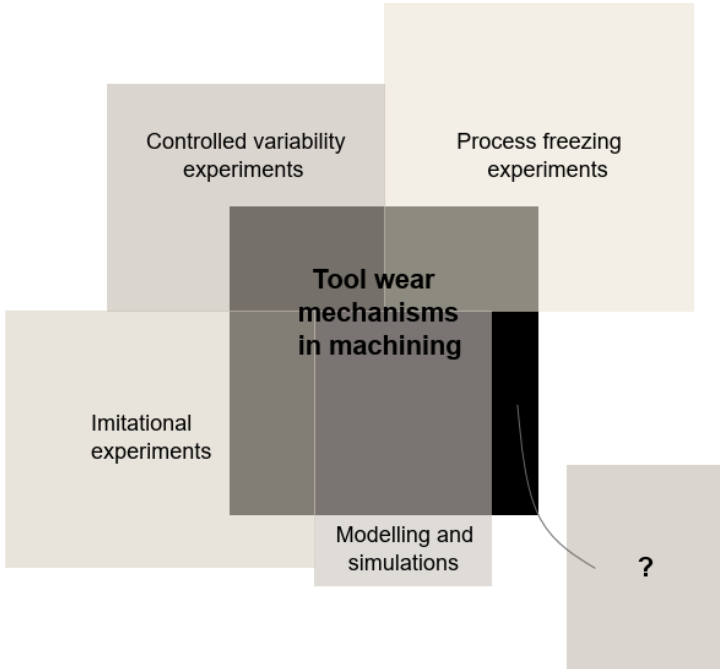


Printed by Media-Tryck, Lund 2024 NORDIC SWAN ECOLABEL 3041 0903

LUND UNIVERSITY

Division of Production and Materials Engineering
Department of Mechanical Engineering Sciences
Faculty of Engineering

ISBN 978-91-8039-962-3